Modelling secondary organic aerosol formation : from chemical mechanistic modelling to empirical modelling

Author:
Singh Peterson, Lila

Publication Date:
2007

DOI:
https://doi.org/10.26190/unsworks/6588

Modelling Secondary Organic Aerosol Formation: from Chemical Mechanistic Modelling to Empirical Modelling.

THE UNIVERSITY OF NEW SOUTH WALES

Lila Singh Peterson

April 2007

A thesis submitted for the degree of Doctor of Philosophy in the Faculty of Science.

ORIGINALITY STATEMENT

'I hereby declare that this submission is my own work and to the best of my knowledge it contains no materials previously published or written by another person, or substantial proportions of material which have been accepted for the award of any other degree or diploma at UNSW or any other educational institution, except where due acknowledgement is made in the thesis. Any contribution made to the research by others, with whom I have worked at UNSW or elsewhere, is explicitly acknowledged in the thesis. I also declare that the intellectual content of this thesis is the product of my own work, except to the extent that assistance from others in the project's design and conception or in style, presentation and linguistic expression is acknowledged.'

Signed .....

Date .....

Acknowledgements

The period of time that I have been chipping away at this thesis can more accurately be measured by life events than by the number of days. Whoever said that time was linear? During the four and a bit years I have lived in five houses, owned three cars, had three part-time jobs, lost my Stepfather, got engaged, then married, and celebrated (and am still celebrating) the birth of my daughter who is now 2 years old. The constant factor through all these events has been these studies which have been both my sanctuary and solace, and a frustrating and challenging endurance test (mainly on the sunny days).

The thought of not completing these studies a few months ago made me consider the cast of support that has gathered around me gently nudging me along the road. For these people can I take a moment to pause and say 'Thankyou'.

First and foremost I wish to convey my most heartfelt gratitude to my husband, Dr Fu. Without your constant 'dusting off' and pointing up at sky and world beyond my computer, I would never have managed to pull this together. Thankyou to my daughter, Mishti Moonbeam (Sienna), I am so looking forward to sitting under a tree with you just watching the leaves and the clouds without a timetable. Deepest gratitude to you too, Mum, for your constant support and help on the seemingly small stuff (that amounts to the really big stuff) and for being such a wonderful example of what a Mum can be.

I would like to acknowledge how very, very lucky I have been with my supervisors Dr Merched Azzi and A/Prof. Michael Box. I have felt a bit guilty listening to other students complain about how unavailable and unhelpful their supervisors are, something I have not experienced. I am grateful for the direction and support but also for the opportunity to be autonomous and choose what direction I would like to follow... a difficult balance to supervise. I'd especially like to thank Michael Box in these final stages of submission for making himself available to me, and in one case for giving up

his Easter Monday to accommodate me. I can't express how appreciative I am for your time, wisdom and humour.

Another person who has given up their personal time and energy to help me advance this work is Dr Martin Cope. I have really benefited from our discussions about air quality modelling and I feel inspired by your knowledge as a scientist.

My experience as a CSIRO student has been enriching and rewarding and for that I'm grateful for the creed and ethos of those around me, namely Graeme Batley, Dennys Angove, David French, Anne Tibbett, Rob Heywood and Rob Hynes in addition to those already mentioned.

Finally, I would also like to acknowledge the financial support received from the Australian Postgraduate Award (APA), University of NSW Maths top-up Scholarship and the CSIRO top-up scholarship.

Abstract

The work presented in this thesis is primarily concerned with modelling the formation of secondary organic aerosols (SOAs). SOAs cannot easily be measured with direct analytical chemical methods; indirect methods like applying organic carbon to elemental carbon ratios and utilising computer models have been employed to provide an estimate of the SOA mass concentrations in ambient air. The five models presented in this work were either developed or assessed using environmental chamber data.

Chamber experiments were undertaken using initial isoprene concentrations in the range of 22 ppb to 343 ppb, with the reactive organic carbon (ROC) to NOx ratios in the range of 2.0 to about 18. Chamber experiments were also performed for the α-pinene / NOx system with initial α-pinene concentrations ranging from 79 ppb to 225 ppb, with ROC/NOx ratios varying from 5.5 to about 41. All of the experiments were performed without the addition of propene or seed aerosol. Background aerosol levels were very low for the experiments presented in the thesis and so homogeneous nucleation processes were considered to occur in the chamber in addition to absorption and oligomerisation formation processes. Initial nucleation events resulting from the photooxidation of isoprene could be detected once the aerosol diameter was greater than 12 nm. In the α-pinene system, new particles formed via homogeneous nucleation processes were detectable in the 100-200nm diameter range.

The models presented range in complexity from the near explicit Master Chemical Mechanism to an empirical model whose key feature is its simplicity. The mechanistic model provides an insight into the SOA formation pathways and the influence of varying the initial experimental conditions and the duration of photooxidation on the simulated SOA composition. The aim of the empirical model is to simulate the SOA mass concentration produced during a chamber experiment. The development of the model is intentionally simple so that it can be applied to any hydrocarbon and has been applied successfully to isoprene and α-pinene chamber experiments. In this way, the

empirical model is presented as an alternative approach to predicting the temporal variation in SOA mass concentrations.

An analysis of the partitioning absorption models developed by Odum et al. (1996) and Hoffmann et al. (1997) has informed the development of the SOA module which has been coupled to a 3D atmospheric model. Embodied within the SOA module is the gas / aerosol partitioning theory which includes the model proposed initially by Pankow et al. (1994) and by Odum et al. (1996).

TABLE OF CONTENTS

ACRONYMS

CCN	Cloud Condensation Nuclei	Page 10, Chapter2
COC	Condensable Organic Compounds	Page 65, Chapter 5
CSIRO	Commonwealth Scientific and Industrial Research Organisation,	Page 24, Chapter 3
EPA	Environmental Protection Agency	Page 42, Chapter 7
EUPHORE	European Union Photooxidation Reactor	Page 31, Chapter 3
FTIR	Fourier Transform InfraRed Spectroscopy	Page 2, Chapter 1
GCMS	Gas Chromatography Mass Spectrometry	Page 16, Chapter 2
HC	Hydrocarbon	Page 16, Chapter 2
IPCC	Intergovernmental Panel on Climate Change	Page 9, Chapter 1
NEPC	National Environmental Protection Council	Page 7, Chapter 1.
NEPM	National Environmental Protection Measure	Page 7, Chapter 1
NMR	Nuclear Magnetic Resonance	Page 16, Chapter 2
NSW	New South Wales, Australia	Page 8, Chapter 2
PM_1	Particulate Matter with a diameter less than 1 μm	Page 9, Chapter 2
$PM_{2.5}$	Particulate Matter with a diameter less than 2.5 μm	Page 9, Chapter 2
PM_{10}	Particulate Matter with a diameter less than 10 μm	Page 7, Chapter 2
ppb	Parts per billion	Page 30, Chapter3
ROC	Reactive Organic Compounds	Page 2, Chapter 1
ROC/NOx	ratio of Reactive Organic Carbon to NOx	Page 2, Chapter 1
SAR	Structural Activity Reactions	Page 49, Chapter 4
SMPS	Scanning Mobility Particle Sizer	Page 34, Chapter 3
SOA	Secondary Organic Aerosol	Page 1, Chapter 1
SOAPEM	Secondary Organic Aerosol Profile Empirical Model	Page 3, Chapter 1
Tg C yr^{-1}	Teragrams of carbon per year	Page 6, Chapter 1
μm	Micrometre	Page 5, Chapter1
UV	UltraViolet	Page 23, Chapter 3
WHO	World Health Organisation	Page 8, Chapter 2
ZAP	Zero Air Plant	Page 26, Chapter 3

Chapter 1: Overview

The intention of this thesis is to explore and develop modelling methods for quantifying the formation of secondary organic aerosols (SOAs) in both the photochemical reaction chamber and ambient environment. Large concentrations of SOAs raise significant health concerns and may impact on visibility and the radiative balance of the atmosphere. Background information pertaining to aerosols and the current methods employed to study aerosol are presented in Chapter 2 along with a general overview of air pollution and the associated impacts of bad air quality.

The current state of knowledge on the quantity and type of SOAs in our atmosphere has largely been determined by coupling chamber experiments with modeling techniques, and both complex chemical mechanistic type models and empirical models have furthered our knowledge in this field. Three models have been developed and are presented in this work. An empirical model, an SOA chemical mechanism and an SOA module that was designed to be coupled to a three dimensional airshed model are presented. The three models have different aims and are based on very different approaches, and levels of complexity.

To develop and evaluate the models presented in this thesis, environmental chamber experiments were performed. Chamber experiments were used to study the formation mechanisms and overall SOA formation yields from the photooxidation of isoprene. Experiments were also performed for the α-pinene/NOx system. Information pertaining to the environmental chamber and associated instruments is presented in Chapter 3 along with a discussion of the experimental procedures and data treatment.

Chapter 4 discusses the development and results of an extension to the gas phase isoprene chemical mechanism (Master Chemical Mechanism (v 3.1)) to incorporate the formation of SOA. Isoprene is one of the most abundant hydrocarbons generally found in rural airsheds, and until recently, isoprene was thought to produce less than significant quantities of SOA. Recently, chamber experiments have found that the SOA

forming potential of isoprene is much higher than previously thought (Kroll et al., 2005; Böge et al., 2006).

Isoprene environmental chamber experiments were undertaken to determine the variation in SOA yields in response to different initial isoprene and NOx concentrations. Data collected from the NOx analyzer, ozone analyzer, particle classifier and counter, and fourier transform infrared spectroscopy (FTIR) provided further information from which formation pathways could be verified against the existing gas phase mechanism developed by Pinho et al. (2005). An SOA extension of the existing mechanism incorporates the recent advancements reported in the literature: from the identification of new particles in ambient $PM_{2.5}$ as isoprene photooxidation products to condensed phase reactions to form further products. Formation pathways for the tetrols and 2-methylglyceric acid were incorporated into the mechanism, in addition to partitioning of condensable organic products with boiling points in excess of 450 K. Condensed phase reactions to form peroxyhemiacetals were also added to the SOA mechanism and follow the methodology of Johnson et al. (2004).

In Chapter 4, the composition of the simulated SOA was compared to the initial isoprene and NOx chamber concentrations. Although a direct correlation between these two variables could not be observed, it was found that the SOA composition was different for different ratios of reactive organic carbon (ROC) to NOx. The composition of the simulated SOA was also found to vary throughout the chamber experiments as a result of varying precursor concentrations.

The purpose of Chapter 5 was to analyse the capabilities and limitations of the popular SOA partitioning models developed by Odum et al. (1996) and Hoffmann et al. (1997). Both models are based on the absorption partitioning theory proposed by Pankow et al. (1994). Pankow et al. (1994) proposed that condensable products behave as quasi-ideal solutions that partition to the aerosol phase by absorbing onto the surface of available aerosol. The models are, therefore, based entirely on the absorption mode of SOA formation, and neglect both homogeneous nucleation of SOA and condensed phase

reactions to form SOA. Despite these obvious limitations, both models are tested with a SOA sample of known composition derived from the 1,3-butadiene/NOx system with mostly good results.

The Odum model is most often applied to chamber data to derive parameter values for one or more products. The model also produces agreeable results when the parameter values of the species identified in the SOA sample are summed together as two products and substituted into the model to calculate individual and net SOA yields. The Odum model, however, does not produce good results when actual parameter values for two or three products are substituted into the model. The model products when fitted to the chamber data are theoretical products only, otherwise the products must represent the characteristics of the whole system of products, rather than a few individual products.

The Hoffmann model is more complex than the Odum model and results from Chapter 5 indicate that the best results were obtained by fitting the Hoffmann model to chamber data. This model is very successful at simulating the temporal variation of mass concentration over time when the modelled products represent the whole system. The Master Chemical Mechanism was employed to determine the temporal fraction of the hydrocarbon consumed by each of the three oxidants. Like the Odum model, the Hoffmann model did not produce good results when the characteristics of actual species (identified in the literature) were substituted into the model. A preliminary version of the work described in Chapter 5 has been presented at a Clean Air Conference in 2003 and a paper supporting the presentation was published in the CASANZ Conference Proceedings 2003 (Singh et al., 2003).

An empirical model named the SOA Profile Empirical Model (SOAPEM) is introduced in Chapter 6. The strength of this model is that it can estimate the temporal formation of SOA mass concentration throughout a chamber experiment, given only the initial hydrocarbon and NOx concentration. The model was developed for isoprene photooxidation chamber experiments and was able to represent the time that SOA became detectable in the chamber (defined as the time when the SOA diameter was

greater than 12 nm) and the maximum aerosol concentration produced by the experiment. The model was also applied to α-pinene chamber experiments with satisfactory results.

Due to the variation in experimental conditions/set-up of chambers from laboratory to laboratory, it is not recommended that SOAPEM be applied directly to other laboratories' chamber data. The concept underlying the model, however, could easily be adopted by other laboratories. The model is presented as a very different approach to modelling SOA. In the context of air pollution studies, if a number of chamber experiments were undertaken with a mixture of hydrocarbons representing the hydrocarbon burden in ambient air, SOAPEM could provide a platform to predict the SOA profile of further experiments in addition to providing a maximum aerosol mass concentration of SOA for those conditions modelled.

Chapter 7 similarly introduces an SOA module that has been designed to be coupled to The Air Pollution Model (TAPM). TAPM is the most widely used 3D air quality model in Australia and New Zealand and is favoured by consultants and government departments undertaking environmental impact assessments. The module relies on an emissions inventory, meteorology and Carbon Bond 99 mechanism embodied within TAPM to produce spatial estimates of SOA mass.

The SOA module described in this chapter incorporates SOA formed from six groups and individual species dominant in the ambient environment, namely paraffins, olefins, toluene, xylene, isoprene and terpenes. The Odum model is applied in the SOA module to estimate the product yields and partitioning characteristics of the products derived from the reaction of the six hydrocarbons with the dominant oxidant. In line with the findings from the work presented in Chapter 5, the model's products are theoretical products whose parameters characterize the whole of the system rather than actual products. A portion of the SOA is retained in the module between time-steps to represent the condensed phase oligomerisation reactions (Morris et al., 2006). Spatial estimates of $PM_{2.5}$ and SOA produced from the photooxidation of isoprene, terpenes

and olefins are distributed across the Greater Melbourne study area. The SOA module is a first version of development and it is expected that further stages of development will include the addition of hydrophilic SOA formation routes. The constant oligomerisation rate used in the SOA module also warrants further investigation, since the SOA module responds with sensitivity towards it.

Chapter 2: Air Pollution, Aerosols and SOA

2.1 Air Pollution

Air pollution is an issue that Londoners have known for centuries. Bad air quality was known to affect human health from as early as the 12th Century when English royalty, Queen Eleanor of Provence and Henry II's wife, Eleanor of Aquitaine were reported to have fled from their residences during periods of 'unendurable' air pollution. The word 'smog' was coined by London residents as air pollution was an inevitable part of day to day life illustrated by the Shakespearean play Macbeth, in which the three witches chorus "Fair is foul, and foul is fair: Hover through the fog and filthy air". In 1306, Edward I forbad the burning of sea-coal in London: infringement meant the death penalty, and so the first recorded 'air quality' law was passed (Urbinato, 1994). In 1661, the scientist John Evelyn wrote "Fumifugium, or the Inconvenience of the Aer and Smoake of London Dissipated" that proposed remedies for London's air pollution including the tending of large public gardens and parks. And so the first act of air pollution management was proposed.

Despite the attention that air pollution issues raised, in early December, the Great Smog of 1952 descended over London. Because of the cool air, Londoners began to burn more coal than usual, the cool air acted as an inversion layer and trapped in the smog. Over the following six days, more than 4,000 people died, and 8,000 more died in the following months, mainly from respiratory tract infections caused by mechanical obstruction to the airways. As a result of the Great Smog of 1952, the Clean Air Acts of 1956 were enacted to ban black smoke and dirty fuels in industry (Camps, 1976)

In addition to aerosols, gas phase air pollutants and air toxics are also of concern to government authorities because they too, pose health risks to the public and can negatively impact on the environment and natural earth systems. Most governments have mitigation policies in place to regulate and monitor the concentration of air pollutants like ozone, nitrogen dioxide, carbon monoxide, sulfur dioxide and air toxics including dioxins, benzene, lead and other metals.

The National Environmental Protection Council (NEPC) of Australia is currently appraising a national environmental protection measure (NEPM) for atmospheric concentrations of $PM_{2.5}$. NEPM standards are currently in place for the larger size particulate matter less than 10 μm (PM_{10}) and other non-particulate air pollutants. The goal in Australia is that by 2008 an average of 0.05 mg/m^3 over 24 hours would be exceeded a maximum of 5 days per year. The NEPC has estimated that the health benefit of meeting this goal would be about $4 billion. Because this thesis is primarily concerned with aerosols, an account of air quality policy in reference to the (gaseous) air pollutants and air toxics will not be included.

2.2 Aerosol

2.2.1 Aerosol types

As defined by Finlayson and Pitts (2000), aerosol may be of a solid or liquid phase and vary in size from 0.002 to 100 μm. 'Aerosols' differ in definition from 'particles' in that they are either solid or liquid particles suspended in a gas, whereas particles are only in the solid phase. They can be either emitted directly into the atmosphere as primary aerosol (such as sea salt, dust, etc.), or formed in-situ from chemical reactions occurring in the atmosphere, which are referred to as secondary aerosol. Secondary aerosols that have an organic compound are referred to as secondary organic aerosol (SOA). Sulfates and nitrates derived from photochemical reactions occurring in the atmosphere are examples of secondary inorganic aerosols.

SOAs are formed from the photodegradation of volatile organic compounds (VOCs) in the atmosphere. VOCs can be released from man-made sources such as, vehicles and industry which are referred to as anthropogenic sources. Similarly, VOCs can be emitted from vegetation in which case they are referred to as biogenic emissions. Chung et al. (2000) found that more SOA is produced from biogenic sources than from anthropogenic sources. Atmospheric aerosols can have a concentration of up to 10^7 to 10^8 particles/cm^3 (Seinfeld and Pandis, 1998, p408). Griffin et al. (1999) estimate the total emission of atmospheric aerosol to be about 6000 Tg/yr. Six general groupings of

aerosols exist: dust, sea salt, elemental carbon (soot), organic carbon, sulfate, and nitrate aerosols (Lack, D. 2003, p10). The organic carbon group comprises primary organic emissions (like aromatics from combustion sources), biogenic primary sources (pollens, spores) and secondary organic aerosol (from biogenic and anthropogenic emissions).

A typical composition of atmospheric aerosol with a size fraction less than 10μm in diameter consists of about 18% elemental carbon, 20% organic carbon, 6% nitrates, 17% sulfates, 6% ammonium, 2% chlorides and 30% dust and salt (Lack, D. 2003, p 10).

2.2.2 Impacts of aerosols

Human Health Impacts

Worldwide today, more deaths are attributed to air pollution than to automobile accidents (WHO and World Bank, 2004). The World Health Organization reports that reliance on solid fuels, including coal and biomass fuels for cooking and heating, is still a reality for more than three billion people worldwide. As a result, the 'World Health Report 2002' states that 2.7% of the global burden of disease and 4.6 million deaths per year can be attributed to indoor air pollution. In more developed countries, a strong dependence on burning fossil fuels still exists. A push towards renewable and 'green' energy technology is emerging as the impact of burning fossil fuels, particularly realized through climate change scenarios, are becoming more widely accepted. In Australia, about 2400 deaths are attributed to air pollution each year (CSIRO, 2004). In urban Australia, the estimated health cost resulting from exposure to air pollution is calculated to be between $100/kg and $300/kg of particulate matter (Robinson, 2005). To place these costs in context, a typical wood-heater releases about 20 kg of emissions annually, which places the health costs at $2000 to $6000 annually per heater.

A good example of the effects of particulate pollution on public health occurred in Dublin. When the $PM_{2.5}$ pollution was reduced in 1990, there were 15.5% fewer respiratory deaths and 10.3% fewer cardiovascular deaths per year (Riessel, 2005).

Recent studies have reported that an increase in 10 $\mu g/m^3$ of PM_{10} over 24 hours can result in an increase in the daily mortality rate by 1% (Morgan, 1993). The NSW Department of Health estimated that during 1991-1996, in Melbourne, an increase of 1 $\mu g/m^3$ of $PM_{2.5}$ resulted in a 0.38% increase in all-cause deaths and an increase of 1.18% in respiratory deaths during that period (Simpson et al., 2000).

Other health effects linked to particulate pollution range from chest colds to heart attack, cancers and overall reduced life expectancy (Dockery et al., 1993). There is some debate regarding the impact of the actual composition of the particulates as to how they correlate with different types of illness and the severity of illness. The United States of America's Environmental Protection Agency (EPA) also monitors and reports on the concentration of particulates less than 1 μm ($PM_{1.0}$). An association between the size of the particulates and specific health effects has not been identified as yet.

Aerosols and climate change

Climate change refers to a statistically significant variation in either or both the mean state of the climate, or its variability over a prolonged period of time (Houghton et al., 2001). The Intergovernmental Panel on Climate Change (IPCC) attributes these changes to natural internal processes or external forcing, or to persistent anthropogenic changes in the composition of the atmosphere or land use (Houghton et al., 2001). Collectively, the perturbation in the energy balance of the atmosphere is called climate forcing or radiative forcing. Radiative forcing is a measure of the change of heating rate (W m^{-2}) of the earth due to a specific atmospheric species and/or as a result of land-use changes or other events. A positive forcing indicates that there is more radiation absorption and (possible) global warming, whereas a negative forcing indicates a net atmospheric cooling. The Intergovernmental Panel on Climate Change (IPCC) 2007 Working Group 1 reports that aerosol forcing contributes -0.50 W m^{-2} to the overall energy balance, and that the effect from the post industrial increase in concentration of greenhouse gases is about 2.3 W/m^2.

All atmospheric aerosols can scatter and absorb radiation, thereby modifying the radiative balance of the atmosphere (IPCC, 2001). This phenomenon is referred to as direct aerosol forcing in which the particle composition influences the absorption and reflection properties of an aerosol. Fine aerosol (diameters between 0.1 and 2.0 μm) have sizes close to wavelengths in the visible, which have stronger climatic impacts than aerosol of a larger size per unit mass (Kanakidou et al., 2005). Aerosols can have a positive or negative net radiation forcing because they both scatter and absorb radiation to some degree. Carbonaceous particles are strong absorbers whilst sulfates are efficient scatterers and mineral dust is known to be mildly absorbing (M. Box, personal comm.).

Indirect aerosol forcing is a change in forcing by clouds due to the presence of aerosols (Pilinis et al., 1995). Cloud properties can be altered by an increase in the number of particles which act as cloud condensation nuclei (CCN). Hegg and Kaufman (1998) observe that the CCN diameters that are most relevant to indirect forcing were those greater than 0.1 μm.

Aerosols and visibility

Substantial concentrations of aerosols result in reduced visibility due to absorption and scattering of visible radiation. A reduction in visibility results in safety concerns in congested centres. Visibility issues may also impact on tourism expenditure which might have quite significant repercussions for a city/town dependent upon tourism. Another consequence of poor visibility is the blurring of satellite images which may impact on defensive and scientific endeavors.

A reduction in visibility also impacts on a community's quality of life by affecting aesthetics. The best way to illustrate the effect of aerosols on visibility is by observation. Figure 2.1 depicts a street scene in South Korea where the effect on visibility from air pollution is apparent.

Figure 2.1: Seoul, South Korea, 11am May 2002 (Photo courtesy of Dennys Angove)

2.3 Secondary Organic Aerosols

Hildermann et al. (1994) estimated that for a typical smog episode in Los Angeles, 40% of the total aerosol burden consists of secondary aerosol. Secondary aerosol is distinct from primary aerosol in that it is produced in-situ from chemical reactions occurring in the atmosphere. Secondary organic aerosol is a subset of secondary aerosols which have an organic or carbonaceous component. In the urban airshed, carbonaceous aerosol can account for up to 50% of the average annual $PM_{2.5}$ mass, and up to 90% of the total organic aerosol mass is estimated to consist of SOAs (Baltensperger et al., 2005). As determined from urban air studies, the types of SOA encountered are typically carbonyl compounds, nitrated derivatives, organic acids, phenols and aromatics (Hildermann et al., 1994).

2.3.1 The formation of SOAs

SOAs are formed in the atmosphere when a hydrocarbon initially degrades photochemically to produce semi-volatile compounds which can then partition between the aerosol and gas phase as shown in Equation 2.1.

$$HC + ox \xrightarrow{hv} P_1 + P_2 + ... \quad (2.1)$$

where *ox* is the primary oxidant which includes NO_3 the nitrate radical, OH the hydroxyl radical and O_3 which is ozone. P_1, P_2 ... are the products formed from the reaction.

The products produced in Equation 2.1 can undergo further reactions to form more condensable species adding to the net SOA yield of the system. Note that light is not essential in the case of the ozonolysis reactions where O_3 reacts with the HC to form condensable products. Many ozonolysis chamber experiments are undertaken in the dark to form SOA (Presto et al., 2005).

There are several SOA formation processes. Initially SOA is formed via a process of homogeneous nucleation. This SOA is often referred to as 'seed' aerosol or 'new particles' because the aerosol partitions directly from the gas phase to the aerosol phase. In this mode, aerosol can condense, or 'drop out,' given certain favourable conditions. This occurs when molecules in the parent compounds collide and form molecular clusters. When the system becomes saturated they reach a saturation concentration, and the amount of product that condenses is the quantity in excess of its saturation concentration (Odum et al., 1996). When no initial seed aerosol is introduced to the chamber prior to experiments, the gas phase concentration is required to become 'supersaturated' before SOA can drop out.

Another SOA formation process can occur once there is seed aerosol in the system. Once the organics have begun to condense, an organic layer can form on the surface of the particles through a process of absorption. Photooxidation products whose gas phase

concentrations are below saturation concentrations are able to partition onto an absorbing organic aerosol. This process can occur at low gas-phase concentrations. The main requirement for partitioning is that the condensable product is semi-volatile, that is, it has an intermediate to low saturation vapour pressure so that it can exist in both phases (aerosol or gas phase). These compounds are generally highly polar. This process is referred to as collective saturation and it occurs when an organic layer is established on particles without any species reaching gas phase saturation levels with respect to its pure liquid (Odum et al., 1997). This mechanism for SOA formation is often referred to as 'heterogeneous nucleation'.

Coagulation is an important process and occurs when SOA sticks together to form larger particles. This process can be observed when the particle numbers monitored in the chamber suddenly decrease but the particle volume is detected to continue to increase. When viewing SMPS data, the aerosol population migrates along the particle diameter size and the growth of particles is observed. This can be attributed in part to coagulation.

A third formation process occurs via condensed phase reactions to form oligomers. Baltensperger et al. (2005) defines an oligomer molecule as being distinct from a polymer on two scores: oligomers do have a similar structure to a polymer, in that it comprises a repetitive series of small molecular units that combine to form a compound of intermediate molecular mass, whereas polymers are regarded as having high molecular mass. The second main difference is that the removal of a single structural unit will have a negligible effect on a polymer compound, but will change the properties of an oligomer.

Condensed phase association reactions forming polymers and oligomers have been detected for several species (Jang and Kamens 2001; Baltensperger et al., 2005; Dommen et al., 2006; Surratt et al., 2006). Gao et al. (2004) studied oligomer formation for seven different hydrocarbon systems and found oligomers present in aerosol samples

regardless of the initial particle acidity. They speculate that oligomer formation is a ubiquitous phenomenon in ambient aerosol.

Several oxidation steps may be involved in the formation of some SOAs (Böge et al., 2006). Kroll et al. (2006) identified that almost as much SOA is produced from the photooxidation of isoprene as is produced from the photooxidation of methacrolein, which is one of the dominant primary products of isoprene photodegradation. An isoprene chamber experiment will therefore produce SOA from the isoprene system as a whole, which will include the SOA formation from the primary and secondary oxidation products and so on. Böge et al. (2006) suggests that SOA may be produced from several oxidation steps.

Presto et al. (2005) compared the preference between the formation of new particles (homogeneous nucleation) or the absorption of a compound onto existing aerosol. In these experiments, two injections of α-pinene were introduced into a chamber. The second injection resulted in a minor increase in particle number, but a significant increase in aerosol mass, indicating the preference for condensable species to be absorbed onto an existing surface than to homogeneously form new aerosol.

The role of biogenic compounds

Biogenic compounds are the main precursors forming SOAs (Chung et al., 2000). Guenther (1995) estimated that total hydrocarbon emissions of 1150 TgC/yr are emitted from biogenic sources and 98 TgC/yr from anthropogenic sources. Of the biogenic sources, 500 TgC of isoprene is emitted annually (Guenther, 1995). Due to the sheer volume of isoprene emitted, its aerosol forming potential has become a topic of interest. As other biogenic compounds are being discovered and their aerosol forming potentials determined, it is becoming more apparent that the net potential for aerosol formation from biogenic compounds can be significant from an air pollution perspective.

Until recently, isoprene was not considered to produce significant amounts of SOA (Pandis et al., 1991). The actual SOA formation mechanism produced from isoprene photooxidation has been the subject of a number of recent papers, and includes laboratory synthesis studies, chamber sampling analysis, and mechanism modelling (Limbeck et al., 1996; Claeys et al., 2004a; 2004b; Edney et al., 2005; Matsunaga et al., 2005; Kourtchev et al., 2005; Ion et al., 2005; Wang et al., 2006; Surratt et al., 2006; Kroll et al., 2006; Dommen et al., 2006). Some of the dominant ambient biogenic hydrocarbons that are important producers of SOA are illustrated in Figure 2.2.

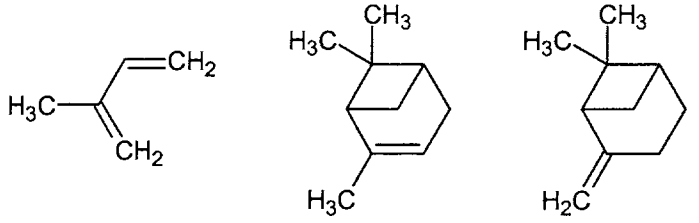

(1). Isoprene (2). α-pinene (3). β-pinene

Figure 2.2: Some of the dominant SOA precursor biogenic compounds found in ambient air.

2.3.2 Analysis of SOAs

Field studies

Due to their partitioning characteristics, it is all but impossible to measure the mass concentration of SOAs directly through ambient measurement. A condensable organic compound could occupy either a gas or aerosol phase depending on the ambient conditions, and so a sampling program one day may collect aerosol from a range of compounds that would not exist in the aerosol phase the following day, if the ambient conditions were different. For example, a slight temperature increase would cause a change in results, since the degree of partitioning from gas to aerosol is temperature dependent (Odum et al., 1996; Hoffmann et al., 1997).

Another limitation on field sampling is that many SOA compounds have not been identified. For example, a component of $PM_{2.5}$ often collected from field sampling is

referred to as a 'humic-like substance', because its identity and origin have not been determined (Limbeck et al., 2003). $PM_{2.5}$ samples often collect SOAs in addition to primary aerosols and other secondary materials. In recent years, components of the $PM_{2.5}$ sample have been identified as comprising species known to be SOA, but this is still a minor fraction of the total sample (Claeys et al., 2004b)

As analytical chemistry techniques have evolved, a larger fraction of the $PM_{2.5}$ sample can be identified although their origins are still tentatively determined. Recently, the combination of environmental chamber photo-oxidation studies and $PM_{2.5}$ monitoring have identified common species like tetrols and 2-methylglyceric acid. As a result, the list of known SOAs derived from various hydrocarbon photooxidation regimes is growing.

Laboratory analysis of SOAs

Laboratory studies of SOAs and their formation pathways are usually undertaken using environmental chambers which are often referred to as 'smog chambers'. There are many analytical chemistry techniques that identify and/or quantify groups of similar compounds. Some of the most commonly used methods for SOA identification and/or quantification are:

1. ElectroSpray Ionization – Mass Spectrometry (ESI-MS)
2. Matrix-Assisted Laser Desorption /Ionization (MALDI)
3. Nuclear Magnetic Resonance – Gas Chromatography Mass Spectrometry (NMR-GCMS).
4. Fourier Transform InfraRed spectrometry (FTIR)
5. High Performance Liquid Chromatography (HPLC)

Environmental chamber experiments

Environmental chamber experiments allow researchers to isolate photooxidation reactions that produce SOA. The decomposition of precursor compounds and products

can be monitored with a range of instruments, thereby allowing SOA formation pathways to be identified.

The influence of the physical and chemical parameters on SOA formation can also be evaluated using chamber experiments. Physical parameters like the intensity of the ultraviolet light, the relative humidity and temperature have been shown to have an influence on the amount of SOA formed in a given system. Many researchers also use additives like propene and aerosol seeds to speed up the reaction, however recent studies indicate that these additions do have direct and indirect effects on the chamber experiment. In a mixed system, Lack et al. (2003) found that the addition of propene (which does not form SOA directly), does contribute to the SOA mass concentration resulting primarily from the toluene/NOx system.

Two types of seed aerosol are generally used in chamber studies: ammonium sulphate and ammonium sulphate /sulphuric acid seed. Czosche et al. (2003) studied the influence of wet and dry seed aerosol on chamber experiments and found that wet acidic aerosol acted as a catalyst for heterogeneous SOA growth and formation. The yield associated with SO_2 experiments should similarly be considered cautiously, as recent work has reported that the uptake of glyoxal by the ammonium sulfate and mixed ammonium sulfate-sulfuric acid aqueous aerosol (introduced in seeded chamber experiments) can lead to the formation of low volatility, high molecular weight glyoxal adducts (Liggio et al., 2005). Since two of the oxidation products produced from isoprene are glyoxal and methylglyoxal, it is possible that some of the yield observed from isoprene photooxidation experiments has formed through this process, in an acidic pre-seeded environment.

Takakawa et al. (2003) found that an increase in chamber temperature resulted in a decrease in SOA formation since an increase in temperature resulted in an increase in the saturation vapour pressure. As mentioned earlier, a species with a lower saturation vapour pressure is able to more efficiently partition to the aerosol phase. Odum et al.

(1996) and Hoffmann et al. (1997) also found that the gas to particle partitioning was reduced at higher temperatures.

Seinfeld et al. (2001) theorized that increasing the relative humidity in dry (less than 5% relative humidity) systems in monoterpene systems should result in an increase in the mass of condensed matter and the amount of liquid water in the SOA phase, which favoured the formation of SOA. In contrast, Dommen et al. (2006) found that varying the relative humidity during isoprene photooxidation experiments had a negligible effect on the amount of SOA produced. The differences in these studies may be indicative of different SOA formation processes between systems.

Due to these variations, it is often difficult to compare experimental results from two different chambers. Although many air quality models depend on a common yield value for a species (which is considered to be the aerosol forming potential of a particular hydrocarbon), a standard experimental procedure that can be applied across laboratories has yet to be accepted.

The experiments presented in this thesis were undertaken at Lucas Heights Technology Park using the Commonwealth Scientific and Industrial Research Organisation's (CSIRO's) chamber, which is described in detail in Chapter 3. There are several chambers worldwide that contribute to SOA research. Some of these chambers and their predominant characteristics are featured in Table 2.1. They are listed in this section to provide a comparison with the CSIRO chamber. This will provide background for subsequent chapters in which results obtained by international groups are compared with CSIRO chamber data.

Table 2.1: International environmental chambers and their main features.

Name/location	Permanent or portable?	Dimensions (m x m x m)	Volume (m^3)	Special features (Reference)
CSIRO	Permanent	2 x 3.7 x 2.5	18	Low aerosol background. (Hynes et al., 2005)
EUPHORE, Valencia Spain.	Permanent			Outdoor dome structure. No need for artificial light source. (Skov et al., 1992)
Carnegie Mellon Institute, Pennsylvania	Non permanent		10	Chamber inside a temp. controlled room. (Presto et al., 2005)
CE_CERT Bourns College	Permanent		2 x 90	Temp. controlled room, chamber collapses progressively during expt to maintain pressure. (Song et al., 2005)
Toyota Central Labs, Japan	Non permanent	1 x 2 x 1	2	Temperature controlled room. (Takakawa et al., 2003)
Chapel Hill North Carolina	Permanent	9 x 12 x 6	320	Outdoor triangular structure. Mixing fans within chamber. High RH% (45-100%). (Kamen et al., 1999)
Caltech, California Institute of Technology.	Moveable framework with twin collapsible chambers		2 x 28	2 light sources argon ARC and blacklight. Temp controlled. Experiments undertaken at ~20°C and 40 - 50% relative humidity. (Kroll et al., 2005)
Paul Scherrer Institut, Villigen, Switzerland	Permanent		27	4 xenon arc lamps. (Dommen et al., 2006)

2.3.3 Modelling of SOA formation and quantities

Computer models have been developed to either predict the mass of SOA produced in the ambient environment, or to map the formation routes and to identify possible species involved in the formation of SOA. Examples of both of these models are presented in this thesis.

Most models depend on the concept of 'yield', which is the ratio of the amount of SOA formed from a chamber experiment to the amount of hydrocarbon consumed in the experiment. In this context, the yield is often considered to be a constant value specific to a hydrocarbon and identifies the aerosol forming potential of that hydrocarbon.

The SOA model that is most often incorporated into air quality models is the equilibrium absorption partitioning model developed by Odum et al. (1996). The Odum model is widely used to determine properties of two or more theoretical products. The main assumptions behind the Odum model are that at equilibrium, the condensable products behave as quasi-ideal solutions and the degree of partitioning that occurs between the gas and the aerosol phase is a function of the saturation vapour pressure, molecular weight and activity coefficient of the product. The amount of aerosol partitioned from the gas phase in the Odum model is a function of the amount of aerosol in the system in addition to the product yield and the partitioning coefficient.

Many other models have been developed as extensions to the Odum model that incorporate physical variables like temperature and humidity (Takakawa et al., 2003; Griffin et al., 2000). Barthelmie and Pryor (1999) applied the Odum model as a six product model rather than as a two product model. The Hoffmann model is an extension of the Odum model that considers the amount of SOA produced by each of the oxidation reactions with the precursor hydrocarbon (Hoffmann et al., 1997). This model is, therefore, also an equilibrium absorption model and is based on the absorption mode of SOA formation like the Odum model.

Some 3D air quality models incorporate both a partitioning component to quantify the SOA concentration and a chemical mechanism to group and transport chemical species (Bowman et al., 1997; Strader et al., 1999). In these models, SOA can be produced explicitly by a species or by a lumped group of similar species.

The Master Chemical Mechanism (MCM) has been employed in this thesis to model the SOA formation pathways resulting from isoprene photo-oxidation. The MCM is a near implicit chemical mechanism that describes the detailed degradation of volatile organic carbon in an environment akin to the Earth's atmosphere (Jenkin et al., 1997). In this work, an SOA module is developed within the current gas-phase chemical mechanism which consists of 598 reactions and 185 species (Pinho et al., 2005). The main assumption behind the development of the isoprene mechanism and other non-studied species in the MCM, is that the kinetics and products of an unstudied reaction are assumed to be the same, by analogy, with a similarly structured species participating in a studied reaction (Jenkin et al., 1997; Saunders et al., 2003; Jenkin, 2004).

Airshed models often employ a combination of both mechanistic models and empirical models (like the Odum model) to determine SOA mass concentrations spatially. The Air Pollution Model (TAPM) is employed extensively within Australia to assess the environmental impact of new developments. An SOA module has been developed and is presented in this thesis to couple to TAPM – CTM modeling system which consists of a prognostic meteorological model and a chemical transportation module (CTM).

One limitation of the current models employed in airshed modeling (including the TAPM-CTM model) is that they all assume that the net SOA mass of the atmosphere will be the sum of the individual SOA masses produced from a hydrocarbon (or group of hydrocarbons if lumped). Odum et al. (1997) found that adding the yields determined from individual chamber experiments was equal to the net yield returned from a chamber experiment with a mixture of hydrocarbons. This is the case when the absorption of SOA is considered in isolation. Lack et al. (2003) found that although propene did not produce SOA in its own right, when added to another system, it

increased the mass of SOA produced in the chamber. One reason for this finding might be that condensable products were formed in the propene system but have not reached a critical diameter so cannot 'drop out' from the gas phase. When the propene system is combined with the toluene system, seed aerosol may be formed from the toluene system which acts as a surface onto which the propene condensable products are able to condense. As Odum et al, 1997 specify, a condensable product does not need to reach a critical saturation to be adsorbed onto the surface of another aerosol species. In this case, the net SOA mass concentration is a reflection of both of these systems, however the yield returned from the combined system is not the sum of the yields returned by the individual systems (which would be zero for the propene system). It is also possible that the binary system of propene and toluene produce SOA via a very different mechanism to that of toluene or propene. Another explanation for this observation may be that the added SOA mass concentration formed in the binary system may be a result of oligomerisation rather than partitioning.

Chapter 3: Experimental Set-up and Data Analysis

3.1 Chamber Facility

All experiments presented in this thesis were performed within the indoor chamber facility located at the Commonwealth Scientific and Industrial Research Organisation's site at Lucas Heights. The chamber description, preparation and associated instrumentation have been discussed previously by Angove et al. (2000) and by Hynes et al. (2005). Since the chamber experiments are central to this thesis, a detailed account will be given in this chapter.

3.1.1 Environmental chamber description

The environmental chamber has a rectangular shape with a width of 1.98 m, length of 3.71 m and is 2.46 m in height. This amounts to a total volume of 18.1 m^3 and a surface area of 42.7 m^2. The chamber is supported by an aluminium frame and highly polished aluminium walls to maximise reflection. Internally, the frame is covered by a FEP Teflon skin (Dupont 3 mil (0.075 mm thick)). The light transmittance of the Teflon film has been further discussed by Hynes et al. (2005).

An external ultraviolet (UV-A) lighting module of forty blacklight tubes (36W Sylvania Blacklight Blue 350) is located at each end of the chamber, all tubes are fitted with a highly polished aluminium reflector. The UV tubes emit radiation over the range of 350 – 390 nm, with a peak intensity at 366 nm (Hynes et al., 2005). Each tube can be turned on and off individually, so that the amount of UV light can be controlled as required. The change in the internal chamber temperature is dependent upon the number of UV tubes that are turned on for a given chamber experiment. In the experiments presented here, only 50% of the tubes were used which resulted in a maximum temperature increase of 7°C. This occurred over the duration of a ten hour experiment.

Figure 3.1 shows an internal view of the smog chamber showing one of the two light modules which are mounted at either end of the chamber, and the input/output panels on either side.

Figure 3.1: Internal picture of the CSIRO's environmental chamber facility. (Photo courtesy of Dennys Angove)

The photolysis rate (J_{NO_2}) for the NO_2 conversion to NO and O_3, was used as a measure of the UV intensity. This was achieved by injecting a certified NO_2/He mixture (0.4% BOC Gases) and monitoring the NO, NO_2 and O_3 concentrations. J_{NO_2} was calculated using Equation 3.1:

$$J_{NO_2} = k_{NO+O_3}[O_3][NO]/[NO_2] \quad (3.1)$$

where the NO, NO_2 and O_3 concentrations (molecule cm^{-3}) are represented by the bracketed quantities and

$$k_{NO+O_3} = 1.4x10^{-12}\ e^{-1310/T}\ cm^3\ molecule^{-1} \quad (3.2)$$

where T is temperature in Kelvins (Atkinson et al., 2004).

Two external fans located underneath the chamber provide constant air movement across the external teflon surfaces, which in turn aids in the mixing of gases in the chamber. The two input/output panels located on the side of the chamber provide access to the chamber for instrument sample lines and sensors. The flow rates of reactant and carrier gases into the chamber are controlled by an external panel which houses twelve mass flow controllers (UCF 7300 series). A Binos dry calibrator was regularly used to calibrate the mass flow controllers and an uncertainty of 2% was determined. The flow

rates were also measured using the wet bubble technique at the commencement of experiments with the resulting flows found to agree with those measured using dry calibration. The flow rate calculated was corrected for temperature and vapour pressure according to the following equation:

$$flow\ rate = k\ \frac{P - \rho^{\circ}_{L}}{P} \tag{3.3}$$

where k is the measured flow rate, P is the ambient pressure and ρ°_{L} is the liquid vapour pressure of water at standard temperature and pressure.

A comparison between the wet calibration technique and the dry calibration technique for the mass flow controllers with the largest degree of error (MFC 5) on the chamber control panel is presented in Table 3.1. An average error of 13.5% was determined for this mass flow controller (MFC 5) based on this data.

Table 3.1: A comparison between flow rates obtained from the wet calibration method and the dry calibration method for a 100mL mass flow controller.

WET CALIBRATION			DRY CALIBRATION		
Anticipated Flowrate (mL/min)	Measured Flowrate (mL/min)	% error of MFC	Anticipated Flowrate (mL/min)	Measured Flowrate (mL/min)	% error of MFC
100	113.33	13.3	100	112.4	12.2
85	96.81	13.9	85	95.95	12.9
63	70.2	11.1	63	70.97	12.9
37	42.35	14.4	37	41.37	11.8
15	17.21	14.7	15	16.32	10.9
Average error		13.5			11.7

The measured flow rates for the wet and dry calibrations identified in Table 3.1 agree quite well in relation to the discrepancy between each of the measured flow rates and the expected flow rates. This result may cast some doubt on the method of determining the expected flow rate but will not have an impact on the experimental data presented in this thesis. The mass flow controllers in these experiments were only used to import NO and NO_2 which were monitored with chemiluminescence.

The primary hydrocarbon reactants used in the smog chamber experiments were isoprene (99+% purity, Aldrich Chemicals) and alpha pinene (99+%, Aldrich Chemicals). The makeup gas used to replace the air removed by instruments whilst sampling was highly purified air obtained from the zero air plant. The carrier gas used was scrubbed reticulated N_2 (Linde gases).

A block diagram of the chamber laboratory at CSIRO, Lucas Heights site is presented as Figure 3.2. During the period of this study, the FTIR system was upgraded from an external 31.5 m (white) cell through which air was extracted at a flow rate of 7.5 mL/min, to an internal cross-chamber long path system. The FTIR upgrade involved placing retro-reflectors on either side of the chamber so that the infra-red path-length was extended to 148 m. Apart from improved sensitivity, the in-situ mirrors have reduced sample flows significantly because the sample air is analysed in-situ in the chamber rather than being extracted as in the previous system. This has allowed the experiments to run for up to 16 hours without requiring input zero air to keep the chamber inflated.

CSIRO's Zero Air Supply

Zero air is purified air that has been supplied by a zero air plant (ZAP) located on the floor directly above the chamber. It can be fed into the chamber via the muffler system located on the laboratory wall near the chamber. The reactant and carrier gases are located outside the building and fed via tubing to the control panel where they are directed to the instruments or the chamber, as required.

Expected page number is not

in original print copy

3.2 Instrumentation

Ozone Analyser

Ozone was measured using an API 400 UV Photometric Analyser which has been calibrated against a California Air Resources Board certified O_3 primary standard (Hynes et al., 2005). The analyser is calibrated prior to each experiment by measuring against an O_3 generator which is set to a concentration dependent upon the experimental requirements. As an example, calibrations taken two and a half years apart are presented in Figure 3.3.

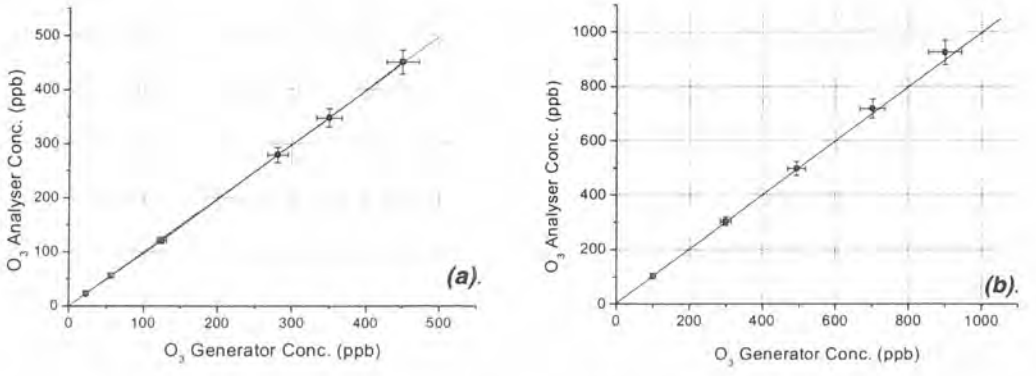

Figure 3.3: Comparison of ozone calibrations – February 2004 (a) and August 2006 (b).

The accuracy of the ozone analyser is regularly maintained and monitored. A comparison between calibrations made in February 2004 and those made in August 2006 indicate that the ozone analyser has maintained a high level of consistency during this period. The consistent performance of the ozone analyser provides some support for the estimated 5% error associated with the ozone measurements.

Chemiluminescence Analyser

NO and NO_2 were measured using a Monitor Labs 9841B Chemiluminescence Analyser (NOx). Unlike NO, NO_2 measurements cannot be determined directly by the analyzer. The analyzer groups all NOx species as NOy, where:

$$NOy \equiv NO + NO_2 + HNO_3(g) + PANs + \text{some organic nitrates.}$$

NO_2 can be estimated as NOy – NO, assuming that NO and NO_2 are the only NOx species present. In this work, the NO_2 concentrations reported are supported by FTIR analysis. The chemiluminescence analyzer was calibrated prior to each experiment with a certified NO/N_2 mixture (1.09 ± 0.05%; BOC Gases), precision diluted by N_2 via the gas panel. Representative calibrations are given in Figure 3.5 for different gain settings. Gain settings are used to determine the level of sensitivity of the photomultiplier tube (PMT) which consists of a cylindrical container, into which emitted light due to chemiluminescence enters. It was determined that a larger gain setting resulted in a larger calibration error as observed in Figure 3.4, and so gain settings for these experiments were less than 6.0. The error associated with chemiluminescence measurements is estimated to be at most 5%.

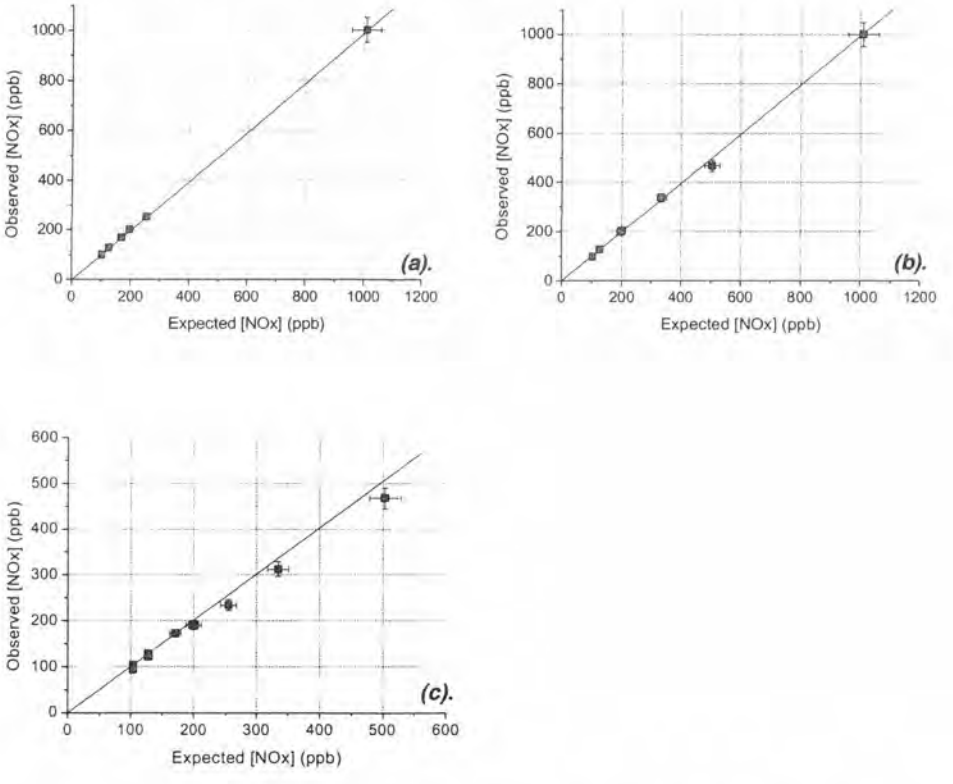

Figure 3.4: The effect of the instrument gain variable on the NOx calibration at gain settings of 5.594 for *(a)*, 6.396 for *(b)* and 6.677 for *(c)*.

FTIR Measurements

NO_2 concentrations were also measured using FTIR. A comparison between the chemiluminescence analyzer and FTIR measurements is presented in Figure 3.5 for experiment E203, in which the initial NO concentration was 92ppb and the initial NO_2 concentration was 2ppb. There is good agreement between the FTIR and chemiluminescence analyzer for the NO_2 concentration until it reaches a peak concentration of about 80ppb. The chemiluminescence trace plateaued while the FTIR determined NO_2 concentration declined. This occurred because the FTIR measured only NO_2 unlike the chemiluminescence analyser which measured NOy-NO (as discussed earlier).

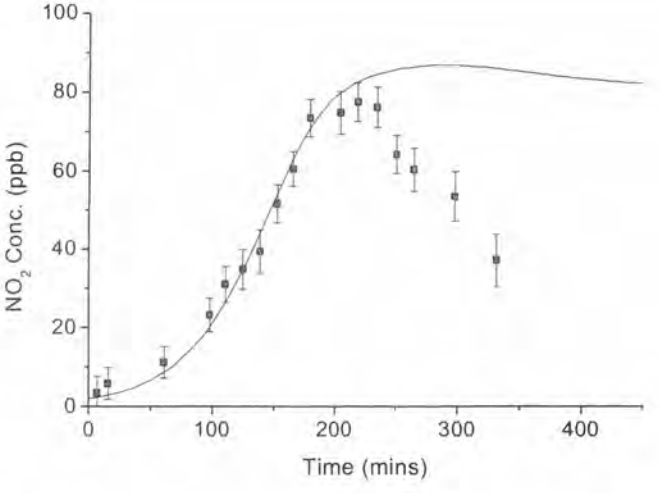

Figure 3.5: A comparison between the NO_2 concentration monitored during E203 by FTIR (symbols) and by the chemiluminescence analyzer (line).

FTIR was also used to measure the degradation of isoprene and α-pinene concentrations in addition to the formation of their oxidation products during chamber experiments. Two of the major isoprene photooxidation products, methyl vinyl ketone (MVK) and methacrolein were not detectable during the first set of experiments due to their low concentrations and the FTIR detection limits. Once the FTIR system was upgraded,

both MVK and methacrolein were detectable because the pathlength of the cell was extended from 31.5 m to 148 m. The cell was mounted on a Nicolet Magna 550 spectrometer fitted with a MCT detector. Spectra were obtained at a resolution of 0.25 cm^{-1} and 64 scans, with some experiments at 512 scans to ensure that necessary detail was not missing from the lower resolution scans. For the second tier of experiments using the in-situ white cell FTIR, spectra were obtained at a resolution of 1 cm^{-1} and 512 scans, where no gas extraction was required. The same spectrometer and detector were used with the long path mirror set.

Isoprene calibration spectra were obtained by injecting known concentrations of isoprene into the chamber with the lights turned off. Figure 3.6 shows a typical isoprene calibration spectrum. A comparison of the reference spectrum obtained in this study with that supplied by EUPHORE is given in Figure 3.7. The calibration plots produced for the CSIRO and EUPHORE reference spectra are presented in Figure 3.8. The absorbance height of the peak at 893 cm^{-1} is used as the comparative feature.

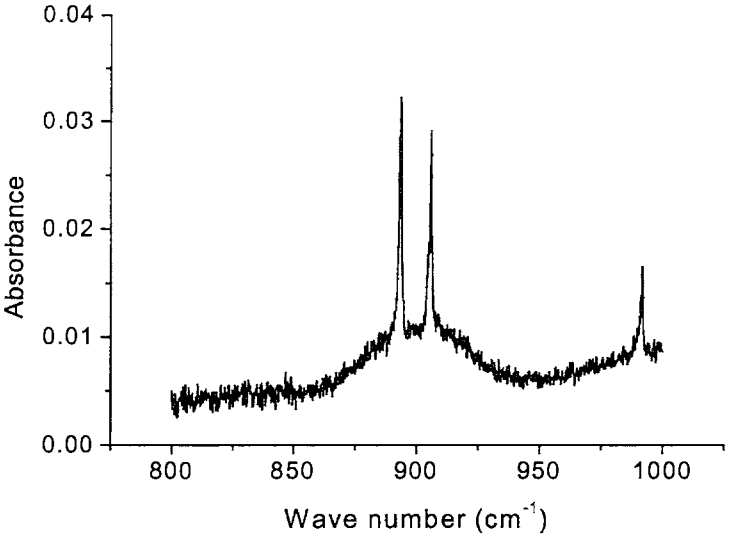

Figure 3.6: CSIRO Calibration Spectrum for 1010 ± 27 ppb of isoprene.

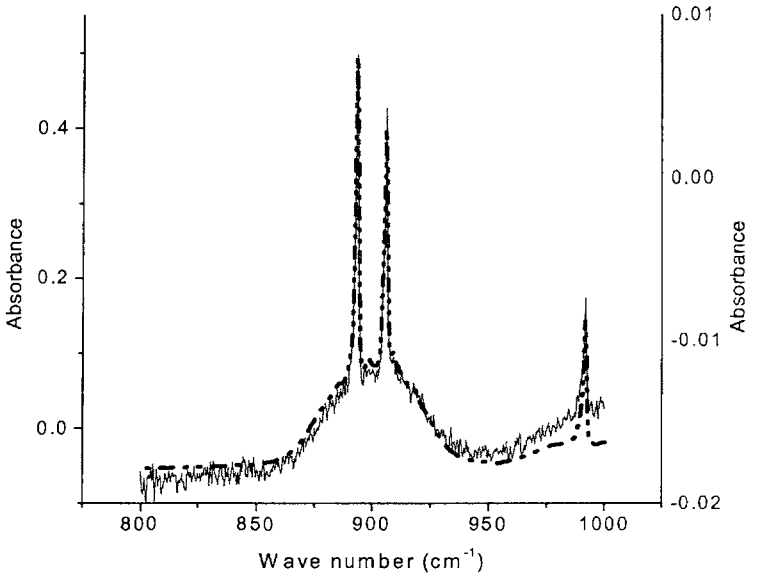

Figure 3.7: FTIR reference spectra for isoprene obtained from CSIRO (solid line) and EUPHORE (dotted line) chamber runs. Note that the spectra are for different concentrations.

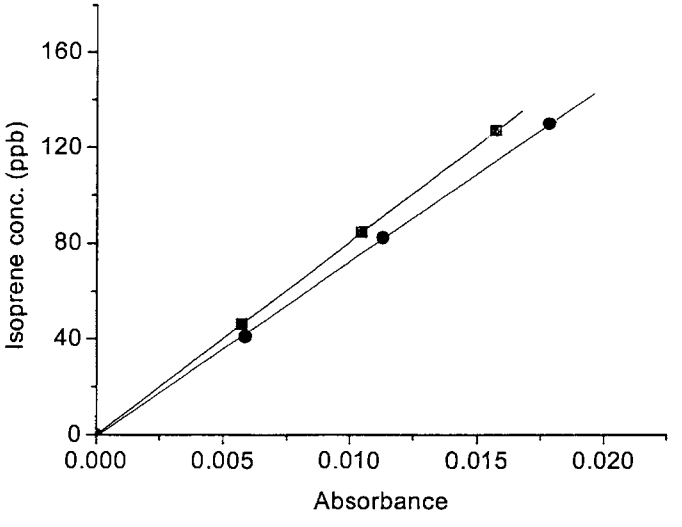

Figure 3.8: CSIRO (black diamond) and EUPHORE (blue square) calibration plots for the isoprene peak featured at 893 cm^{-1}.

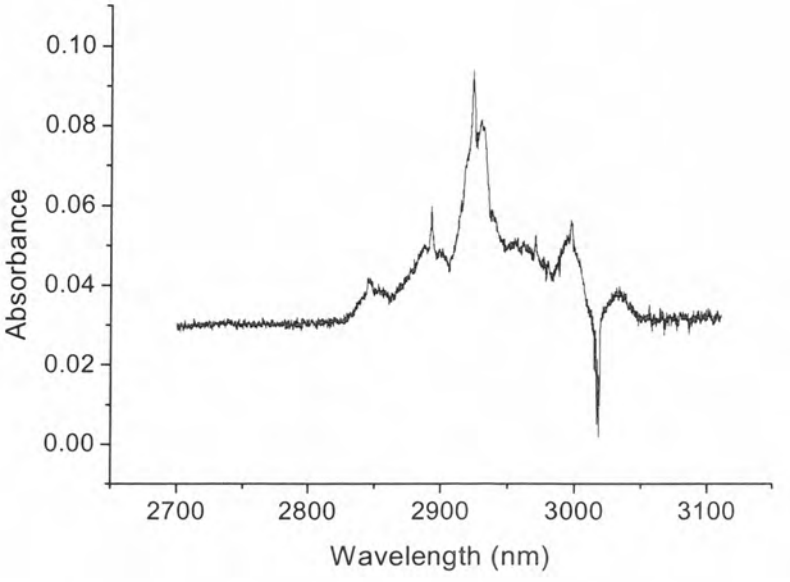

Figure 3.9: The calibration spectrum for α-pinene concentration at 367 ± 2 ppb.

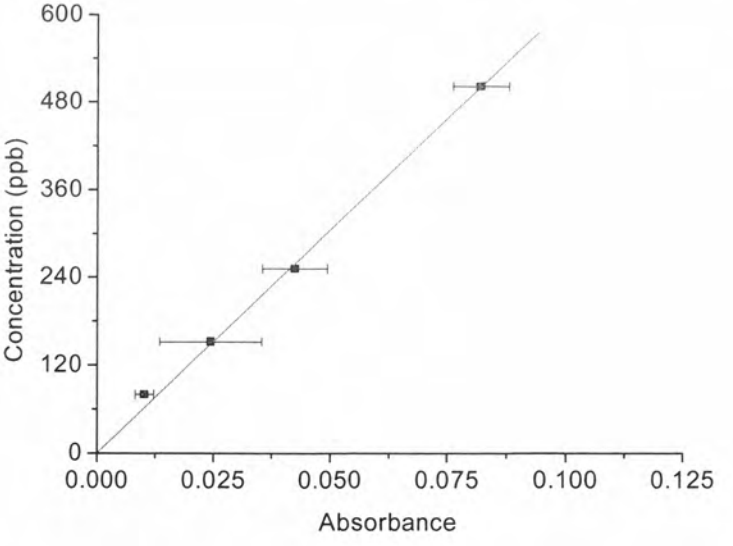

Figure 3.10: The α-pinene calibration plot.

Calibration spectra were also obtained for α-pinene following the method described for the isoprene spectra. A typical calibration spectrum is presented in Figure 3.9 and the α-pinene calibration plot is presented as Figure 3.10. The concentration of isoprene or α-pinene at various times throughout an experiment was determined from the absorbance values obtained from the FTIR spectra using an application of the Beer Lambert law:

$$A = \varepsilon c l \qquad (3.4).$$

where A is the absorbance, ε is the molar absorption coefficient (L mol^{-1} cm^{-1}) , c is the concentration (mol L^{-1}) and l is the cell path length (cm).

A comparison between the CSIRO and the EUPHORE isoprene reference spectra showed that the isoprene concentrations were within 5.5% with respect to peak area, and within 14.4% when using the peak height. Similarly, a comparison of the CSIRO and EUPHORE α-pinene spectra showed only a 6.4% difference based on peak area and 8.8% based on peak height. This comparison provides some further assurance of the accuracy of the CSIRO and EUPHORE isoprene and α-pinene reference spectra.

The errors associated with FTIR measurements are calculated for each measurement. They are determined as a ratio of noise in the spectrum to the absorbance of the feature in the spectrum and are, therefore, relative errors. The errors vary from 1 – 2% initially when features are large and increase up to about 33% when the feature being measured is almost undetectable and can be up to 3 times smaller that the spectral noise. The minimum detection limits for the FTIR system (post upgrade) are presented in Table 3.2. The minimum detection limit was identified as the concentration in which the associated error was at 33% or greater.

Table 3.2: FTIR detection limits.

Compound	Isoprene	*α- Pinene	MVK	Methacrolein	CO	HCHO
Conc. (ppb)	6	<40	12	8	6	6

* denotes prior to FTIR upgrade and where none of the experiments nudged the lower limits

SMPS Measurements

Aerosol number and volume concentrations were measured using a TSI 3071A Classifier and a TSI 3022A Condensation Particle Counter (CPC). To improve stability at high flow rates and at the low end cut-off, mass flow controllers were fitted to the classifier. This had the advantage of adding control in setting the excess, sheath and monodisperse flows. The detectable particle size ranges were 12nm to 670nm for isoprene and 27nm to 1000nm for α-pinene. For the α-pinene experiments, it is likely that the actual nucleation events were not observed. The aerosol was initially detected at around 12 nm for the isoprene system and at around 80nm for the α-pinene system.

The aerosol produced from the isoprene system was consistent in distribution for each experiment, with an almost log normal distribution profile observed. The TSI Classifier segments the aerosol into bins of equal log diameter ranges. The TSI manual specifies that the error attributed to the particle diameter is within 2% and that the concentration can be measured within 5%. The average aerosol diameter towards the end of an experiment (around 8 to 16 hours) converged at about 80 nm. The aerosol produced from the α-pinene system was much larger in size with mean aerosol diameters converging towards 1 μm at the end of an experiment (around 6 to 8 hours). The mass concentration of α-pinene derived aerosol was extrapolated assuming a log normal distribution for aerosol greater than 1 μm. A typical aerosol number profile for an isoprene experiment is depicted in Figure 3.12.

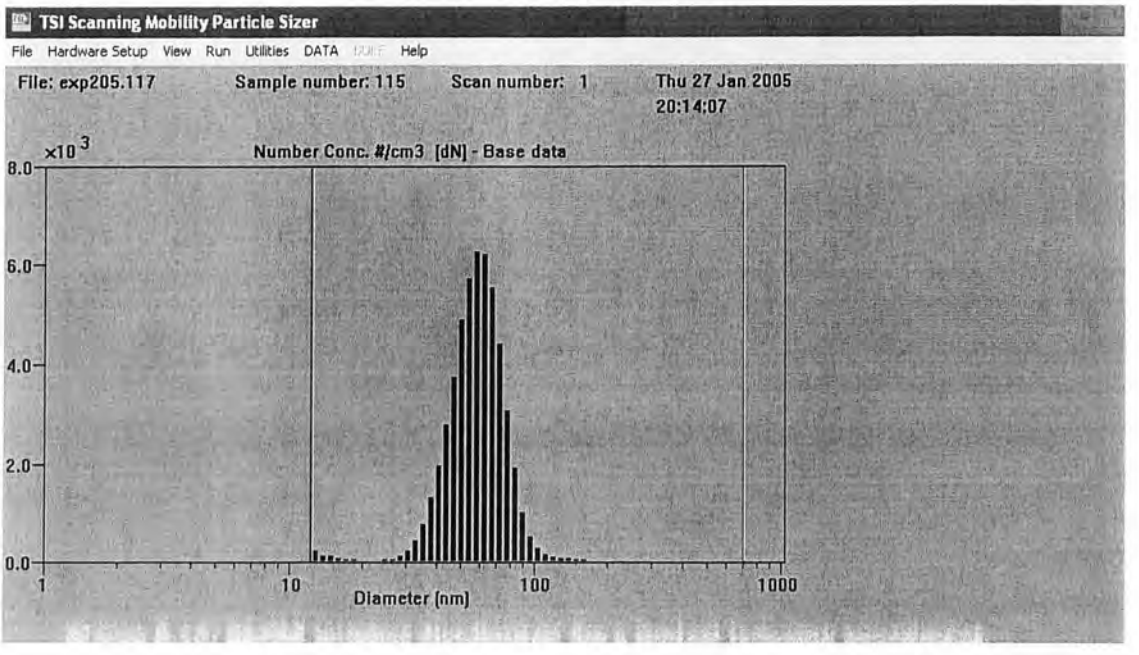

Figure 3.12: SMPS number distribution for a typical isoprene experiment.

3.3 Experiments

3.3.1 Experimental procedure

The same experimental procedure was applied to all of the experiments with the exception of the injection of the hydrocarbon. Prior to the commencement of each experiment, the chamber was baked for 10 hrs and flushed with purified air for two days. As a result, the background aerosol number and mass concentration was in the range of 0.0002 – 0.02 $\mu g/m^3$. The experimental procedure followed was to seal the chamber once the instruments had been calibrated and the chamber had been flushed with zero air. The two fans located underneath the chamber were turned on after the reactants had been injected into the chamber.

Different injection techniques were used for the α-pinene and isoprene experiments because the boiling point of isoprene (34 °C) was much lower than α-pinene (156 °C) and more likely to vapourise before being injected into the chamber. The introduction of isoprene into the chamber was performed by injecting a known concentration into a

clean glass bulb (flushed with N_2 gas) via syringe. The inlet to the bulb was then connected to a N_2 gas stream and its outlet was connected to the chamber. It was then heated very slowly to about 50°C to make sure that the reactant had completely evaporated. The sample line was then flushed with the N_2 carrier gas for 10 minutes to make certain that the entire hydrocarbon had entered the chamber.

In the case of the α-pinene experiments, the method used for the isoprene experiments was trialled. In this instance, the α-pinene had oxidised before being injected into the chamber, as precipitate appeared on the surface of the glass bulb. The injection technique adopted for the α-pinene experiments was to syringe the required quantity directly into the chamber through the import panel located on the side of the chamber. As described previously, the chamber was baked and flushed extensively after each experiment to remove any residuals in the chamber. Pre-experimental calibrations indicate that no contamination of the chamber resulted from this style of direct injection.

The required volume of NO was then injected into the chamber using the mass flow controllers on the control panel and monitored using the chemiluminescence analyser.
For each experiment, thirty minutes were allocated for the mixing of NO and hydrocarbon gases. The first FTIR spectrum was taken to ascertain whether the hydrocarbon concentration had reached the concentration required, and that the gases were mixed in the chamber. Another FTIR spectrum was then taken to check that the chamber concentrations detected by the first spectrum were consistent. The experiment commenced by turning on the UV lighting such that J_{NO_2} was at 0.41 min^{-1}. The photolysis rate chosen for all of the experiments (isoprene and α-pinene) was J_{NO_2} at 0.41 min^{-1} since it represented normal daytime radiation intensity (Seinfeld et al., 2001).

O_3, NO and NO_y concentrations were recorded at regular intervals of 1 minute. In the case of the FTIR measurements, they were initially collected at 15 minute intervals and then at 30 minute intervals towards the end of an experiment. The FTIR sample stream

was closed between samples in order to reduce the extraction of air from the chamber. In this set of experiments, makeup gas (zero air) was not introduced into the chamber until 400 minutes into the experiment. The duration of experiments varied according to the initial concentrations of the precursor gases and onset time of aerosol formation.

3.3.2 Schedule of experiments

The chamber experiments performed for this thesis at the CSIRO facility at Lucas Heights are presented in Table 3.3. The matrix identifies each experiment in terms of the initial precursor concentrations.

Table 3.3: Matrix of isoprene (I) and α-pinene (A) experiments presented in the thesis.

[HC] top [NOx]	0-20 ppb	21–50 ppb	51–100 ppb	101–150 ppb	150-200 ppb	201ppb +
0–20 ppb	I					
21–50 ppb		I	I, A		I	A
51–100 ppb			I		A, A	I, A
101–150 ppb			I		I, A, A	I, I
151–200 ppb						
201 ppb +			I	I, I, A,	I, A	I, A

The ambient concentrations of isoprene and α-pinene vary enormously depending on the location of the site. Ambient concentrations of isoprene in the United States have been measured between 1 and 21 ppb (National Health Institute, Report on Carcinogens, 2007). The focus of the experimental program was to try to make the precursor concentrations as close to ambient as possible. The limitation of un-seeded experiments at very low concentrations is that it takes a long time to reach nucleation. It is not possible to undertake sample gas extraction for the FTIR system during such a long experiment and using make-up gas to fill out the chamber is also not an option at such small initial precursor concentrations. Our initial FTIR set-up required sample extraction, which was the only method employed to determine isoprene and α-pinene concentrations and so it was necessary to do experiments with initial hydrocarbon

concentrations greater than ambient. With the FTIR upgrade, the FTIR detection limits were much lower and sample gas extraction was not necessary, which enabled a few experiments to be undertaken with low initial precursor concentrations.

The isoprene photooxidation experiments were undertaken in two separate programs about a year apart. The FTIR system was upgraded during this interval from short to long path. The experiments with the experimental number prefix of 2** were performed prior to the upgrade and those denoted with a 3** were undertaken after the upgrade. The main difference between the programs is that primary isoprene photooxidation products, methyl vinyl ketone and methacrolein, could not be detected in the first program but could be detected in the second program. Other products like NO_2 and HNO_3 could be detected in the first program but are not identifiable post FTIR upgrade due to strong interference by water vapour.

The α-pinene experiments were also undertaken in two separate programs in a manner similar to isoprene. The concentration of the α-pinene was the only hydrocarbon monitored by FTIR in both programs. The initial conditions for isoprene and the α-pinene photooxidation experiments are summarised in Table 3.3 and 3.4, respectively. The background aerosol concentrations are an average of the five preceding time steps before the experiment commences. The α-pinene experiments have on average a higher background aerosol mass concentration than the isoprene experiments. This is indicative of the larger aerosol sizes detected during nucleation, and hence the higher SMPS range setting used for α-pinene compared to isoprene.

Table 3.3: Isoprene Photooxidation Experiments.

Expt.	Initial $[C_5H_8]$ ppb	Initial [NO] ppb	Initial $[NO_2]$ ppb	ROC/ NOx	Temp. (°C)	RH % @~24°C	Backgrd. Aerosol ($\mu g/m^3$)
201	100	235	18	2.0	22.6	6.2	0.012
202	90	51	1	8.8	22.6	6.4	0.005
203	188	106	2	8.8	23.2	10.1	0.002
204	201	135	4	7.1	21.5	7.2	0.020
205	343	240	3	6.8	21.7	9.3	0.004
206	105	254	7	2.0	24.6	7.8	0.0002
207	188	255	6	3.5	21.8	7.2	0.155
210	128	251	8	2.5	20.9	7.4	0.007
211	16	20	1	3.8	23.2	6.1	0.001
303	257	105	0	11.3	21.0	6.5	0.001
304	73	34	1	10.6	23.1	5.8	$1x10^{-5}$
306	76	108	2	3.5	22.1	4.2	0.004
307	25	40	1	3.0	21.9	1.0	0.053
308	232	80	11	13.2	23.0	2.8	0.0001
309	153	44	0	14.4	22.7	3.4	0.002

Table 3.4: Photooxidation experiments for α-pinene.

Expt	Initial $[C_{10}H_{16}]$ ppb	Initial [NO] ppb	Initial $[NO_2]$ ppb	ROC/ NOx	Temp (°C)	RH% @~24°C	Backgrd Aerosol ($\mu g/m^3$)
230	203	241	3	8.3	22.5	7.2	0.009
231	192	245	8	7.6	21.8	7.6	0.018
232	166	98	0	16.9	21.0	6.6	0.019
233	134	241	4	5.5	21.8	7.0	0.340
235	167	98	0	17.0	21.1	6.6	0.688
236	205	114	3	17.5	21.1	6.6	0.390
237	79	50	3	14.9	21.8	6.4	0.303
311	225	55	0	40.9	21.2	5.0	0.039
312	172	89	0	19.3	21.5	5.6	0.034
313	173	140	2	12.2	23.4	4.0	0.169

3.4 Data Analysis

The raw data were smoothed as little as possible in order to preserve small fluctuations in aerosol numbers that may be significant. Once an experiment had been completed, concentrations of O_3, NO, NOy - NO and NO_y were returned from the ozone and NOx (chemiluminescence) analysers. Hydrocarbon concentration was determined from FTIR analysis.

Aerosol data were collected using the TSI SMPS software determination of number and volume concentrations for specific bin sizes. The aerosol mass concentration was calculated based on the assumption that all aerosol counted were spherical with a constant density. A density of 1.4 g/cm^3 was assumed when calculating aerosol mass derived from isoprene and α-pinene photooxidation (Stroud et al., 2004). Many researchers have previously used an arbitrary value of 1 g/cm^3 , Stroud's work focused on aerosol derived from oxidized aromatics. Although the structure of an aromatic is not similar to an isoprene compound, this density estimate is consistent with the conservative SOA estimates (as a worst case scenario). More recently, Surrat et al. (2006) determined a density of 1.25 g/cm^3 for aerosol formed from isoprene photooxidation chamber experiments. Number distributions returned from the CPC were ordered according to a median bin size. Volume and mass concentrations were then calculated once wall loss processes, which account for the Brownian motion and gravitational settling of particles 'sticking' to the chamber walls, were corrected for.

3.4.1 Wall loss corrections

The corrections for the loss of aerosol to the walls were applied to the number and volume distributions measured directly and indirectly by the classifier and condensation particle counter. Wall loss corrections based on the aerosol's diameter were calculated using a pseudo first order rate expression for aerosol mass concentration decay (Seinfeld et al., 2001):

$$dN(Dp)/dt = -\beta(Dp)N(Dp) \tag{3.5}$$

where N represents the number of particles, Dp the diameter of the particles and β is the loss rate coefficient. Loss of aerosol in each bin size is attributed largely to wall loss but can also be due to coagulation processes which are especially dominant in the smaller diameters.

In order to calculate β for each size bin, a number of assumptions were made:

1. The wall loss commenced once the peak of the number population (per bin) was observed.
2. The data range used to calculate β (for each bin size) started with the number peak and ended once three consecutive time points had particle numbers less than 0.5.

The loss rate coefficient, β, was determined by fitting Equation 3.5 to a plot of particle number versus time (sec) as shown in Figure 3.13. β were determined from the line of best fit for each individual bin size (Stroud et al. 2004).

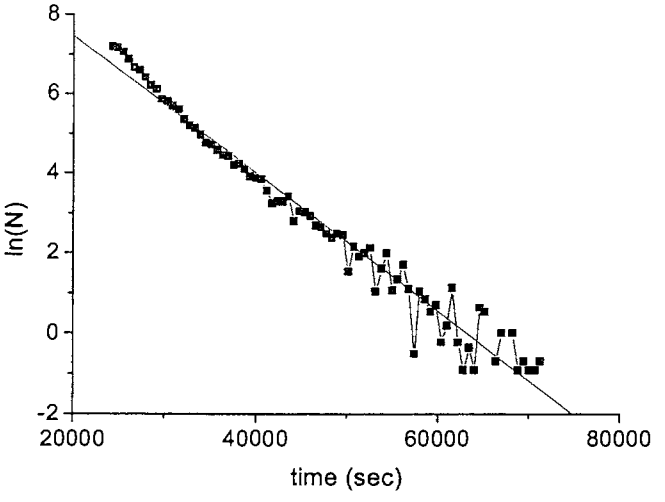

Figure 3.13: Ln(N) versus time (sec) for the experiment E52.

The constants a, b, c and d were determined by fitting the experimental chamber data plot of β against *Dp* to Equation 3.6 as depicted in Figure 3.14.

$$\beta(Dp) = a + b\exp\left[-0.5\left(\ln(Dp/c)\right)/d\right)^2] \quad (3.6)$$

where $\beta(Dp)$ is the loss rate coefficient for the bin size with diameter *Dp*

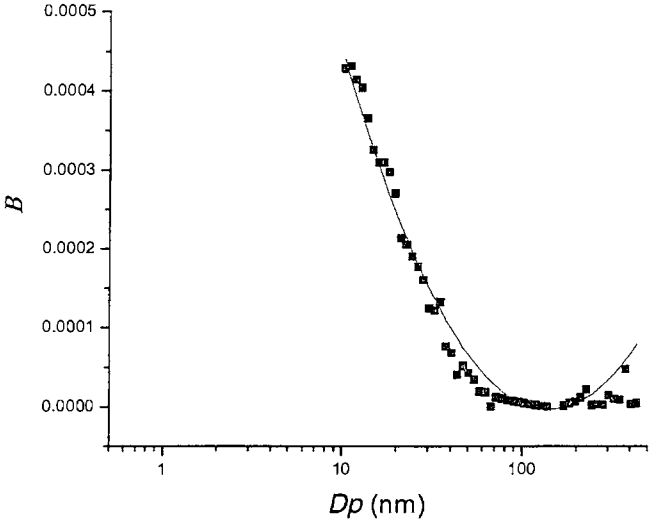

Figure 3.14: A fit of Stroud's wall loss equation to chamber data of E52.

3.4.2 Error estimation

Cumulative errors were calculated for all results: they included components of instrument errors, human error (experimental) and errors attributed to the assumptions made as detailed in Table 3.3. The cumulative errors associated with aerosol mass calculations from chamber experiments are calculated as 7% (TSI errors) plus 2% associated with the assumption that all aerosol is geometric and spherical, which results in an error of ± 9% of the aerosol mass concentration.

The mass flow controllers have mainly been used to regulate the input of NO, NO_2 and NOx in the experiments presented in this thesis. The error associated with the mass flow controllers (presented in Table 3.3) have not been incorporated in the data analysis

because the import of NO and NO_2 into the chamber was monitored by chemiluminescence and so errors are associated with this measurement only.

Table 3.3: Errors attributed to instruments, techniques and assumptions

Instrument/Lab technique/Assumption	*Estimated Error*
1. Ozone Analyser	5%
2. TSI Classifier - bin size association	2%
3. TSI CPC – number calculation	5%
4. Chemiluminescence	5%
5. FTIR – measurement	1 – 33%
6. Purity of hydrocarbons, NO, NO_2	1 – 2%
7. Injection of hydrocarbon – chamber	0.005 μL
8. Assumption – geometrically spherical aerosol	1%
9. Number of aerosol lost to the chamber walls (over corrected for coagulation)	2%
10. Time increment, 3 minute interval (measurements)	180 secs

O_3, NO, NO_2 and NOx measurements have an error of 5% each, whilst the initial NO, NO_2 measurements have a 1-2% error associated with purity. The initial hydrocarbon concentrations have an error of up to 2% relating to the purity of the compound plus an additional 0.005 μL error if the concentration required was syringed from the bottle. Once in the chamber, these errors are lost if monitoring with FTIR because the FTIR is a relative measurement. In order to measure a concentration by FTIR a calibration spectrum is required. If the same detail of care and the same technique is applied to the injection of the hydrocarbon (during the experiment as it was with the calibration), then this error will be consistent, and hence lost in a relative system. A yield calculation therefore embodies both errors associated with the mass concentration (9%) and with the consumption of the hydrocarbon (FTIR relative error). Similarly, an error of 2% has been assigned to SMPS data largely due to assumptions made about density and wall loss (which includes loss processes also due to coagulation) as discussed previously.

Chapter 4: Simulations of secondary organic aerosol formation during the photooxidation of isoprene using the Master Chemical Mechanism (MCM v3.1).

4.1 Introduction

Global biogenic emissions have been estimated to be approximately ten times more abundant than anthropogenic emissions (Guenther et al., 1995). Of the biogenic emissions, almost 45% of biogenic emissions are comprised of isoprene (Guenther et al., 1995). In North America, isoprene oxidation represents the dominant source of summertime ozone (Fan and Zhang, 2004). Environmental chamber studies of isoprene report SOA yields in the range 0.2 – 1.0%, depending upon initial conditions (Pandis et al., 1991; Kroll et al., 2005; Dommen et al., 2006). An estimate of the global isoprene emission rate (Guenther et al., 1995) is ~500 Tg/yr, resulting in the formation of up to 5 Tg/yr of isoprene-derived SOA, thereby making isoprene photooxidation a significant contributor to global SOA production. As such, SOA produced from the photooxidation of isoprene can be potentially significant in terms of global climate and human health effects.

Aerosol sampling has identified isoprenoid-like polyols and an acid species as major components of the ambient $PM_{2.5}$ (Limbeck et al., 2003; Claeys et al., 2004a and 2004b; Ion et al., 2005; Kourtchev et al., 2005). Laboratory synthesis studies and chamber photooxidation experiments have identified these species as 2-methylthreitol, 2-methylerythritol (which are stereoisomers of 2-methylbutan-1,2,3,4-tetrol and collectively referred to as tetrol) and 2-methylglyceric acid (Claeys et al., 2004a; Wang et al., 2005; Edney et al., 2005). Several formation pathways have been proposed for these compounds. Claeys et al. (2004) proposed that the diastereoisomeric tetrols were produced in the condensed-phase from the products C_5 1,2-diols and 1,4-diols. In a later study by Claeys et al. (2004b), the tetrol and 2-methylglyceric acid were synthesized by reacting H_2O_2 and H_2SO_4 in aqueous solutions with isoprene to form tetrol, and with methacrolein and methacrylic acid to form 2-methylglyceric acid. Edney et al. (2005) conducted chamber experiments using isoprene/NOx/air mixtures in both the presence

and absence of SO_2 and concluded that an acidic environment catalyses SOA growth. However, it is not essential for the formation of the tetrol and 2-methylglyceric acid (depicted in Figure 4.1).

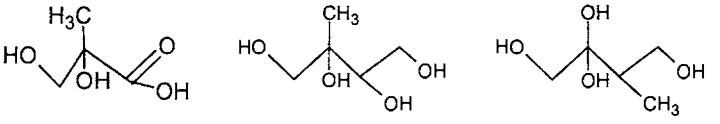

Figure 4.1: 2-methylglyceric acid and the stereoisomers of 2-methylbutan-1,2,3,4-tetrol (collectively referred to in the mechanism as tetrol) respectively.

Böge et al. (2006) found that the tetrols could also be formed from the C_5 1,2-diols in the gaseous phase and considered that this pathway is representative of low NOx conditions similar to those found in forested regions. Böge et al. (2006) suggested that the dominant pathway for the formation of tetrol is through the acid catalysed oxidation of isoprene to form the isomeric isoprene monoxides 2-methyl-vinyloxirane and 2(1-methyl-vinyl)oxirane in the gas-phase, which in turn react with H_2O_2 to form tetrol in the condensed phase.

Kourtchev et al. (2005) observed significant concentrations of ambient tetrol and 2-methylglyceric acid and hypothesised that the photooxidation of isoprene may participate in the early stages of new particle formation, particularly in the boreal forest environment. Angove et al. (2006) observed the formation of the tetrols, threitol and meso-erythritol, from the photooxidation of 1,3-butadiene, which has a similar molecular structure to isoprene, and proposed that these compounds were the endogenous seed species required for SOA formation in the butadiene/NOx system.

Oligomer formation has been observed in photooxidation experiments using initial isoprene concentrations of 500 ppb (Surratt et al., 2006) and 180 ppb (Dommen et al., 2006). An analysis of the composition of isoprene-derived SOA found that the main precursors for oligomer formation were formed from self-oxidation reactions of 2-methylglyceric acid and oxidation reactions of tetrol (Surratt et al., 2006). This

formation has not been represented in the following mechanism but would be the next logical step in the mechanism's development. Oligomers comprised of organic nitrates were identified in the above study but could not be quantified although they were identified as a likely SOA precursor. Similarly, hydroperoxides were also found to be a possible SOA precursor. In the low NOx experiments (<1ppb of NOx), Surratt et al. (2006) found that up to 60% of the SOA mass concentration was composed of peroxides. Surratt et al. (2006) state that hydroperoxides are expected to be the dominant gas phase species in the low NOx experiments; they also suggest that the hydroperoxides further participate in condensed phase reactions with aldehydic species to form high molecular weight species, like peroxyhemiacetals.

The high NOx experiments reported by Surratt et al. (2006) were initiated with NOx concentrations between 800-900 ppb. The CSIRO experiments presented in this chapter were performed with NOx concentrations in between these two scenarios and with significantly less isoprene (500 ppb of isoprene used in Surratt et al.,2006 work). Since the precursor concentrations are significantly different, the findings of Surratt et al. (2006) are applied tentatively to this work. Johnson et al. (2005) and Surratt et al. (2006) have both found that the initial NOx concentrations directly influence the SOA yield.

Previous studies have alluded to the occurrence of association reactions of organics in the aerosol phase (Tobias and Ziemann, 2000; Jang and Kamens 2001). Jang and Kamens (2001) observed that aldehyde functional groups could participate further in SOA formation in the aerosol phase via hydration, polymerisation and acetal/hemiacetal formation with alcohols. Heterogeneous reactions between carbonyls and hydroxylated carbonyls with the tetrol species threitol and meso-erythritol were proposed to form hemiacetal species in the 1, 3-butadiene system (Angove et al., 2006). Johnson et al. (2004) modelled the formation of peroxyhemiacetals produced from the reactions of aldehydes with hydroperoxides.

The aim of this study is to present a mechanism for SOA formed in the isoprene-NOx system. The approach reported by Johnson et al. (2005) for simulating SOA formation produced from the photooxidation of toluene has been adopted in this work. Initially gas/aerosol partitioning dynamics were introduced into the mechanism and as discussed in the Johnson et al. (2005) study, a large species independent scaling factor indicated that other SOA forming mechanism were required to be represented in the mechanism, like the condensed phase association reactions. Johnson et al. (2005) identified several potential association reactions such as the formation of peroxyhemiacetals (from the reaction of nitrated organics and aldehydes with hydroperoxides), hemiacetal/hemiketal formation, aldol condensation reactions and the polymerization of aldehyde species. In the work presented in this chapter, the formation of peroxyhemiactels is simulated from the reaction of several carbonyls / aldehydes and organic nitrates / PANS with hydroperoxides. An analysis of the simulated SOA composition at key times throughout the experiments is presented as a relative study that indicates that the initial precursor concentrations influence the composition of SOA which varies throughout an experiment. These observations are consistent with the findings of Johnson et al. (2005), Johnson et al. (2006) and Surratt et al. (2006).

The gas phase isoprene photooxidation MCM was developed by Pinho et al. (2005). The SOA formation routes were added to this existing mechanism once the gas phase mechanism was applicable to the CSIRO chamber experiments, which is discussed in the following section. The original gas phase mechanism was downloaded from the Master Chemical Mechanism version 3.1 (http://www.chem.leeds.ac.uk/MCM). Structural diagrams of each of the species identified in the mechanism are presented on the MCM website. As previously mentioned this work was produced as part of a collaboration*. A complete listing of the gas phase isoprene mechanism amended from Pinho et al. (2005) with the SOA formation routes is presented in the appendix (attached as a CD).

*Dr Sam Saunders from the University of WA identified the likely branching ratios and reaction rate coefficients of the SOA formation pathways using Structural Activity Relationships (SAR) calculations.

4.2. Experimental Details

Isoprene/NOx in air irradiations were performed in the 18 m^3 indoor environmental chamber located at the CSIRO laboratories in Lucas Heights, Australia. The chamber facility has been previously described in detail in Chapter 3. Table 4.1 summarises the initial conditions used for 12 non-seeded experiments and includes measured background and experimental aerosol mass concentrations.

Table 4.1: Initial conditions and precursor concentrations for the isoprene/NOx environmental chamber experiments.

Expt	C_5H_8 ppb	NO ppb	NO_2 ppb	ROC/Nox	Temp. (°C)	RH% at ~ 24°C	Max. Aerosol Mass Conc. µg/m^3	Background Aerosol Mass Conc. µg/m^3
E201	100	235	18	2.0	22.6	6.2	no SOA	1.2E-04
E202	90	51	1	7.8	22.6	6.4	*	5.0E-04
E203	188	106	2	8.7	23.2	7.0	*	2.0E-03
E206	105	254	7	2.0	24.6	7.8	no SOA	2.0E-04
E210	128	254	6	2.5	20.9	7.4	*	7.0E-03
E211	16	20	1	3.8	23.2	6.1	*	1.0E-03
E303	257	105	0	11.3	21.1	4.3	13.6	9.0E-04
E304	73	34	1	10.6	23.2	2.4	2.5	1.3E-03

* indicates that the maximum aerosol mass concentration was not reached.

Chamber dependent reactions were included in the mechanism as described by Hynes et al. (2005). The auxillary mechanism is presented in Table 4.2. For the isoprene mechanism, the most sensitive chamber dependent reactions were the $h\nu$ + wall → NO_2 and the NO_2 → 0.5 HONO + 0.5 wall – HNO_3 reactions listed in Table 4.2.

Table 4.2: Chamber dependent auxillary reactions from Hynes et al. (2005).

Reaction	Parameter	Upper/Lower limits
$h\nu$ + wall → OH	J_{NO_2} (0.0015) ppbv s^{-1}	J_{NO_2} (0.0075-0.0030) ppbv s^{-1}
$h\nu$ + wall → NO_2	J_{NO_2} (0.0015) ppbv s^{-1}	J_{NO_2} (0.0075-0.0030) ppbv s^{-1}
NO_2 → 0.5 HONO + 0.5 wall – HNO_3	$1x10^{-6}$ s^{-1}	(0.5-2.0) x $10^{6}s^{-1}$
N_2O_5 → 2wall-HNO_3	$1x10^{-20}cm^3molecule^{-1}s^{-1}[H_2O]$;	(0.1-10)x $10^{-20}cm^3molecule^{-1}s^{-1}$
	(0.3-1.8)$x10^{17}$molecules cm^{-3} @ 298K	
	for $[H_2O]$ = 1200-7400 ppmv	
Wall-HNO_3+$h\nu$→OH+NO_2	J_{HNO_3}	(0.5-2.0) J_{HNO_3}
HNO_3→wall-HNO_3	$1x10^{-4}s^{-1}$	(0.5-2.0)$x10^{-4}s^{-1}$
NO_2→wall	$2x10^{-7}s^{-1}$	(1.0-4.0)$x10^{-7}s^{-1}$
O_3→wall	$2x10^{-7}s^{-1}$	(1.0-4.0)$x10^{-7}s^{-1}$
$[HONO]_0$	Varied from 0.0-1.0 ppbv	

4.3 Model Development

4.3.1 Gas-phase isoprene/NOx photochemistry

The basis for the SOA formation mechanism is the Master Chemical Mechanism (MCM) v3.1, a near explicit chemical mechanism that describes the detailed degradation of emitted volatile organic compounds and the subsequent formation of ozone and other secondary products (Jenkin et al., 1997). The MCM gas-phase oxidation scheme for isoprene consists of 598 reactions and 185 species. Pinho et al. (2005) extended the MCM isoprene mechanism by adding extra photolysis channels for methacrolein (MACR) and methyl vinyl ketone (MVK) as well as $O(^3P)$ reactions with isoprene, MACR and MVK. The SOA mechanism developed in this study builds on the mechanism developed by Pinho et al. (2005).

For this work, the photolysis rates were calculated using the chamber lamp spectrum, the cross sections and quantum yields for each molecule of interest. The actinic flux was estimated using the method described by Hynes et al. (2005), and the photolysis rates were determined using equation 4.1.

$$J = \sum_{\lambda} \sigma(\lambda)\phi(\lambda)F(\lambda) \qquad (4.1)$$

where J, σ, F and φ represent the photolysis rate, absorption cross section, actinic flux and quantum yield, respectively. A description of each photolysis reaction rate used in the MCM is described by Jenkin et al. (1997). Additional chamber-dependent reactions were incorporated into the MCM gas phase mechanism following Hynes et al. (2005).

In order to reduce complexity in the model the isomers 2-methylthreitol and 2-methylerythritol have been represented as the single species, tetrol. The mechanism of Pinho et al. (2005) was initially modified by including reaction channels for the formation of tetrol from various first generation unsaturated methyl-butene diols. This is illustrated in Figure 4.1 for one of the product methyl-butene diols.

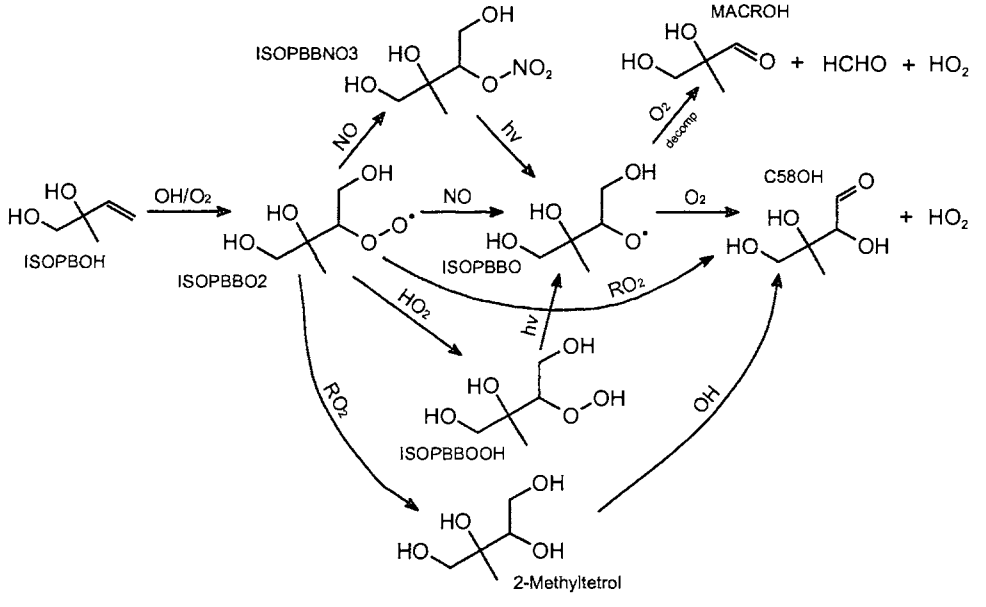

Figure 4.1: The formation pathway for the tetrol species (gas phase) as incorporated into the Master Chemical Mechanism.

The specific rate coefficients for the new reactions were calculated using Structure Activity Relationships (SAR) by Dr Sam Saunders of the University of Western Australia. An SAR calculation (Kwok and Atkinson, 1995) for OH/O_2 addition to 2-methylbut-3-ene-1,2-diol (or ISOPBOH in the MCM v3.1) shows that the addition of

OH to the double bond has a branching ratio of 0.9, thus dominating H-abstraction by OH radicals from the tertiary OH group, as presently depicted in the MCM v3.1. The SAR rate coefficient is 4.7 x 10^{-11} cm^3 $molecule^{-1}$ s^{-1}, and the product is a new peroxy radical in the model, labelled ISOPBBO2. This radical decomposes as per MCM protocols with the tetrol forming from ISOPBBO2 reacting with the peroxy radical pool. The rate coefficient is 2.0 x 10^{-12} cm^3 $molecule^{-1}$ s^{-1}, and the reaction channel has a branching ratio of 0.1. The second ISOPBBO2 + RO_2 channel has the same branching ratio and forms 2,3,4-trihydroxy-3-methylbutanal, or C58OH in the MCM. The second pathway for tetrol formation is from OH/O_2 addition to (2E)-2-methylbut-2-ene-1,4-diol, or ISOPAOH in the MCM. SAR calculation shows that OH addition to the double bond has a branching ratio of 0.97, and a rate coefficient of 2.3 x $10^{-10}cm^3molecule^{-1}s^{-1}$. A second new peroxy radical, ISOPAAO2, is formed rather than the two hydroxybutenal structures HC4CCHO and HC4ACHO in the MCM.

The formation of the tetrol arises from reaction of ISOPAAO2 with the radical pool, with a rate coefficient of 3.0 x 10^{-12} cm^3 $molecule^{-1}$ s^{-1} and a branching ratio of 0.1. The second ISOPAAO2 + RO_2 channel has the same branching ratio and forms a new species 1,3,4-trihydroxy-3-methylbutan-2-one, labelled C59OH. The third pathway is from OH/O_2 addition to 3-methylbut-3-ene-1,2-diol, or ISOPDOH in the MCM. SAR calculation shows that OH addition to the double bond has a branching ratio of 0.87, and a rate coefficient of 9.5 x 10^{-11} cm^3 $molecule^{-1}$ s^{-1}. A third new peroxy radical, ISOPDDO2, is formed rather than the hydroxybutenal structure HCOC5 in the MCM. The formation of the tetrol again arises from reaction of ISOPDDO2 with the peroxy radical pool, with a rate coefficient of 2.0 x 10^{-12} cm^3 $molecule^{-1}$ s^{-1} and a branching ratio of 0.1. The other ISOPDDO2 + RO_2 channel has the same branching ratio and forms 2,3,4-trihydroxy-2-methylbutanal or C57OH in the MCM.

Decomposition of tetrol by reaction with OH forms 2,3,4-trihydroxy-3-methylbutanal (C58OH), 1,3,4-trihydroxy-3-methylbutan-2-one (C59OH) and 2,3,4-trihydroxy-2-methylbutanal (C57OH) with branching ratios 0.56, 0.22 and 0.22, respectively. The

SAR calculation gives an overall OH rate coefficient of 1.9 x 10^{-11} cm^3 $molecule^{-1}$ s^{-1}. The pathway for the formation of 2-methylglyceric acid is shown in Figure 5.2.

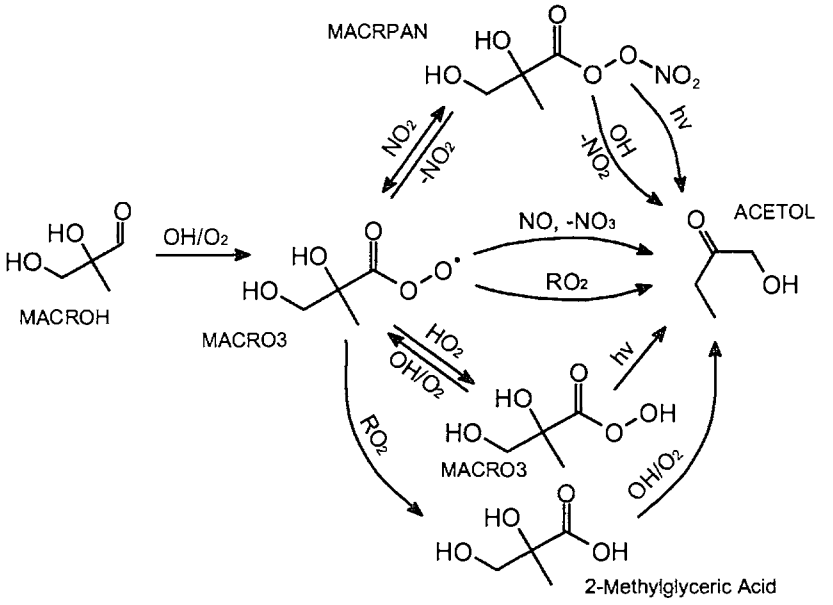

Figure 5.2: The formation pathway for the 2-methylglyceric acid species (gas phase) as incorporated into the Master Chemical Mechanism.

The second modification is a mechanism for the formation of 2-methylglyceric acid. The species 2,3-dihydroxy-2-methylpropanal, or MACROH in the MCM, is assumed to undergo OH attack at the tertiary OH group. However, SAR analysis suggests that OH attack should occur at the aldehydic hydrogen with a new peroxyacyl radical labelled MACRO3 forming after O_2 addition. The overall rate coefficient for OH attack is estimated at 3.4 x 10^{-11} cm^3 $molecule^{-1}$ s^{-1}. The SAR calculation shows that the branching ratio for the formation of MACRO3 is about 0.6, and 0.4 for the formation of hydroxy(methyl)malonaldehyde or C3MDIALOH in the MCM. A new PAN species forms from the reaction of MACRO3 and NO_2. The 2-methylglyceric acid is produced from the reaction of MACRO3 with the peroxy radical pool and with HO_2 (minor channel). The MACRO3 + RO_2 ($+O_2$) reaction has an estimated rate coefficient of 1.0 x 10^{-11} cm^3 $molecule^{-1}$ s^{-1} and a formation branching ratio of 0.3. The main gas-phase decomposition route for the 2-methylglyceric acid is by reaction with OH/O_2, forming 1-hydroxyacetone (ACETOL in the MCM) with a rate coefficient of 1.5 x 10^{11} cm^3 $molecule^{-1}$ s^{-1}.

4.3.2 Gas to Particle Transfer

The SOA mechanism was developed by firstly partitioning selected species from the gas to the aerosol phase according to the equilibrium absorption model of Pankow et al. (1994). This model contains an equilibrium partitioning coefficient, which represents the extent to which a species can partition from the gas to the aerosol phase. The aerosol phase concentration of each species was calculated using Equation 4.2 (Odum et al., 1996):

$$C_a = K_p \times C_g \times C_{om} \tag{4.2}$$

where C_a is the concentration of the species in the condensed phase ($\mu g/m^3$), C_g is the gas phase concentration of the species ($\mu g/m^3$), C_{om} is the total mass concentration of the condensed organic material ($\mu g/m^3$) and K_p is the equilibrium partitioning coefficient ($m^3/\mu g$). The partitioning coefficient was calculated using Equation 4.3:

$$K_p = \frac{7.501\times10^{-9} RT}{MW_{om}\zeta p_L^{\circ}} \tag{4.3}$$

where R is the ideal gas constant (8.314 J K^{-1} mol^{-1}), T is temperature (K), MW_{om} is the mean molecular weight of the condensed material (g mol^{-1}), ζ is the activity coefficient which was assumed to be 1.0 (Johnson et al., 2004) and p_L° is the liquid vapour pressure (Torr). It is assumed that aerosol particles are principally comprised of the same types of molecules, and so a value of 1.0 for the activity coefficients for all partitioning oxidation products is realistic is an assumption shared by several authors (Johnson et al, 2004). Where a value of 1.0 might not be appropriate could be for the condensed phase association reaction products.

Partitioning coefficients were calculated for each product that has a normal boiling point above 450 K (including tetrol and 2-methylglyceric acid) as suggested by Johnson et al. (2004). Partitioning coefficients were calculated for 88 species in total, which included those identified in SOA samples by Matsunaga et al. (2003) such as glycoaldehyde and hydroxyacetone. The liquid vapour pressure was estimated using the Clausius-Clapeyron equation:

$$\ln\left(\frac{p_L^\circ}{760}\right) = \frac{-\Delta S_{vap}(T_b)}{R}\left(1.8\left(\frac{T_b}{T}-1\right)-0.8\left(\ln\frac{T_b}{T}\right)\right) \quad (4.4)$$

where T_b is the normal boiling point and ΔS_{vap} is the entropy change of vaporization at T_b.

Boiling points were estimated using the fragmentation method modified by Stein and Brown (1994). Values for $\Delta S_{vap}(T_b)$ were determined using the Trouton-Hildebrand-Everett rule (Jenkin, 2004). Following Jenkin, (2004) and Johnson et al. (2004), the partitioning was represented as a dynamic equilibrium with $K_p = k_{in} / k_{out}$, where k_{in} is an absorption rate coefficient and k_{out} is a rate coefficient for desorption. In all partitioning reactions, k_{in} = 6.2 x 10^{-3} m^3 μg^{-1} s^{-1} as suggested by Jenkin (2004). The k_{out} values depend on the average molecular weight of the absorbing organic medium. The initial value, k°_{out}, assumes an average molecular weight for the absorbing organic medium (MW°_{om}) of 130 g mol^{-1}. At each subsequent time step, k_{out} values were corrected by multiplying k°_{out} by (MW_{om}/MW°_{om}), where MW_{om} is the actual average molecular weight of the absorbing organic medium calculated at each time step. As found by Jenkin (2004) and Johnson et al. (2004), a species-independent scaling factor was required to adjust the partition coefficients in order to correct for the observed aerosol mass concentrations. This also has the effect of delaying or increasing the onset of aerosol formation in the simulations.

4.3.3 Condensed phase reactions

The mechanism was further developed by adding condensed phase association reactions between the predominant hydroperoxide species (depicted in Figure 4.3) and the predominant aldehyde and –ONO_2 -substituted carbonyls (depicted in Figure 4.4).

As mentioned in section 4.1, hydroperoxides were identified by Surratt et al. (2006) as being likely to participate in condensed phase reactions with aldehydic species to form high molecular weight species, like peroxyhemiacetals. Hydroperoxides are a dominant

gas phase product and have been used in this mechanism as the main precursor in the association reactions to form peroxyhemiacetals.

Aldehydes were chosen as a precursor for the formation of peroxyhemiacetals due to the abundance of glyoxal and methylglyoxal identified as a gas phase product from the photooxidation of isoprene (Pinho et al., 2005). Glyoxal and methylglyoxal were identified as species dominant in the SOA sample collected from the photooxidation of 1,3-butadiene by Angove et al. (2006) and of toluene by Johnson et al. (2004). These products are known to polymerise readily and so have been identified as a possible precursor for condensed phase association reactions (Johnson et al., 2004). Carbonyls were identified as a likely precursor for condensed phase reaction in the 1,3-butadiene system by Angove et al. (2006) and since the structure of 1,3-butadiene and isoprene is very similar and gas phase products have been identified as being very similar, it is likely that carbonyls are a precursor for the formation of peroxyhemiacetals in the isoprene system. For this reason, the association reaction between hydroperoxides and aldehydes have been extended to incorporate carbonyls.

Organic nitrates were identified in the simulated SOA returned from incorporating only the partitioning of gas to aerosol of the products (with normal boiling temperatures greater than 450 K). Organic nitrates were also considered by Surratt et al. (2006) to be likely SOA precursor compounds. The isoprene mechanism has also been extended to incorporate the dominant PAN species identified in the simulated SOA sample (returned from only the partitioning reactions) as it was considered likely that these species also reacted further in the condensed phase.

The species chosen as precursors for the association reactions were the dominant species identified in the simulated SOA sample resulting from the inclusion of partitioning in the mechanism. An arbitrary number of species was chosen in response to the species – independent scaling factor which is also the method developed by Johnson et al. (2004).

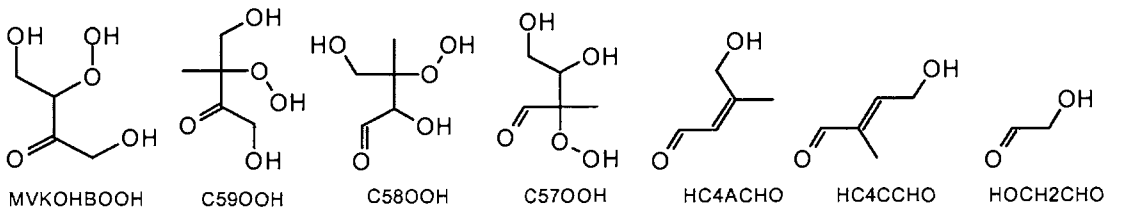

Figure 4.3: The hydroperoxides (structures 1 - 4) and the aldehydes/carbonyl (structures 5-7) used as peroxyhemiacetal precursor compounds and named according to MCM nomenclature.

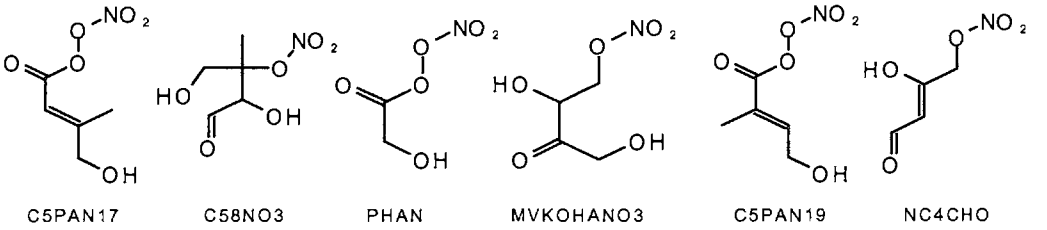

Figure 4.4: Nitrate substituted species used as peroxyhemiacetal precursor compounds and named according to MCM nomenclature.

This led to 36 peroxyhemiacetal species being considered in the simulation. The formation of stable peroxyhemiacetal adducts are assumed to proceed via a simplified association reaction between hydroperoxide and carbonyl species (Johnson et al., 2004):

$$ROOH + R'C(=O)R'' \rightarrow ROOC(OH)R'R'' \quad (4.5)$$

The association rate coefficient was arbitrarily chosen by finding the best fit to the onset time of the SOA growth. The partitioning coefficients for all adducts were calculated as described in the previous section. The peroxyhemiacetals possessed very low estimated vapour pressures, and were assumed not to desorb into the gas-phase.

4.4. Results

4.4.1 Modelled gas phase and SOA mass concentration

Figures 4.5 to 4.8 compare observed (continuous traces or symbols) and simulated (dashed lines) reactant/product gas phase profiles as well as SOA mass concentration profiles for experiments E201, E202, E203, E206, E210, E211, E303 and E304. The initial ROC/NOx ratios and length of each experiment varied for the experimental suite. As a result of improved FTIR signal-to-noise, MVK and MACR are included in E303 and E304. For purposes of clarity, simulation of the latter has been presented using a solid line.

In all cases, at the end of each experiment the simulated NO and NO_y-NO profiles are within 10% of the observed NO and NO_y-NO concentrations. In the latter case the simulated result is larger than the observed. This is attributed to the simulated NO_y-NO results being calculated as the total concentration of nitrate species, some of which were not efficiently detected by the chemiluminescene analyser. The simulated O_3 profiles for E203, E210 and E304 are also within 10% of the observed results. In the case of E303, the simulation rises steeply in accordance with observations. At the point of inflexion (~240 mins), the simulated O_3 concentration is 63 ppb less than observed. Unlike the observed result which plateaus at ~390 ppb, the simulation increased steadily, reaching 414 ppb at 600 min. The O_3 profile plateaus off in E303 due to the lower precursor species concentrations, this may be attributed to the variation in simulated O_3 concentration compared to experimental.

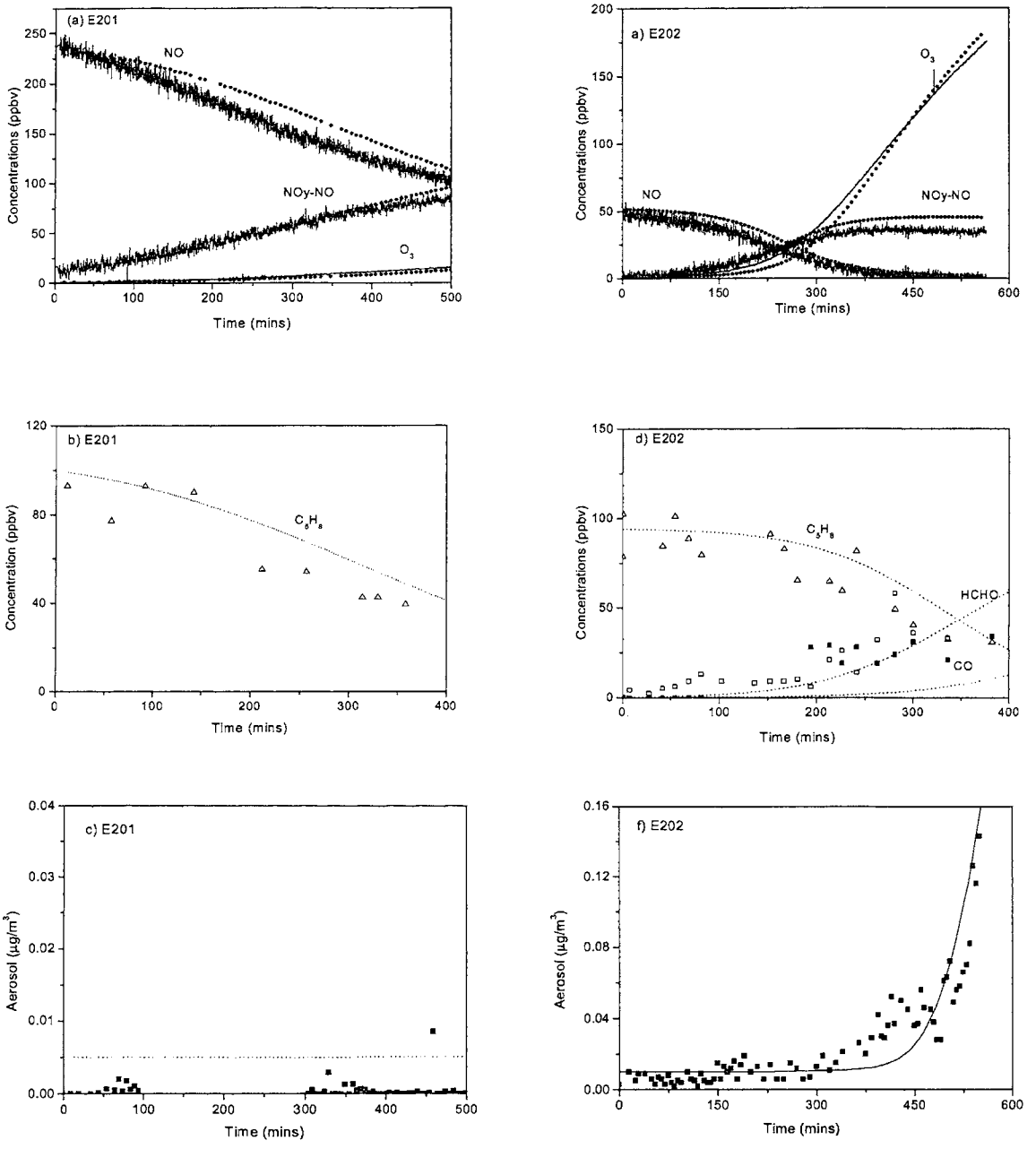

Figure 4.5: Comparison between observed gas phase and SOA mass concentration (continuous instrumental traces or symbols) and simulated MCM model (dashed lines) profiles for experiments E201 and E202.

NB: E201 The SMPS was taken offline between 100 and 300 minutes to check settings and calibrations. This experiment was repeated and is presented as E206.

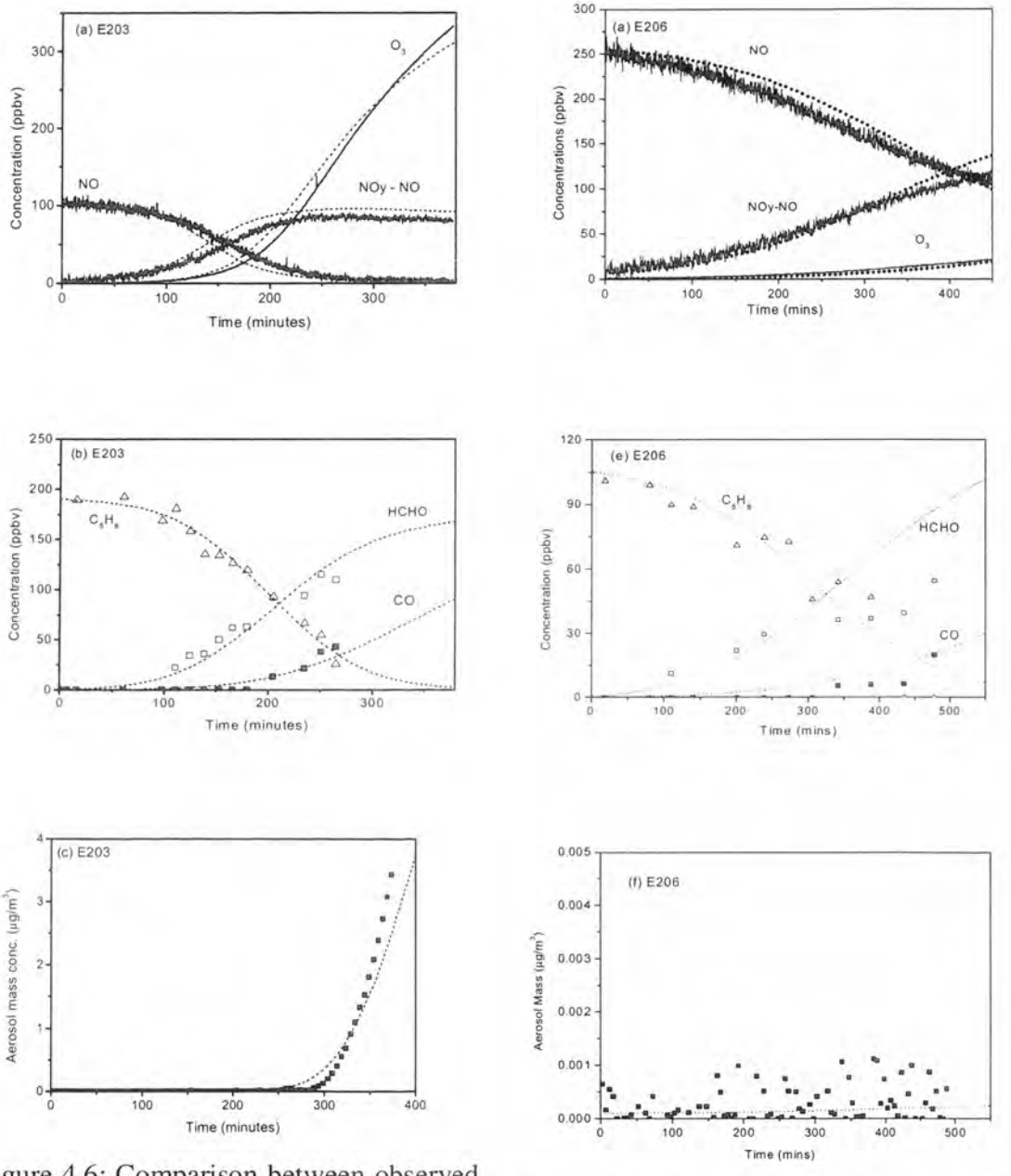

Figure 4.6: Comparison between observed gas phase and SOA mass concentration (continuous instrumental traces or symbols) and simulated MCM model (dashed lines) profiles for experiments E203 and E206.

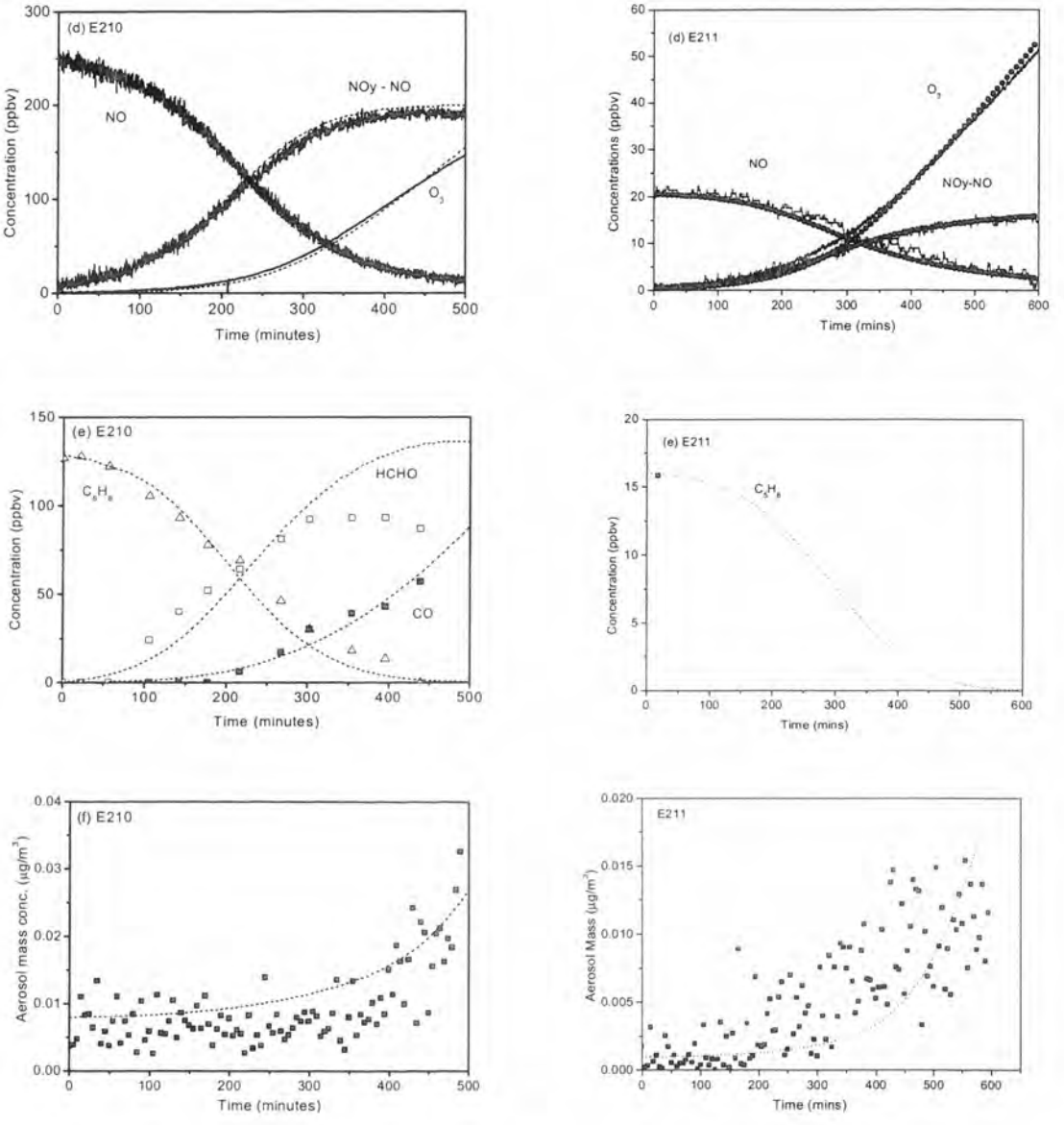

Figure 4.7: Comparison between observed gas phase and SOA mass concentration (continuous instrumental traces or symbols) and simulated MCM model (dashed lines) profiles for experiments E210 and E211.

NB: The concentrations of HCHO, CO and most of the C_5H_8 concentrations were below the FTIR detection limit for E211.

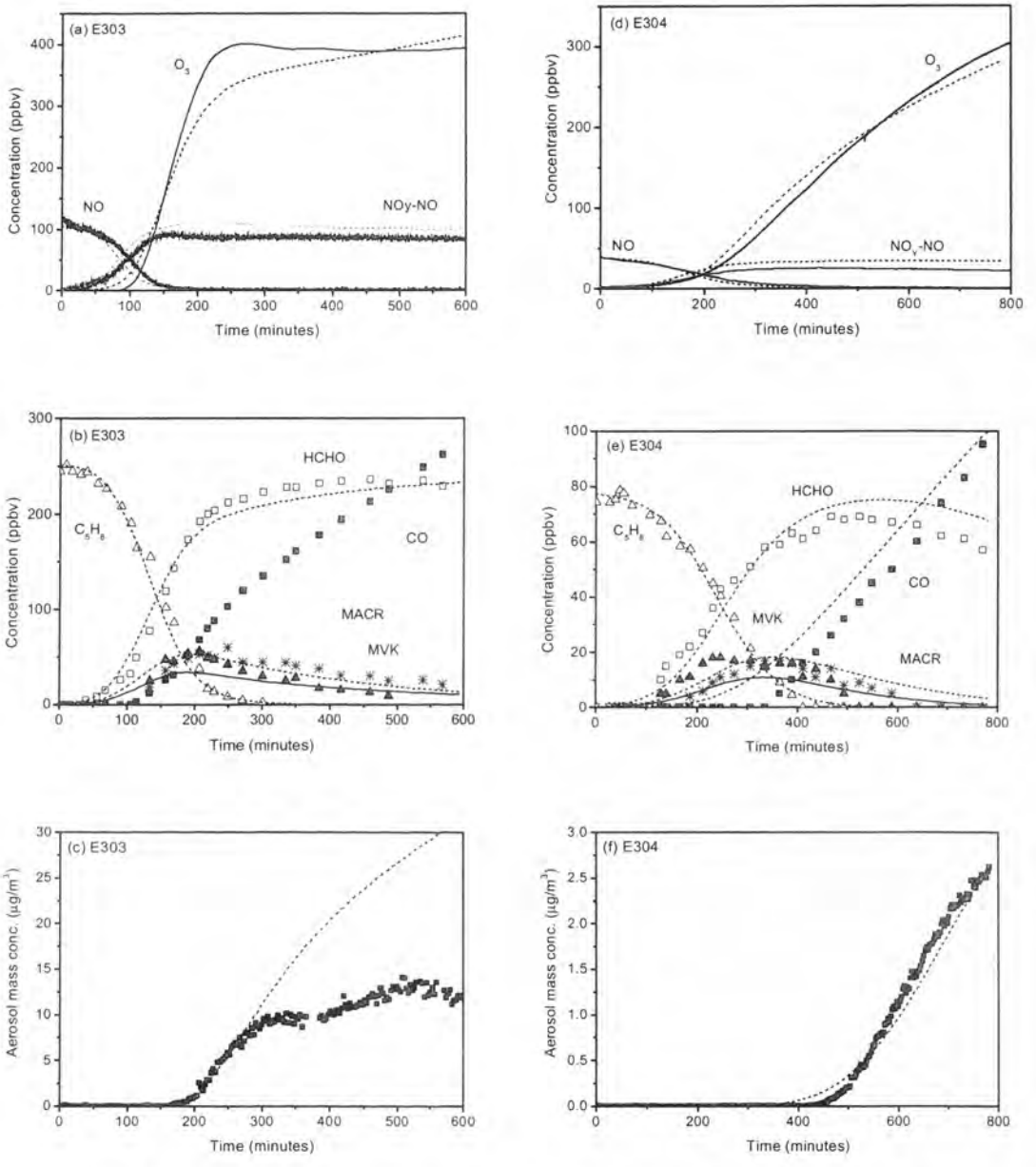

Figure 4.8: Comparison between observed gas phase and SOA mass concentration (continuous instrumental traces or symbols) and simulated MCM model (dashed lines) profiles for experiments E303 and E304.

The model simulations for isoprene are within 5% of the observed results. The simulated and observed profiles for CO are in good agreement for E203 and E210. In the case of E303 the simulation underpredicted CO, the maximum difference being 14% at the end of the experiment. In the E304 simulation, the CO concentration was overpredicted by a maximum of 20% at ~588 mins but approached the observed result near the end of the experiment. In the case of HCHO, the simulations were in good agreement with observed results up to the points of inflexion. Thereafter, for experiment E303, the model overpredicted the concentration of HCHO by less than 5%. By the end of experiment E304 the HCHO concentration was underpredicted by 19% and notably, by 52%, for E210.

In both E303 and E304 the modelled concentration profiles of MVK (dashed) were higher than those obtained for MACR (solid). The 10 to 50% uncertainty in the observed MVK (solid triangles) and MACR (stars) data make it difficult to be conclusive when comparing the observed and simulated profiles. It is probable that the concentration of MACR was not always less than that of MVK. In experiment E303, the simulated peak concentrations of MVK and MACR were 55 ppb and 33 ppb at ~200 mins, respectively. Observed MVK and MACR concentrations appeared to increase from ~120 mins, reaching peak concentrations of 56 ± 6 ppb and 53 ± 6 ppb at ~200 mins, respectively, which was similar to the simulation. MVK appeared to decay at a faster rate than MACR and was not detected after ~500 mins, whereas MACR was still present at the end of the experiment. In the simulation, both MVK and MACR were present at the end of the experiment.

In experiment E304, MVK was detected at ~125 mins which was ~60 mins before that of MACR. The peak concentration of MVK of 18 ± 3 ppb occurred at ~247 mins and that of 17 ± 3 ppb for MACR at ~336 mins. The simulated peak concentrations were 18 ppb at ~353 mins for MVK and 10 ppb at ~333 mins for MACR. Similar to experiment E303, MVK decayed more rapidly than MACR and was not observed after ~525 mins. MACR was not observed after ~637 mins, which is in close agreement with the

simulation, whereas, the model predicted that MVK would be present in the chamber, was not observed.

As shown in Figures 4.5c, 4.5f, 4.6c and 4.6f, the onset of SOA formation occurs close to the time that the NO concentration becomes limited. The model accurately simulates this condition. In the case of experiment E303, as the concentration of isoprene approaches zero, the observed SOA formation plateaus at a mass concentration of ~10 $\mu g/m^3$ at ~300 mins, and at ~360 mins the mass concentration increases to a peak of 13.6 $\mu g/m^3$ at ~530 mins.

4.4.2 Modelled SOA Composition

Table 4.3 compares modelled SOA compositions for experiments E203, E210 and E303 at the times when SOA onset occurred, and when NO and isoprene concentrations were depleted. The SOA species were classified into 6 groups. No species was permitted to belong to more than one group. The order of grouping was: peroxyhemiacetals (36 species; 20 species were nitrated), organic nitrates (22 species), hydroxycarbonyls/carbonyls (31 species), hydroperoxides (23 species), tetrols (8 species) and diols/alcohols (7 species). The tetrol group also included 2-methylglyceric acid. Contributions to the peroxyhemiacetal group by nitrated species are given in parentheses in Table 4.3.

Table 4.3: A comparison of aerosol composition simulations for experiments E203, E210 and E303

Expt/aerosol component	**E203 Composition (mass conc.%)**			**E210 Composition (mass conc.%)**			**E303 Composition (mass conc.%)**		
	SOA onset, 220 mins	NO depletion, 260 mins	Isoprene depletion, 405 mins	SOA onset, 405 mins	NO depletion, 460 mins	isoprene depletion, 560 mins	SOA onset, 60 mins	NO depletion, 190 mins	isoprene depletion, 300 mins
Peroxyhemiacetals *(nitrated)*[a]	40.9 *(26.1)*	81.7 *(64.0)*	98.0 *(94.1)*	30.4 *(26.3)*	52.0 *(47.0)*	81.2 *(77.4)*	2.78E-03[c]	97.9 *(94.3)*	99.0 *(96.0)*
Organic nitrates	36.6	13.0	1.42	55.7	39.5	15.2	59.6	1.60	6.46E-01
Hydroxycarbonyls and carbonyls	10.6	2.68	3.09E-01	7.52	4.86	2.08	40.4	2.83E-01	1.43E-01
Hydroperoxides	11.9	2.69	2.50E-01	6.42	3.74	1.53	2.40E-03	1.93E-01	1.50E-01
Tetrols[b]	1.27E-02	1.45E-02	8.00E-03	1.13E-03	8.29E-04	3.86E-04	1.14E-04	1.54E-02	3.18E-02
Diols and alcohols	6.16E-02	4.54E-02	1.49E-02	1.93E-01	2.02E-01	1.19E-01	2.17E-04	7.37E-03	4.69E-03
SOA Mass ($\mu g/m^3$)	0.0145	0.0752	2.15	0.0090	0.0135	0.0342	0.0102	0.623	11.1

[a] Mass concentration % in parentheses refers to the contribution by those peroxyhemiacetals which are nitrated.
[b] The tetrol grouping also includes 2-methylglyceric acid
[c] Negligible contribution by nitrated peroxyhemiacetals

Expected page number is not

in original print copy

The tetrol concentration in experiments E203 and E210 decreased from SOA onset to that time when isoprene was considered to have been depleted by a factor of ~1.6 and ~2.9 respectively. In contrast, in experiment E303, the tetrol concentration increased by ~280 times. The diols/alcohol concentrations in experiments E210 and E303 increased ~14 and ~22 times, respectively and decreased in E203 by ~4 times.

A detailed description of the tetrol mechanism and the methylglyceric mechanism (with rate coefficients) are included in the Appendix which includes structural diagrams of the reactants in the new mechanism.

4.5.Discussion

In general, the model performed well for most gas-phase species when compared to the observed chamber data. Simulation of the SOA mass concentrations agreed with the observed data with respect to SOA onset time and the initial rate at which the SOA mass concentration increased. In the two experiments E201 and E206 where SOA was not observed, SOA was also not generated by the model.

However, the model could not account for the observed levelling-off in the SOA mass concentration in E303, which has been observed in other studies (Angove et al., 2006; Dommen et al., 2006; Surratt et al., 2006). The simulation showed that the aerosol mass concentration continued to rise over time, suggesting that a more complex mechanism for aerosol growth is required. The low saturation vapour pressure species such as tetrols, the complex organic peroxides and peroxyhemiacetals are formed explicitly in the mechanism and ineffectively irreversibly adsorbed once they have partitioned from the gas phase. As a result, the aerosol mass concentration tends to build up until all condensable organic species in the gas-phase are depleted.

The apparently bimodal nature of Fig. 4.6(c) is perhaps due to two aerosol growth phases: one due to isoprene and its related oxidation products, and a second due to methacrolein, whose oxidation product (2-methyglyceric acid) represent a major contribution to isoprene aerosol mass (Surratt et al., 2006). The bimodal nature of

the SOA profile will be discussed in further detail in Chapter 6. Clearly, more work is required to capture the effects of photochemical aging on SOA in the model which may account for the decrease in aerosol mass concentration observed towards the end of the experiments.

Results from the aerosol composition simulations in Table 4.3 demonstrate that the initial isoprene and NO concentrations influence the aerosol composition. The calculated aerosol composition varies throughout an experiment, with most of the aerosol mass constituted by peroxyhemiacetal species at the end of a simulation.

Several studies have recently discussed potential formation routes for the tetrol and 2-methylglyceric acid found in various ambient $PM_{2.5}$ samples. In this work, the formation of the tetrols has been represented as the nucleating species for SOA growth. The calculated yields of tetrol and 2-methylglyceric acid in the condensed phase were less than the yields suggested by other chamber studies (Edney et al., 2005; Böge et al., 2006). This indicates that other formation pathways, additional to the gas-phase routes, need to be incorporated into the model. Böge et al. (2006) suggest that epoxydiol intermediates may form from hydroxyhydroperoxides or hydroperoxy radicals, which could undergo condensed phase hydrolysis to form the tetrols. Alternatively, reaction of key unsaturated butene diols with H_2O_2 on acidic particles could occur. As Surratt et al. (2006) surmise, these processes require more consideration.

These simulations can be compared with the isoprene SOA analyses undertaken by Surratt et al. (2006). The experimental conditions used in this study represent intermediate NOx concentrations (of less than 250 ppb) when compared to the 'low NOx' and 'high NOx' experiments of Surratt et al. (2006). Under very low NOx conditions, Surratt et al. (2006) observed mostly polyols and organic hydroperoxides in the SOA. Under high NOx conditions, hydroxynitrate compounds and acidic species, based on the structure of 2-methylglyceric acid, tend to dominate the SOA composition. In these simulations, the hydroperoxides accounted for no more than 12% of the total SOA mass and the tetrols less than 0.01%.

Possible reasons for the discrepancy between this study and that of Surratt et al. (2006) could also be due to the simple equilibrium model used to describe aerosol growth, as well as large uncertainties in the calculated boiling points and saturation vapour pressures of key hydroperoxide and polyol species. The simple peroxyhemiacetal formation pathway makes assumptions about a condensed-phase process of which little is presently known, and the assumed association rate constant may skew the SOA composition towards peroxyhemiacetals over individual nitrated aldehydes and organic hydroperoxides, which are assumed to be rapidly converted into peroxyhemiacetals. Surratt et al. (2006) did, however, observe hemiacetal dimers in the SOA and speculated that peroxyhemiacetal oligomers could form due to the large amounts of organic peroxides measured in the SOA, thus providing some justification for the assumption that peroxyhemiacetals are produced in the SOA.

In Figure 4.7, the simulated concentrations of RO_2, HO_2 and OH (if not completely consumed) at the end of the experiments that produced SOA, are compared to the experiments that produced no SOA. When these results are compared to the onset times for E203 (222 mins), E210 (395 mins) and E303 (58 mins), there is an indication that the SOA forms once the NO and/or isoprene is almost completely consumed. Conversely, in E206 no SOA is reported to have formed after almost 500 minutes of irradiation, at the same intensity as the other experiments. In this case, the HO_2 and RO_2 species are still building to a peak and there is still some OH in the system. This may suggest that once the NO concentration has been suppressed, the ratio of RO_2 / OH increases (less OH), and the peroxy – peroxy reactions forming the tetrols becomes more dominant as illustrated in the mechanism.

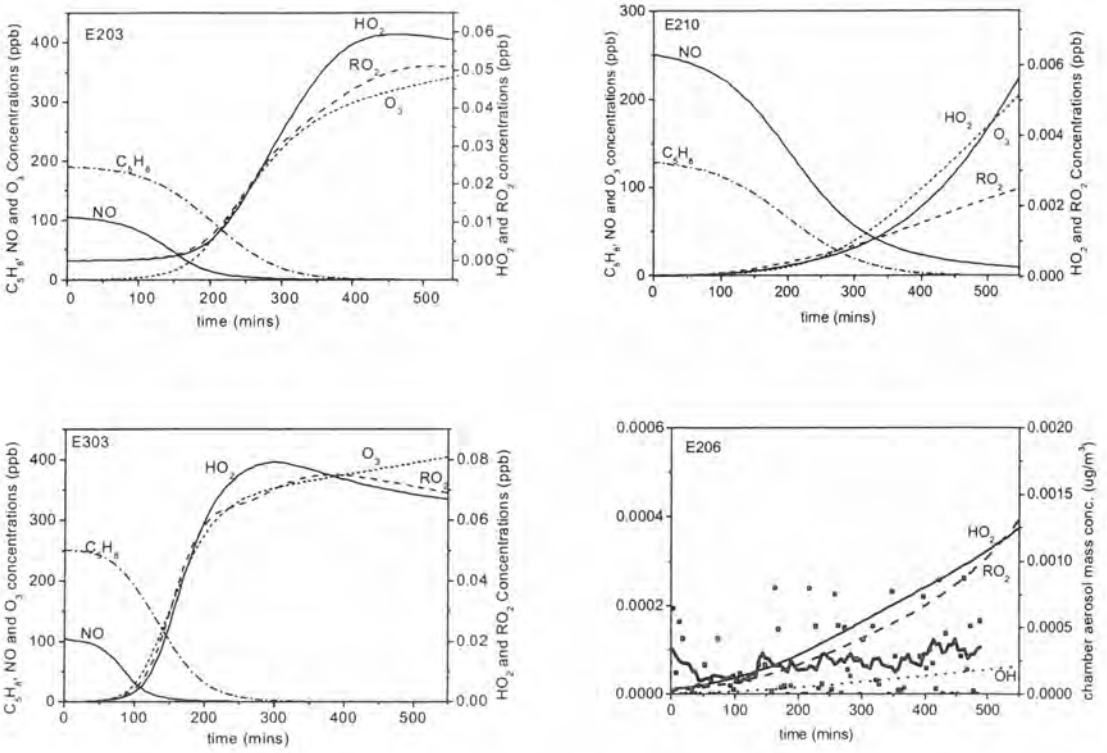

Figure 4.9: SOA forming experiments E203, E210, E303 and the non SOA forming experiment E206. Aerosol detected at about 160mins for E303, 255 mins for E210 and around 250 mins for E303. The E206 panel also includes the aerosol detected for the experiment (symbols) and the average aerosol conc. (thick line).

4.6. Conclusions

A model for SOA formation derived from the photodegradation of isoprene in NOx has been developed and tested against environmental chamber experiments conducted over a wide range of ROC/NOx values. The model appears to reproduce the observed gas-phase species profiles reasonably well. The model also successfully simulated the SOA onset time and the initial increase in aerosol mass concentration for the majority of experiments performed over a photochemical window of 6 to 8 hours. The model overestimated the simulated mass for the experiment in excess of 10 hours (E303), due to oversimplifications inherent in the equilibrium condensation model for SOA growth. SOA composition simulations indicate that the initial NOx and isoprene concentrations governed the SOA composition, which varied throughout the photochemical window. The influence of the initial NOx concentration on the SOA composition was also reported by Johnson et al. (2004) for the toluene system. In their study of the products derived from the

isoprene system, Surratt et al. (2006) also found that the composition of the SOA varied throughout the experiment. The simulated SOA composition (presented in Table 4.3) indicated that at the end of the three experiments, the peroxyhemiacetal concentration was up to 99% of the total SOA mass concentration. This is more likely to be an indication of the importance of the oligomerisation process once aerosol has formed in the system than of the likely composition of SOA generated from the isoprene system.

The formation of SOA through physical coagulation processes is not represented in the mechanism. SOA is initially generated in the model through partitioning processes and later through the oligomerisation processes. This lack of representation of this physical SOA formation process could possibly account in part for the species independent scaling factor determined by fitting the chamber experiments to the mechanism, however it is more likely that the representation of other association reactions other than the formation of peroxyhemiacetals would improve the species independent scaling factor more significantly than accounting for coagulation processes.

In summary, a crude representation of condensed phase reactions to produce high molecular weight species has been undertaken to improve the results of the SOA simulation. The formation of peroxyhemiacetals has been simulated from the reaction of the precursors aldehydes /carbonyls, organic nitrates / PANs with hydroperoxides. In total 36 species of peroxyhemiacetals were formed to account for the aerosol mass concentration observed from chamber experiments. The number of and type of species chosen were crudely determined by simulating the main SOA species resulting purely from partitioning the dominant gas phase species with normal boiling points in excess of 450 K.

The dominance of the peroxyhemiacetals (up to 99% of the aerosol composition at the end of experiments) indicate that the formation of peroxyhemiacetals is far over estimated and other condensed phase reactions should also be alternatively considered. Surratt et al. (2006) identify the formations of oligomers formed from

self-oxidation reactions of 2-methylglyceric acid and oxidation reactions of tetrol. This would be a likely first point for further development of the mechanism.

Chapter 5: A Comparison of Two Methods of Calculating the Yields of Secondary Organic Aerosol (SOA)

5.1 Introduction

Secondary Organic Aerosol (SOA) is produced during photochemical reactions of reactive organic compounds (ROC) with nitrogen oxides (NOx). Photo-decomposition of a specific hydrocarbon in the presence of NOx forms volatile and semi-volatile products. Some of these products are condensable organic compounds (COCs) and can self nucleate or condense from the gas phase to the aerosol phase, if they have a saturation vapour pressure that is sufficiently low. Once organic matter is produced in a system, other COCs with larger saturation vapour pressures can be adsorbed onto the surface of the aerosol (Odum et al., 1996).

The majority of SOA mass is formed through this absorption process in the α-pinene system (Presto et al., 2005), and this may also be one of the dominant formation processes in the isoprene system since the initial nucleation process produces aerosol with small diameters, as observed at the beginning of chamber experiments. In the isoprene system, the initial mean diameter of the aerosol is less than 20nm, which grows to form aerosol with mean diameters of about 80 nm (refer to Figure 3.12), possibly due in part to coagulation processes. During the absorption process, new COCs are binding to the surface of the existing aerosol, increasing their original size and mass. A larger number of COCs can form aerosol in this manner because they are no longer restricted by vapour pressure (Odum et al., 1996). Recently, chemical reactions occurring between condensed phase species to form oligomers have been identified (Dommen et al., 2006; Surratt et al., 2006).

Several models have been developed to estimate the amount of SOA formed from the photo-oxidation reaction between hydrocarbons and NOx. In this work, two gas/aerosol partitioning models are considered. Both models are extensions of an absorption model developed by Pankow et al. (1994) and focus solely on SOA formed from absorption processes at equilibrium. In order to compare the models'

performances, they will be compared to the experimental yield expression, which is shown in Equation 5.1.

$$Y = M / \Delta HC \tag{5.1}$$

where Y is yield, M is the aerosol mass concentration ($\mu g/m^3$) produced and ΔHC is the mass concentration of the hydrocarbon that has been consumed in the reaction ($\mu g/m^3$).

Equation 5.1 will be referred to as the experimental yield since it is derived from experimental concentrations of mass produced and hydrocarbon consumed. Yield can be defined as the aerosol forming potential of a specific hydrocarbon. A constant yield value for a particular hydrocarbon is incorporated into many air quality models. Takekawa et al. (2003) found that higher aerosol yields were observed during chamber experiments at lower temperatures as opposed to experiments with higher temperatures. Similarly, in Chapter 4 the yield resulting from isoprene photodegradation was found to vary with different precursor concentrations, these findings oppose the assumption of a constant yield for a specific hydrocarbon.

The two models examined in detail in this chapter are referred to as the Odum model and the Hoffmann model. The model developed by Odum et al. (1996) calculates an estimate of the yield. The second model developed by Hoffmann et al. (1997) calculates the amount of aerosol mass produced from the reaction of a hydrocarbon with each of the three oxidants produced photochemically in the atmosphere.

The Odum et al. (1996) model is a static model, and can be used to calculate the SOA yield produced at a specified time in a given system using the equation:

$$Y = M \sum_{i=1}^{I} ((\alpha_i K_{om,i}) / (1 + K_{om,i} M) \tag{5.2}$$

where Y is the yield calculated for a given system, M is the absorbing aerosol mass concentration ($\mu g/m^3$) which is equal to the mass concentration of SOA in the chamber at the time specified, $K_{om,i}$ is the partitioning coefficient, α_i is the stoichiometric ratio that relates the amount of product to the amount of parent hydrocarbon consumed and I is the number of products examined (usually two).

Hoffmann's model is a dynamic model that considers the aerosol mass concentration contributions from each of the three oxidants (ozone, hydroxy radical and the nitrate radical) as a function of time, as depicted in Equation 5.3:

$$M(t) = M_n = M_0 + \Sigma_{ox}\ \Delta ROC_{ox}(t)\ M_{n-1} \sum_{i=1}^{I}((\alpha_i K_{om,i})/(1 + K_{om,i} M_{n-1})) \quad (5.3)$$

where M_0 is the amount of aerosol in the system initially (experimental background in $\mu g/m^3$), t refers to a specific time step, M_{n-1} refers to the amount of aerosol produced in the previous time step, ox refers to the oxidant that is responsible for the consumption of the HC and ΔROC_{ox} is the amount of the hydrocarbon consumed by the oxidant (ox) specified.

Five environmental chamber experiments and a chamber aerosol speciation reported by Angove et al. (2006) have been used to study the Odum and Hoffmann models. The aim of the work presented in this chapter is to identify the strengths and weaknesses of the two models for incorporation into a 3 dimensional air quality model which is presented in Chapter 7.

The Odum and Hoffmann models were assessed using the following procedure:

1. Model parameter values and a yield contribution were determined for every species identified by the analytical aerosol composition work undertaken by Angove et al. (2006). A net yield estimate was then calculated for the Odum and the Hoffmann models and compared with the experimental yield. Since sixteen products were identified in the aerosol sample, each model is treated as a sixteen product model.
2. Parameter values for two hypothetical products for the Odum and Hoffmann models were compared to the calculated parameter values of actual species identified in the first step. This was achieved by fitting the models to the 1,3-butadiene chamber data (Angove et al., 2006). In this context, the models are used as 2-product models and applied in the way described by Odum et al. (1996).
3. A low and a medium saturation vapour pressure product were chosen from those identified in the aerosol sample. The model parameter values calculated in the first step for these products were then substituted into Odum's model to see whether real product values could produce a yield estimate similar to the experimental yield.

5.2 Chamber Experiments and SOA Analysis

A brief account of the experimental details described by Angove et al. (2006) will be provided here, since the experimental data are central to this chapter. The experiments were undertaken at CSIRO's indoor environmental chamber system which has been described in Chapter 3. The UV intensity varied from experiment to experiment and is presented with other initial experimental conditions in Table 5.1. Takekawa et al. (2003) found that the SOA yields were larger when the experimental temperatures were lower, so in Angove et al. (2006) experiments the UV intensity will influence the mass concentration of SOA produced. However, when comparing the J_{NO_2} with the SOA mass concentration and the initial precursor concentrations for each experiment presented in Table 5.1 it seems that the SOA mass concentration is more sensitive to the initial precursor concentrations than the J_{NO_2}. No seed particles were added to the chamber and the background aerosol concentration was less than 5 particles /cm^3 for each of the experiments presented. The initial ROC/NOx ratio varied from 3.5 to 4.0 for the six experiments.

Table 5.1: Initial conditions for the 1,3-butadiene/NOx chamber experiments.

Experiment Number	Initial [C_4H_6] (ppb)	Initial [NOx] (ppb)	ROC/NOx	J_{NO_2}	Aerosol Mass Concentration (μg/m^3)
47	1069	1053	4.06	0.41	8.26
49	897	1028	3.49	0.21	2.03
51	1079	1078	4.00	0.21	8.96
52	1030	1032	4.00	0.83	6.39
53	1019	1075	3.79	0.62	7.81
54	983	1033	3.81	0.42	4.59

The formation of ozone and aerosol was recorded throughout the experiment using an ozone analyser and a scanning mobility particle sizer (SMPS) described in Chapter 3. Similarly, Fourier transform infrared spectroscopy (FTIR) and high

performance liquid chromatography (HPLC) carbonyl derivative analysis were used to determine the initial concentrations of 1,3-butadiene for each experiment.

As reported by Angove et al. (2006), an aerosol sample was collected during experiment 52 over a period of 6 hours on two glass fibre filters in close contact. Aerosol was present only on the front filter, which was taken up in D_2O and analysed using 1H Nuclear Magnetic Resonance (NMR) and Gas Chromatography Mass Spectroscopy (GCMS). The sixteen compounds that were identified by Angove et al. (2006) are presented in Table 5.2 with estimates of the boiling points, change in entropy of vaporisation (ΔS_{vap}) and saturation vapour.

Table 5.2: The sixteen species identified by Angove et al. (2006) in the SOA sample collected during the experiment 52.

Species	Molecular Formula	MW g/mol	T_b K	ΔS_{vap} J/mol/K	Saturation. Vapour Pressure (Torr)
Formaldehyde	$C H_2 O$	30	268.4	93.6	4.55E+03
Formic acid	$C H_2 O_2$	46	383.6	96.6	4.98E+01
Glycoaldehyde	$C_2 H_4 O_2$	60	381.3	106.8	6.27E+01
Glycolic acid	$C_2 H_4 O_3$	76	468.4	107.4	4.36E-01
Glyoxal	$C_2 H_2 O_2$	58	347.5	90.3	4.11E+02
Glyoxylic acid	$C_2 H_2 O_3$	74	447.2	106.4	1.20E+00
Glycerol	$C_3 H_8 O_3$	92	531.9	142.9	2.51E-05
Glyceraldehyde	$C_3 H_6 O_3$	90	490.4	126.5	9.59E-03
Glyceric acid	$C_3 H_6 O_4$	106	542.8	126.5	6.46E-04
Hydroxypyruvaldehyde	$C_3 H_4 O_3$	88	464.3	110.1	2.90E-01
Ketomalonaldehyde	$C_3 H_2 O_3$	86	429.1	93.6	7.35E+0
Threitol	$C_4 H_{10} O_4$	122	585.7	155	1.50E-07
Erythritol	$C_4 H_{10} O_4$	122	585.7	155	1.50E-07
Threose	$C_4 H_8 O_4$	120	561.5	146	5.79E-06
Erythrose	$C_4 H_8 O_4$	120	561.5	146	5.79E-06
Unknown 1**	$C_4 H_7 N O_7$	181	641.4	164.3	5.52E-07
Unknown 2**	$C_4 H_7 N O_7$	181	641.4	164.3	5.52E-07
Unknown 3**	$C_4 H_7 N O_7$	181	641.4	164.3	5.52E-07

*** tentatively identified as threonic/erythronic acid nitrate

5.3 The SOA Models – Applications and Results

5.3.1 Sixteen product model.

Common to both models are the parameters K_{om} and α. The parameter α can be defined as the product yield, that is, a ratio of the amount of product (aerosol and gas phase) over the amount of hydrocarbon consumed. The SOA yield is often referred to as the yield, and can be defined as the ratio of the amount of the product in the aerosol phase to the amount of the precursor hydrocarbon. $K_{om,i}$ is the amount of aerosol that will partition out of the gas phase in equilibrium, given that the COC is assumed to behave as a quasi-ideal solution.

In order to use the Odum and Hoffmann models from first principles, certain properties of each product need to be determined, they are:

(i). the molecular weight of the compound (g mol^{-1}),
(ii). the boiling point (Kelvin),
(iii). the change in entropy, near or at the boiling point ($JK^{-1}mol^{-1}$),
(iv). the saturated vapour pressure of the pure compound of each species (Torr).

The saturation vapour pressure (liquid phase) was determined using the Clausius - Clapeyron equation once the boiling point was estimated from the molecular structure of the species (Stein and Brown, 1994). Change in entropy of vaporisation was estimated by analogy with similar structured species and where possible from other literature. These estimates were calculated by Dr R. Hynes (co-author). From this information, parameter values for the partitioning coefficient, $K_{om,i}$ and stoichiometric constant, α_i were determined for the time at the 'end' of the experiment for each of the products identified by Angove et al. (2006).

Determination of K_{om}

A method for calculating the partitioning coefficient was defined by Pankow et al. (1994) and is presented in Equation 5.4:

$$K_{om,i} = 760\ RT/(10^6\ MW_{om}\ \zeta_i\ \rho^{\circ}_{L,i}) \tag{5.4}$$

where R is the ideal gas constant 8.206×10^{-5} m^3 atm mol^{-1} K^{-1}, T is the temperature at the end of the experiment (307.2 K), MW_{om} is the mean molecular weight of the organic matter in g mol^{-1} (for 1,3-butadiene it is 90). The activity coefficient is ζ_i and for all the compounds is assumed to be 1.0, $\rho^{\circ}_{L,i}$ is the liquid phase saturation vapour pressure in Torr.

Determination of α_i

Pankow et al. (1994) identified a method for calculating the stoichiometric aerosol constant, α_i, using the equation:

$$\alpha_i = C_i / \Delta HC \tag{5.5}$$

where ΔHC is the amount of hydrocarbon consumed and C_i is the total concentration of the compound in both aerosol and gas phases, all in μg/m^3. That is,

$$C_i = C_a + C_g \tag{5.6}$$

where C_a is the concentration of the compound in the aerosol phase and C_g is the gas phase concentration (Pankow et al. 1994; Bowman et al., 1997). The gas phase concentration can be calculated from Equation 5.7:

$$C_g = (y_i \, MW_{om} \, \rho^{\circ}_{L,i} 10^6) / RT \tag{5.7}$$

where y_i is the mole fraction of species i in the aerosol phase and R is 6.2 x10^{-2} Torr m^{3}mol^{-1}K^{-1}.

Once C_g is calculated, C_a can be determined according to Equation 5.8 (Odum et al., 1996; Jenkin, 2004):

$$C_a = C_g \, MK_{om,i} \tag{5.8}$$

where M is the mass concentration of aerosol determined experimentally at the time when all of the 1,3-butadiene has been consumed. Density for this SOA is assumed to be 1.0 g/m^3.

Calculation of yield using the Odum and the Hoffmann model

The α and K_{om} parameter values for each of the sixteen species identified in the aerosol sample were determined and substituted into the Odum model to determine the individual yields of each species. The sum of the yields is therefore the net yield for the experiment which was then compared with the experimental yield.

The Hoffmann model is more complex than the Odum model, in that a mass concentration is calculated from each of the oxidation reactions with 1,3-butadiene. In order to achieve this, the relative consumption of the 1,3-butadiene by each of the oxidants had to be determined. The Master Chemical Mechanism v3.1 (Jenkin et al. 1997) calculated that 68% of 1,3-butadiene was consumed by reaction with the OH radical, 10% by O_3 and 22% by NO_3 radical. An estimate of how much 1,3-butadiene was consumed by each of the oxidants, for each of the time steps, was determined based on these estimates. This mechanism is available from the Master Chemical Mechanism website and the branching ratios applied in this study were sourced from that site with a JNO_2 of 0.81 which is the UV intensity used in experiment 52. The branching ratios are appropriate for all precursor concentrations.

In order to use the Hoffmann model to estimate the aerosol mass concentration, several assumptions were made, one of which is that all of the species identified in the aerosol sample were formed directly from the reaction of 1,3-butadiene with the oxidants and are, hence, first oxidation products. Currently there is little information available about the favoured formation routes for the species identified in the aerosol sample, and so assigning a species to be the product of a particular oxidation reaction was difficult, particularly when a species could be formed from more than one oxidation reaction, such as formaldehyde. Of the products presented in Table 5.2 it was assumed that only formaldehyde and formic acid were produced from the reaction of 1,3-butadiene with ozone, and threonic / erythronic acid nitrate were produced from the oxidation of 1,3-butadiene with NO_3. It was assumed that all other products were produced by the reaction of OH radical with 1,3-butadiene (D. Angove, private communication).

Where there were more than two products in a group, the α and K_{om} parameter values that were calculated for each of the species were then grouped together before being incorporated into the Hoffmann model for each oxidant. For example, the α values for all of the species formed from the OH reaction with 1,3-butadiene were added together to form two α values that represented two hypothetical products resulting from this oxidation reaction: the same method was applied to the K_{om} values. These parameter values were incorporated into the Hoffmann model and an aerosol mass concentration produced from the reaction of OH with 1,3-butadiene was obtained. The mass produced from each oxidant reaction was then added together to derive a final net mass concentration for the sixteen products. The final net yield was determined by dividing the mass concentration of the total amount of 1,3-butadiene consumed by the calculated net mass concentration formed, as shown in Equation 5.1.

5.3.2 Results - sixteen product models

For the experiment E52 (the aerosol sample was collected from this experiment), the initial 1,3-butadiene concentration was 1030 ppb and the initial NOx concentration was 1032 ppb. As discussed in Section 5.3.1, the model parameters for the Odum model were determined for each of the species identified in the aerosol sample taken by Angove et al. (2006). Estimates of boiling points, change of entropy of vapourisation and saturation vapour pressures for each of these species are presented in Table 5.2. Table 5.3 presents the parameter values, $K_{om,i}$ and α, calculated for the Odum model, in addition to the species' concentration in both the aerosol and gas phase (C_a and C_g respectively) and the individual yield contributions.

At the end of the experiment, the aerosol mass concentration was 6.385 $\mu g/m^3$, and 2.275×10^3 $\mu g/m^3$ of 1,3-butadiene was consumed. A yield of 2.81×10^{-3} was derived using the experimental yield expression (Equation 5.1). As presented in Table 5.3, the simulated net SOA yield, which is the sum of all contributions by the sixteen individual compounds (determined from the Odum model), was calculated to be 2.87×10^{-3} $\mu g/m^3$.

Table 5.3: Estimates of the physical and modelling variables calculated for each of the products identified in the SOA sample derived from the photo-oxidation of 1,3-butadiene in NOx.

Species	Molecular Formula	MODELLING PARAMETERS					
		A	K_{om} ($m^3/\mu g$)	Hoffmann's Mass ($\mu g/m^3$)	Odum's Ca ($\mu g/m^3$)	Odum's Cg ($\mu g/m^3$)	Odum's Yield
Formaldehyde	$C H_2 O$	5.09E+05	7.34E-11	3.74E-5	5.43E-01	1.16E+09	2.39E-04
Formic acid	$C H_2 O_2$	2.00E+04	6.54E-09	1.31E-4	1.90E+00	4.54E+07	8.33E-04
Glycoaldehyde	$C_2 H_4 O_2$	5.95E+03	8.12E-09	4.83E-5	7.02E-01	1.35E+07	3.08E-04
Glycolic acid	$C_2 H_4 O_3$	3.53E+01	7.28E-07	2.57E-5	3.73E-01	8.03E+04	1.64E-04
Glyoxal	$C_2 H_2 O_2$	3.14E+04	1.26E-09	3.95E-5	5.74E-01	7.14E+07	2.52E-04
Glyoxylic acid	$C_2 H_2 O_3$	5.61E+01	2.20E-07	1.24E-5	1.79E-01	1.28E+05	7.89E-05
Glycerol	$C_3 H_8 O_3$	3.79E-03	1.02E-03	3.83E-6	5.56E-02	8.56E+00	2.44E-05
Glyceraldehyde	$C_3 H_6 O_3$	2.85E+00	1.19E-05	3.40E-5	4.94E-01	6.49E+03	2.17E-04
Glyceric acid	$C_3 H_6 O_4$	6.43E-02	3.71E-04	2.38E-5	3.46E-01	1.46E+02	1.52E-04
Hydroxypyruvaldehyde	$C_3 H_4 O_3$	2.39E+01	7.05E-07	1.68E-5	2.45E-01	5.44E+04	1.08E-04
Ketomalonalde-hyde	$C_3 H_2 O_3$	1.62E+02	4.36E-08	7.07E-6	1.03E-01	3.69E+05	4.51E-05
Threitol	$C_4 H_{10} O_4$	8.70E-05	3.12E-01	9.17E-6	1.32E-01	6.61E-02	5.79E-05
Erythritol	$C_4 H_{10} O_4$	2.40E-04	3.12E-01	2.53E-5	3.64E-01	1.82E-01	1.60E-04
Threose	$C_4 H_8 O_4$	4.64E-04	1.38E-02	5.89E-6	8.54E-02	9.70E-01	3.76E-05
Erythrose	$C_4 H_8 O_4$	6.96E-04	1.38E-02	8.83E-6	1.28E-01	1.46E+00	5.63E-05
Unknown 1**	$C_4 H_7 N O_7$	5.66E-05	1.64E+02	9.01E-6	1.29E-01	1.23E-04	5.66E-05
Unknown 2**	$C_4 H_7 N O_7$	5.66E-05	1.64E+02	9.01E-6	1.29E-01	1.23E-04	5.66E-05
Unknown 3**	$C_4 H_7 N O_7$	2.36E-05	1.64E+02	3.75E-6	5.36E-02	5.13E-05	2.36E-05
TOTAL				4.54E-4			**2.87E-03**

** tentatively identified as threonic/erythronic acid nitrate

The Hoffmann Model

The α and K_{om} parameter values reported in Table 5.3 were incorporated into Equation 5.3. In accordance with the Hoffmann model, each of the oxidant's reaction with 1,3-butadiene was considered separately so that an aerosol mass concentration formed from each oxidation reaction was determined. The mass concentration formed by each of the sixteen species was presented in Table 5.3. As previously mentioned, the species formaldehyde and formic acid are assumed to be the only products produced from the ozonolysis reaction, the unknowns (tentatively identified as threonic/erythronic acid nitrate) are assumed to be the only products of the nitrate reaction and all the other species are assumed to have been formed from the OH reaction with 1,3-butadiene.

The mass concentrations presented in Table 5.5 were converted to yield contributions using Equation 5.1 in order to maintain a common method of comparison for the two models. The main contributor to the formation of SOA is, therefore, the 1,3-butadiene reaction with OH, followed by the reaction with O_3 and the NO_3 reaction. The net yield calculated from the Hoffmann model is much less than the experimental yield and it is apparent that applying the Hoffman model to estimated parameter values of the 16 products does not produce good results. This may be due to the limitation in assigning one oxidation channel ($OH^{\cdot}$, $NO_3^{\cdot}$ and O_3) to a species observed in the aerosol sample.

Table 5.5: Results of applying the Hoffmann model to chamber observations for Experiment 52.

Mass concentration contributions by oxidant reaction ($\mu g/m^3$). (% of total mass concentration).			Hoffmann's Net Yield	Experimental Yield
$OH^{\cdot}$	$NO_3^{\cdot}$	O_3		
2.6E-4 (58%)	2.18E-5 (5%)	1.68E-4 (37%)	1.62E-7	2.807E-3

The information presented in Table 5.5 compares the yield determined by the Hoffman model (the Hoffman model's estimate of mass divided by the amount of butadiene

consumed) with the experimental yield determined for E52. The SOA mass concentration produced by each of the oxidation channels ($OH^{\cdot}$, $NO_3^{\cdot}$ and O_3) is also presented along with the proportion of the total mass (in percentage) produced by each of the channels. For example, the table shows that 2.6E-04 $\mu g/m^3$ of SOA has been attributed to be formed from the reaction of 1,3-butadiene with the hydroxyl radical which is about 58% of the total mass concentration of SOA produced in the experiment.

5.3.3 Derivation of $K_{om,i}$ and α_i from experimental data

The Odum Model

The second method applied to the models was to determine parameter values (α and K_{om}) for two products by fitting the model to the chamber data. Yield estimates for the five experiments were calculated from Equation 5.1 and a plot of yield versus the final mass concentrations (with one data-point for each experiment) could be produced. The Odum model was then fitted to the experimental plot and the model parameters for two products were determined from the best fit using the Origin software program produced by Microcal Enterprises. This plot is presented as Figure 5.1. A 95% correlation was observed between the Odum model and experimental data.

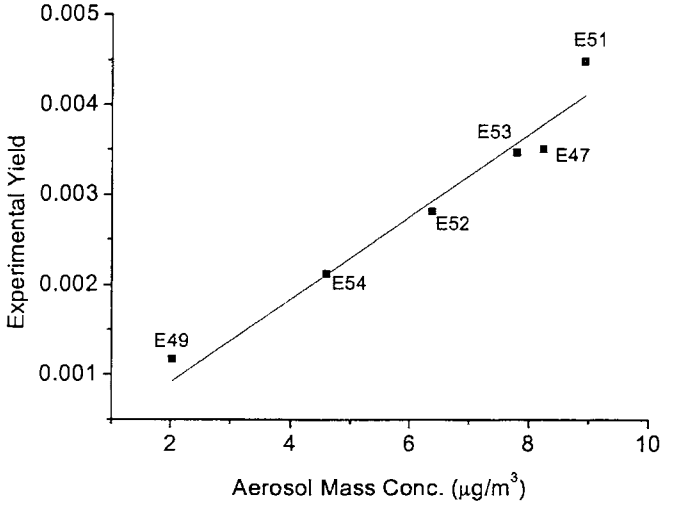

Figure 5.1: Yield versus aerosol mass concentration for six experiments (symbols) are fitted to the Odum model (line).

Assuming a two product model and using the procedure described by Odum et al. (1996), in which the experimental yield is calculated for each of the experiments and plotted against the maximum aerosol mass concentration generated during each experiment. The Odum model is then fitted to the dataset using the non linear fitting function provided in the *Microcal Origin* software program. The fitting function returns a chi- square indicator and a correlation coefficient, the correlation coefficient was used to assess the best fit. The parameter values determined for each product were:

Product 1, $\alpha = 0.0622$ and $K_{om} = 6.0E\text{-}04$ $m^3/\mu g$;

Product 2, $\alpha = 0.4305$ and $K_{om} = 1.0E\text{-}03$ $m^3/\mu g$.

A comparison between these parameter values and those estimated for each of the 16 products presented in Table 5.3, suggests that the K_{om} value of product 1 most closely represents that of glyceric acid (3.71E-04 $m^3/\mu g$) whilst the K_{om} value determined for product 2 is similar to that of glycerol (1.02E-03 $m^3/\mu g$). Based on these estimates, Product 1 most likely represents a low/medium saturation vapour pressure product, and product 2 a mid saturation vapour pressure product.

From the results above, it is apparent from the α values that Product 2 is far more likely to form than Product 1. The 1,3-butadiene system might be well represented as a 1 product model. When the Odum model is applied as 1 product model and fitted to the chamber data, the following plot is produced.

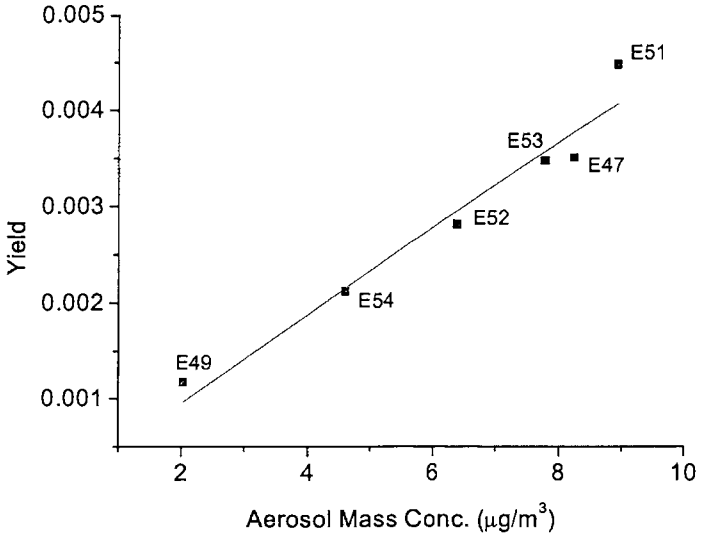

Figure 5.2: The Odum model as a 1 product model is fitted to the chamber data.

When the Odum model is applied as a 1 product model, the α value returned is 6.05E-02 and the K_{om} is equal to 8.0E-03. The species identified in the aerosol sample that have a calculated partitioning ratio closest to Product 1's are threose, erythrose and glycerol, so a low/medium vapour pressure product.

The Hoffmann Model

Fitting the Hoffmann model to experimental data is more complex since the model predicts the aerosol mass concentration for each time step throughout an experiment. The aerosol mass concentration produced and the amount of 1,3-butadiene consumed throughout the experiment was used to calculate the yield produced at each time step. The Hoffmann model (defined in Equation 5.3) was then divided by the total amount of 1,3-butadiene consumed to produce a yield estimate for each time step as shown in Equation 5.9. This model equation was fitted to the experimental plot to define α and K_{om} values for each of the three products (allowing one product to be produced from each oxidation reaction).

Equation 5.9 is essentially Equation 5.1 and Equation 5.3 merged together and is fitted to the experimental data of experiment E52 which is presented in Figure 5.3.

$$Y(t) = (M_0 + \Sigma_{ox}(\Delta ROC_{ox}(t)\ M_{n-1} \sum_{i=1}^{I}((\alpha_i K_{om,i})/(1 + K_{om,i} M_{n-1})))) / \Sigma \Delta ROC_{ox} \qquad (5.9)$$

where $Y(t)$ is the yield calculated per time-step, M_0 is the amount of aerosol in the system initially (experimental background in μg/m^3), t to a specific time step, M_{n-1} refers to the amount of aerosol produced in the previous time step, ox refers to the oxidant that is responsible for the consumption of the HC and ΔROC_{ox} is the amount of the hydrocarbon consumed by the oxidant (ox) specified.

The Hoffman model was fitted to the experimental data (E52) presented in Figure 5.3 as a 3 product model, with one product being produced from each of the oxidation reactions. By fitting the model to the experimental data an estimate of α and K_{om} was determined for each of the three products. The Hoffmann model is very successfully fitted to the chamber data which may in part reflect the large uncertainties associated with the parameter values estimated by the automated fitting function of the Origin software program.

Results of the fitting exercise are:
Product 1 (derived from OH oxidation), $\alpha = 0.005$, and $K_{om} = 0.137$ m^3/μg;
Product 2 (derived from NO_3 oxidation), $\alpha = 1.000$ and $K_{om} = 8.0E\text{-}03$ m^3/μg.
Product 3 (derived from O_3 oxidation), $\alpha = 0.335$ and $K_{om} = 1.0E\text{-}03$ m^3/μg.

The partitioning coefficients of Product 1 are similar to the calculated K_{om} of threitol and erythritol (3.12E-01 m^3/μg) , whereas Product 2's K_{om} is between that of glycerol's (1.02E-03 m^3/μg) and threose/erythrose (1.38E-02 m^3/μg). Product 3's K_{om} is similar to that of glycerol (1.02E-03 m^3/μg). Although the α value for the NO_3 reaction is much larger than the other oxidant's α values, this does not mean that more Product 2 was produced than the other two products. It means simply that the amount of product formed by the NO_3 reaction was the same as the amount of 1,3-butadiene consumed by the NO_3 oxidant (as estimated by the MCM).

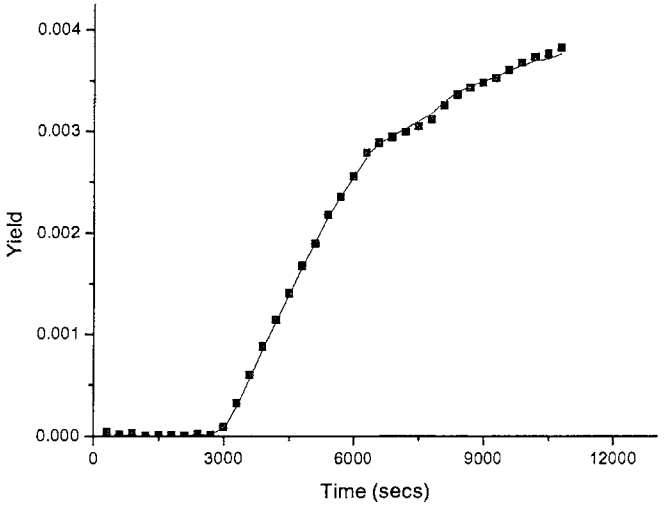

Figure 5.3: The Hoffmann model (line) is fitted to the experimental data (symbols) for E52.

5.3.4 Substitution of real product values into the Odum and Hoffmann models

The Odum Model

Parameter values for actual compounds identified in the aerosol sample were substituted into the Odum model to calculate a yield estimate. Of the sixteen products identified in the aerosol sample, certain products were identified to represent low, middle and high saturation vapour pressure products.

The products formaldehyde, formic acid, glycolic acid, glycoaldehyde, glyoxal and ketomalonaldehyde were grouped as high saturation vapour pressure products as their saturation vapour pressures were greater than 1.0 Torr. Mid saturation vapour pressure products were found to be glyoxylic acid, glycerol, glyceraldehyde, glyceric acid and hydroxypyruvaldehyde which have saturation vapour pressures less than 1.0 Torr but greater than 10^{-5} Torr. The low saturation vapour pressure products were identified to be threitol, erythritol, threose, erythrose and the nitrate species that had saturation vapour pressures less than 10^{-5} Torr.

Of the low vapour pressure group, threose and threitol had vapour pressures in the mid range of the group and so were selected as representative low vapour pressure products. Similarly, glyceric acid and glyceraldehyde were selected as mid vapour pressure products since their vapour pressures were the mid range of vapour pressures in this group. Partitioning coefficients and α parameter values for threose and glyceric acid were then incorporated into the Odum model. Combinations of other low and mid vapour pressure products were also incorporated into the Odum model for experiment E52 to determine whether they produced a yield estimate that is similar to the experimental yield. The results are presented in the following table:

Table 5.6: Yield calculated for E52 using the real products into the Odum Model.

Product 1	Product 2	Calculated Yield from the Odum Model	Experimental Yield
Threose	Threitol	9.766E-05	2.807E-03
Threose	Glyceric Acid	6.222E-05	2.807E-03
Glyceric Acid	Glyceraldehyde	2.460E-04	2.807E-03
Glyoxal	Glyceraldehyde	2.618E-04	2.807E-03

Using Odum as a 2 product model and substituting model parameters with actual calculated values for specific species does not produce a good result. These results are at least, one order of magnitude smaller than the experimental yield. This indicates that the parameter values determined by fitting experimental data to the Odum model as a 2 product model represent theoretical products rather than actual products. This is possibly due to the fact that the saturation vapour pressure of an actual product will be much less than the saturation vapour pressure of a theoretical product that represents the whole system (and a suite of products). The saturation vapour pressure is a very sensitive parameter as both the $K_{om,i}$ and the α are functions of saturation vapour pressure.

Following on from the two product model format, all low saturation vapour pressure products (less than 1.0 Torr) were grouped to represent the first product in the Odum model. All other actual products (medium and high saturation vapour pressure products) were grouped to represent the second product. The saturation vapour pressures of the two lumped products were the combined vapour pressures of their constituents, following Dalton's law of partial pressures. K_{om} and α parameter values were recalculated as the average value for the two products and a yield estimate was determined using the Odum model. The yield was calculated as 2.807×10^{-3} which is the same result as the yield calculated from the sixteen product model exercise undertaken in Section 5.3.2.

The Hoffmann Model

When substituting actual product values into the Hoffmann model, the selection of products was limited. As in Section 5.3.2, only formaldehyde or formic acid (which are both high vapour pressure products) could be used to represent the reaction of 1,3-butadiene with ozone. Similarly, threonic/erythronic acid nitrate (tentatively identified) was the only product that could be used to represent the reaction of the nitrate radical with 1,3-butadiene. The hydroxyl radical reaction with 1,3-butadiene could be represented by numerous products but glyceraldehyde and threose were selected as representatives for the mid and low vapour pressure groups, respectively.

The contribution to the net SOA mass produced by each of the oxidation reactions is presented in Figure 5.4. The products that formed the most SOA resulted from the OH reaction with 1,3-butadiene and the least amount of SOA was produced from the reaction of 1,3-butadiene with NO_3. The net mass of SOA produced by all 3 oxidation reactions for each time-step is compared with the aerosol produced in the chamber (experimental SOA) and is shown in Figure 5.5. This figure illustrates that the Hoffmann model, like the Odum model, should not be applied in this way although this

method produces better results than substituting the parameter values of all 16 products into the Hoffman model (as presented in Section 5.3.2).

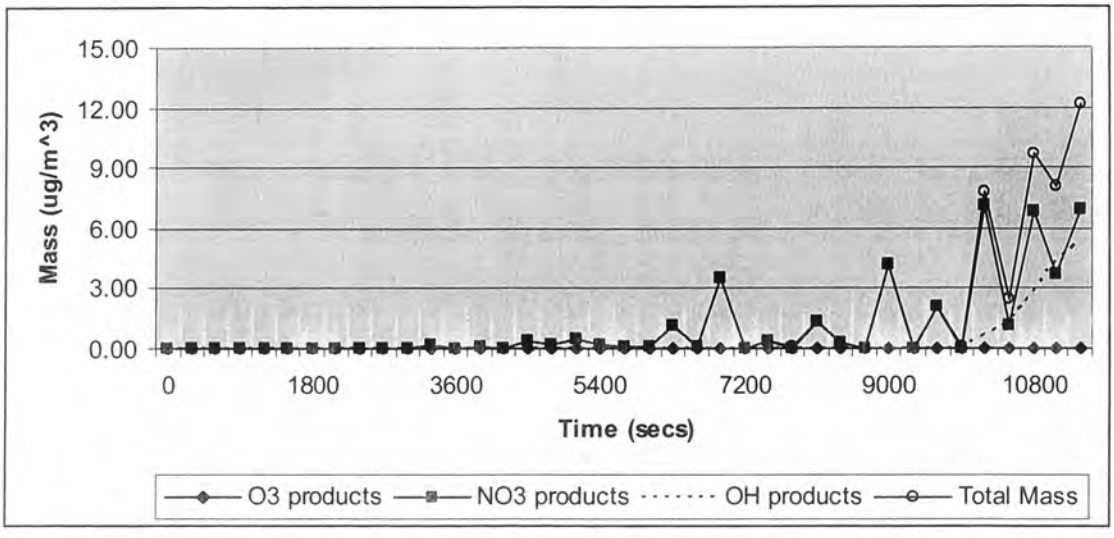

Figure 5.4: Mass concentration values resulting for incorporating 2 and 3 products for each oxidation reaction into the Hoffmann model for E52.

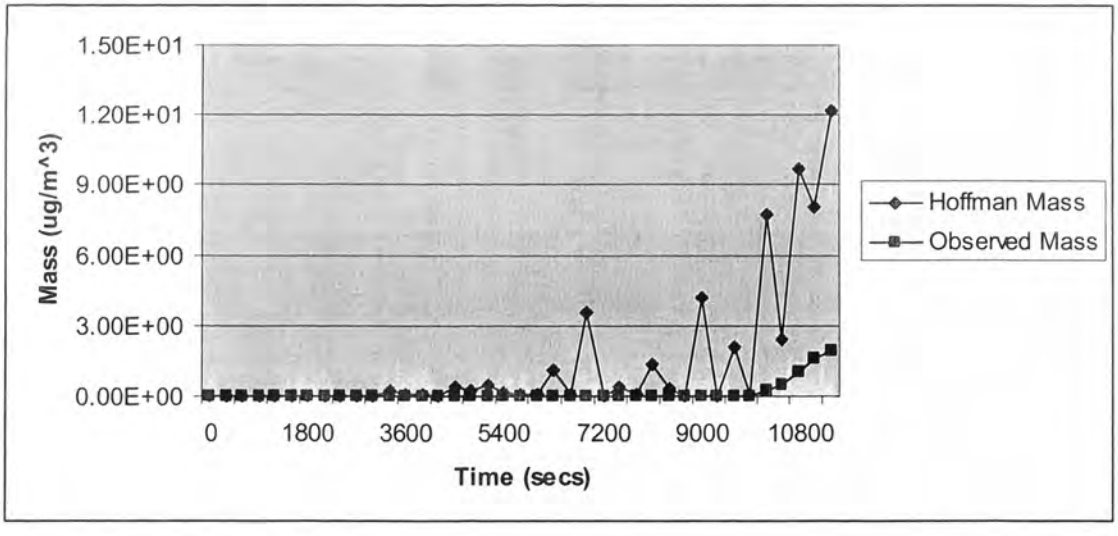

Figure 5.5: Mass concentration formed from the sum of the oxidation reactions using the Hoffman model (shown in Figure 5.4) and the observed mass produced during experiment E52.

5.4 Discussion

When applying the Odum and Hoffmann models as 16-product models, both models produced reasonable estimates of yield when compared with the experimental yield. The Odum model consistently produced results within 10% of the experimental yield for an additional four experiments. The average deviation between the experimental yield and the yield estimates determined by the Odum model was about 3%.

For the Hoffmann model, the species identified in the aerosol sample of Angove et al. (2006) were required to be grouped as products of an ozonolysis, nitrate or hydroxyl radical reaction with 1,3-butadiene. This assumption was made so that the Hoffmann model could be applied in this way, although in reality, some species may be produced by more than one of the oxidation reactions. The grouping of products into a principle oxidation reaction may account for the difference in yield estimates between these results and the experimental yield. For this reason, the Hoffmann model was only applied to one data-set in Section 5.3.2.

The Odum model produced a strong agreement when fitted to experimental data. The parameter values (α and K_{om}) of the two products derived from the fitting exercise may represent a low vapour pressure product and a mid vapour pressure product, although no actual products identified in the aerosol sample collected by Angove et al. (2006) closely represented the fitted product's profile. These results indicate that the two products produced from fitting are in fact hypothetical and represent the whole 1,3-butadiene/NOx system rather than actual products.

The Hoffmann model was similarly fitted to experimental data with good results. A correlation of about 99% was observed between the model equation and the experimental plot. The fit enabled six parameter values for the Hoffmann model to be determined, which represented one product per oxidation reaction. The large uncertainties associated with the estimated parameter values may be indicative of the

experimental suite's initial conditions (ROC and NOx concentrations) being very similar. The amount of UV light was the experimental variable that changed a lot from experiment to experiment and this parameter is not considered in either of these models.

The yield was underestimated when parameter values for actual products were substituted into the Odum model and the Hoffmann model. Combinations of 2 and 3 products produced net yield results that were much lower than the yield calculation by the experimental yield and the observed experimental mass concentration in the case of the Hoffmann model. When combinations of products were grouped together to represent two theoretical products (and their vapour pressures added together to recalculate the model parameters), the yield estimate was found to be the same as the yield calculated from a sixteen product model application. It can therefore be assumed that the saturation vapour pressures are the significant parameter that defines the yield, as both K_{om} and α are functions of the saturation vapour pressure.

In summary, the Odum model can successfully be applied to estimate aerosol yield for 1,3-butadiene using either of two methods: by substituting parameter values of all of the aerosol compositional species, or by fitting the model to chamber data. The Hoffmann model produces the best results when it is fitted to the chamber data.

Chapter 6: The Secondary Organic Aerosol Profile Empirical Model (SOAPEM)

6.1 Introductions

An empirical model is presented that simulates the temporal variation of SOA mass concentration formed during isoprene and α-pinene chamber experiments. There are currently a few modelling techniques that estimate the mass of SOA produced at the end of a time period, or a maximum amount of SOA, but to the author's knowledge, there are none that simulate the evolution of SOA concentrations over time throughout an experiment other than the near explicit MCM model described in Chapter 4. Within an air pollution context, the daily or annual mean values of $PM_{2.5}$ are monitored and reported on. As discussed in Chapter 2, Australia has National Environmental Pollution Measures (NEPMs) which are ambient concentration standards that should not be exceeded. The mass concentrations of SOA in the airshed are important in this context because they form a significant fraction of $PM_{1.0}$ and $PM_{2.5}$ (Baltensperger et al., 2005). Since air pollution events are monitored over time (not as static events), the aerosol mass concentration preceding a high aerosol pollution event and after the event is also significant, and so an indication of the SOA mass concentration over time is important to consider.

The SOAPEM has been developed to address one of the limitations of the current empirical modelling techniques that estimate the amount of SOA formed from a mixture of hydrocarbons. As discussed previously, the net yield of a mixture of hydrocarbons is not the sum of their individual contributions, which is the premise on which most air quality SOA modules are based. The SOAPEM identifies another approach to estimating the net SOA yield for a mixed system from a purely empirical perspective and as such counters the complexity of the SOA formation processes by treating the SOA formation as a whole system rather than as components of individual hydrocarbon reactions. However, the SOAPEM is in its infancy and requires much more chamber data before it can be applied with confidence. It has been presented in this chapter as a potentially different approach to a modelling problem.

If the chamber experiments contain more than one hydrocarbon, the SOA profile produced will be the resultant SOA yield of the mixture, hence alleviating the need to work out the individual yields and add them together. It is also possible that if the chamber experiments were undertaken to reproduce atmospheric conditions and the hydrocarbon mixture was representative of the ambient hydrocarbon burden, the SOA profile produced from these experiments will be a reasonably accurate way of estimating the ambient SOA concentration. In order for a model to be useful within an experimental context (where there is little information available about the composition of the aerosol and the systems are largely unknown), a minimal amount of initial information is desirable. Once SOAPEM has been defined by a suite of chamber experiments, all that is required to produce an SOA profile is the initial concentrations of the precursor hydrocarbon and NOx species as input data.

There is great variation between different laboratories' set-ups and experimental procedures, and as such, experimental results vary. The empirical method described in this chapter is not intended to provide yield estimates for all chambers, but rather is presented as a predictive tool that can be defined by each laboratory. Its strength lies in the fact that once it is defined, the model requires little information to provide an estimate of the temporal variation in SOA mass concentrations throughout an experiment.

The development of the empirical model was based upon three key observations:
(i). The aerosol mass concentration time-series profile of the aerosol mass concentration throughout an experiment follows a distinct sigmoidal shape.
(ii). The SOA reaches a maximum aerosol mass concentration and then either plateaus or declines.
(iii). The time of aerosol formation (onset time) varies from chamber experiment to chamber experiment.

A typical aerosol mass concentration time-series profile for an isoprene photooxidation chamber experiment is presented in Figure 6.1.

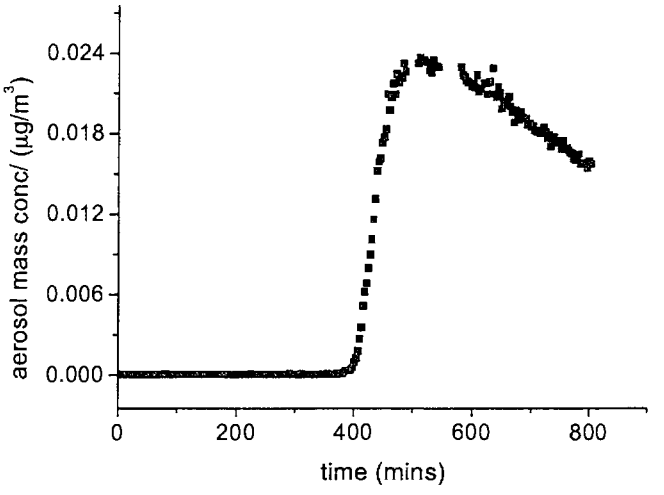

Figure 6.1: Evolution of the SOA mass concentration throughout E304.

Similar time-series profiles have been observed by other laboratories (Jaoui and Kamens, 2001; Takekawa et al., 2003; Stroud et al., 2004; Ng et al., 2006; Presto et al., 2005; Kroll et al., 2006). The majority of chamber experiments presented in the literature have an initial seed concentration introduced before the experiments commence. Consequently, the initial nucleation events are often not observed, and hence the growth of aerosol is presented from the time that the aerosol formation increases rapidly. The effect of pre-seeding an experiment has little effect on the maximum aerosol mass concentration formed during an experiment if the seed introduced to the chamber is dry and non-acidic (Czosche et al. 2003). The maximum amount of SOA formed from these experiments should then be comparable to other laboratory's experiments if the initial conditions are the same.

Kroll et al. (2006) suggest that seeds are necessary for reducing the number of very small particles produced when condensable seed particles are not available. They suggest that the majority of these small seeds are lost to the chamber walls. From the experiments presented here, the initial aerosol is detected at 12 nm and it is the same

population that grows to have a median diameter of about 80 nm. It is possible that much of the smaller aerosol does stick to the chamber walls, and the data are corrected to account for this, but the number and mass concentration is observed to increase and the aerosol population maintains it's log normal distribution profile. In any case, it is imperative for the empirical model described here to incorporate an estimation of onset time (formation of SOA), as it affects the aerosol mass time series profile.

The decline in aerosol concentration after reaching a maximum mass concentration may be due to wall losses or by ageing and further oxidation of the aerosol mass since the chamber is sealed and dilution does not take place. Kroll et al. (2006) observed this effect during isoprene photooxidation chamber experiments where the NOx concentration was less than 1 ppb. They concluded that it was likely a photochemical event and attributed it to be photochemical ageing or oxidative processing of the SOA. AMS results indicate that the aerosol composition changes during this time of mass concentration decrease (Kroll et al., 2006).

Kalberer et al. (2006) found that the oligomers produced from isoprene photooxidation formed soon after SOA onset. They also found that during the experiment the oligomers reached a maximum rate of formation and that the number average molecular weight and weight average molecular weight (which are measures of the molecular size distribution of polymers and oligomers) were either almost constant throughout the experiment or increased slightly. The oligomers studied throughout the experiments reached a maximum chain length which Kalberer et al. (2006) suggested pointed to an efficient termination reaction for the oligomerisation reactions. It is possible that these observations are the result of an artefact caused by the instrumental technique. Although the molecular size growth ceased at some point during the experiment, Kalberer et al. (2006) found that the total mass concentration continued to increase slowly due to further oxidation processes. The longer experiments presented in that work must therefore have a loss process that is greater than the mass increase formed from an oligomerisation process.

The sigmoidal model described here does not simulate the decline in aerosol mass concentration occurring at the end of the experiment as observed for the isoprene / NOx system. This observation is not seen in the α-pinene experiments and has not been observed for other systems discussed in the literature. In the interest of keeping the SOAPEM applicable to many systems, the decline in aerosol mass concentration has not been included.

In the isoprene photooxidation experiments presented in this chapter, it is likely that two oxidation events are observed in the SOA time series profile as presented in Figure 6.2. It can be seen from this figure that the time series profile has two peaks, one earlier in the experiment and a final, larger one at the end. Surratt et al. (2006) found that one of the main primary isoprene oxidation products, methacrolein, when oxidised formed products that readily oligomerised to form SOA. The earlier peak is then thought to be produced from the photooxidaton of isoprene and the second peak formed from the photooxidation of methacrolein. This is one explanation for the two peaks observed, but further exploration is required before that can be clarified. This is another unique feature of the SOA temporal profile formed from isoprene photooxidation.

Equation 6.1 is used as a basis for the development of the empirical model and will be referred to herein as the sigmoidal equation.

$$M(t) = A2 + [(A1 - A2) / (1 + e^{((t-tO)/dT)})] \qquad 6.1$$

where $M(t)$ is the concentration of aerosol mass produced during a chamber experiment ($\mu g/m^3$) and t is time (sec). $A2$ is the maximum aerosol mass concentration produced ($\mu g/m^3$), $A1$ is the concentration of aerosol mass in the chamber prior to the onset of SOA ($\mu g/m^3$), dT is the width (on the t-axis) of the increase in SOA mass concentration and the tO is the pivot point of the curve (measured on the t axis). The four parameters $A2$, $A1$, dT and tO are illustrated in Figure 6.2.

The sigmoidal equation was chosen as it is the simplest formula of the required shape that represents the aerosol mass concentration time-series profile observed from chamber experiments. The intention of this work is not to identify the best fitting function but one that represents the observed shape with variables that could be used to represent the key features of the aerosol mass concentration time-series profile.

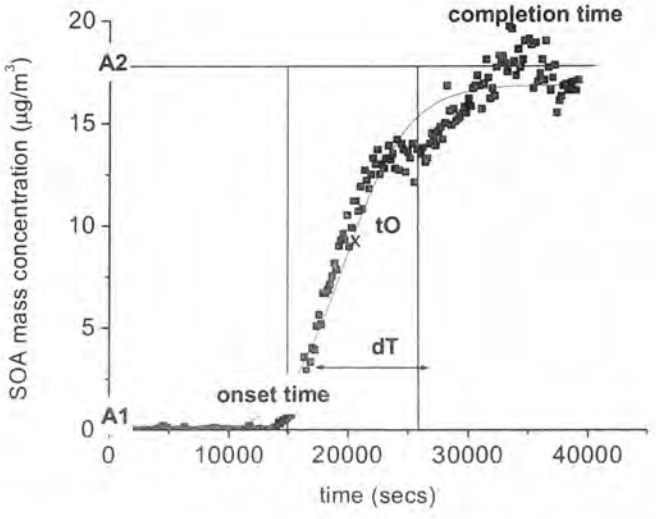

Figure 6.2: Sigmoidal equation parameters (*A1*, *A2*, *tO* and *dT*) when fitted to chamber aerosol mass concentration data collected during experiment E303.

6.2 Experimental Observations

Of the experiments presented in Chapter 3, several were continued long enough to produce a maximum aerosol mass concentration (see below). E304 looks as though it might have reached its maximum aerosol mass concentration, but because there is no decline in the aerosol mass concentration, this is uncertain. This experiment has been retained in the dataset and included in the development of the empirical model in order to test the model's ability to predict SOA profiles for experiments yet to reach their maximum aerosol mass concentration.

The sigmoidal equation was fitted to the four isoprene experiments initially, by using an automated function of the software program *Microcal Origin*, and later by manually fitting the function to the dataset to fine tune the fit. The error estimates for the fit of Equation 6.1 to the SOA profiles were generated from the software program and retained for the manual fit as best estimates. The model parameters and correlation details are given in Table 6.1. It is apparent from the parameter values presented in Table 6.1 that the sigmoidal equation describes the shape of the SOA profile closely since the correlation coefficient, R^2, is greater than 93% in all cases as shown in Figure 6.3.

Table 6.1: Sigmoidal equation fits to SOA formed during the isoprene photooxidation.

Expt	R^2 (%) fit	Sigmoidal Equation Parameters			
		A1 ($\mu g/m^3$)	A2 ($\mu g/m^3$)	tO (secs)	dT (secs)
303	99.2	0.2 ± 0.05	8.4 ± 0.05	16 000 ± 85	2000 ± 70
304	99.7	2E-5 ± 1E-6	2.64 ± 0.02	37 200 ± 75	3450 ± 60
308	94.5	0.07 ± 0.07	5.3 ± 0.05	15 000 ± 170	2100 ± 150
309	93.5	0.005 ± 0.002	1.82 ± 0.04	22 500 ± 300	2000 ± 280

6.2.1 Maximum aerosol concentration

As depicted in Figure 6.1 the aerosol mass concentration reaches a peak and then gradually starts to decline. As discussed previously, most air quality models are interested in determining the maximum aerosol mass concentration, as a worst case scenario. This empirical model is able to simulate the profile of the mass concentration but does not consider the decline in mass towards the end of the experiment which clearly occurs in the isoprene system as discussed previously.

It has been common practise to consider 'yield' as a constant value specific to a hydrocarbon thereby giving an indication of the aerosol forming potential of that hydrocarbon. In this work and described in the literature, the yield of a specific hydrocarbon has been found to vary with the amount of hydrocarbon consumed (Kroll et al., 2005).

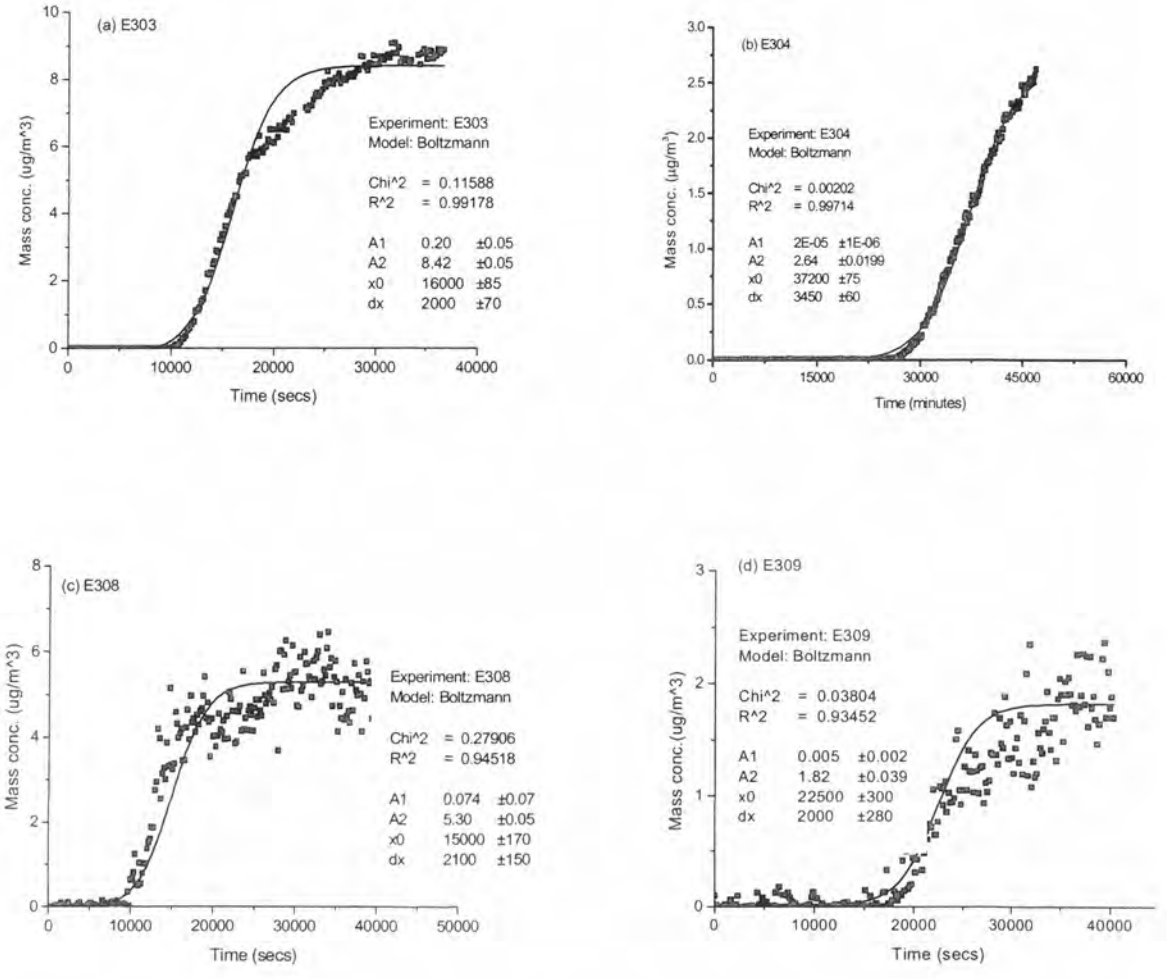

Figure 6.3: The sigmoidal model (line) is fitted to the aerosol mass concentration time-series profiles (closed symbols) for experiments 303, 304, 308 and 309.

A strong correlation between the maximum aerosol mass concentration and the initial isoprene concentration for chamber experiments is observed. Kroll et al. (2005) also comment on the relationship between the hydrocarbon consumption and the amount of SOA produced in the isoprene system. In the experiments of Kroll et al. (2005), initial seed aerosol is introduced to the chamber prior to the experiments (from 10.0 to 25.6 $\mu m^3 / cm^3$), and so only absorption processes and condensed phase reactions would have occurred. This may account for the higher aerosol yields observed by Kroll et al. (2005), however a relationship between the initial isoprene concentration and the amount of aerosol mass produced is observed.

For the isoprene experiments undertaken for this work, an exponential was found to represent the relationship between the initial isoprene concentration and the aerosol mass concentration. A 94% correlation is observed between the isoprene chamber data (symbols) and an exponential as shown in Figure 6.4. An exponential equation (Equation 6.2) has been chosen to represent the relationship between the aerosol mass concentration produced and the amount of isoprene consumed in each experiment because it has the best correlation with the dataset in comparison to other equations (eg. linear, polynomial equations).

As yield can be calculated as the ratio of the amount of aerosol mass produced to the amount of hydrocarbon consumed (as defined in Equation 5.1), the exponential depicted in Figure 6.4 can, therefore, be considered as a yield curve. This indicates that the yield does vary as a function of the amount of hydrocarbon consumed.

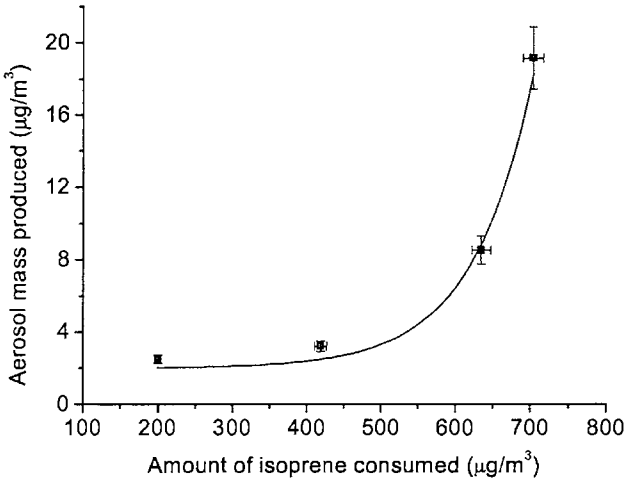

Figure 6.4: The amount of isoprene consumed the amount of SOA produced against the amount of isoprene.

As shown in Figure 6.4, the amount of aerosol mass can be determined from:

$$A2 = (2.02 \pm 0.12) + (0.0027 \pm 0.0005)\, e^{x/(81 \pm 6)} \quad (6.2)$$

where $A2$ is the maximum aerosol mass concentration ($\mu g/m^3$) and x is the amount of isoprene consumed ($\mu g/m^3$).

As with all the parameter relationships presented in this chapter, usually only four experiments are used to identify relationships between the model parameters and observed variables (like precursor concentrations). The equations presented that define these relationships are therefore limited to the range of x values depicted on the x-axis (eg. the amount of isoprene consumed for the onset time determination). With further experimentation and an increasing number of datasets, the relationship between these two variables should become more clearly defined and the need for limits of the x variable may not be required.

6.2.2 The onset time for SOA formation

The second key observation is the relationship between the time that SOA became detectable (with diameters greater than 12 nm) and the square of the isoprene concentration over the NOx concentration, as shown in Figure 6.4. Even though a few laboratories have undertaken experiments without the addition of seeds, the initial time of SOA formation has not been reported in the literature. In our isoprene experiments, the smallest diameter size detectable was 12 nm. Since it is likely that the initial SOA formed is smaller than this, it could only be detected once it had grown past the 12 nm detection limit. The SOA onset time used here is therefore the time that aerosol was observed at this point (12 nm) for at least three consecutive time points. Hence the onset time is, the 'detectable' onset time. The onset time was measured for all chamber experiments including those that were not continued long enough to produce a maximum aerosol mass. Table 6.2 presents the onset time of SOA formation observed for each of the isoprene experiments.

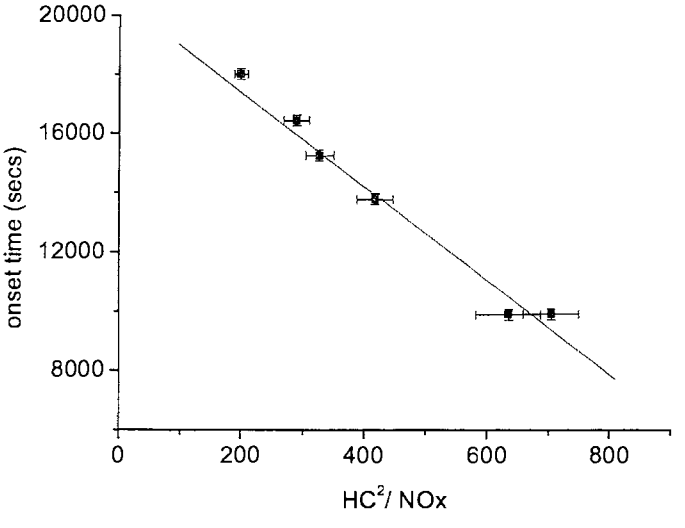

Figure 6.5: The time of SOA onset versus the square of the isoprene concentration over the NOx concentration.

Figure 6.5 shows the onset time of SOA detection compared to the HC^2/NOx for each of the isoprene experiments listed in Table 6.2. The time of SOA onset can be calculated using Equation 6.3:

$$Onset\ time = (20562 \pm 17) - (15.9 \pm 1.1)x \quad (6.3)$$

where the *Onset time* is calculated in seconds, and x is HC^2/NOx which are both in ppb.

Table 6.2: Observed SOA onset times for isoprene photooxidation experiments.

Expt No.	Initial HC conc. (ppb)	Initial NO conc. (ppb)	Initial NO_2 conc. (ppb)	HC^2/NOx	ROC/NOx	Observed onset time (secs)
203	188	106	2	328	8.7	15250
204	201	135	4	291	7.2	16450
303	257	105	0	705	11.3	9900
304	73	34	1	200	10.6	18000
308	232	80	11	635	13.2	9900
309	153	44	0	418	14.4	13800

The relationship shown in Figure 6.5 between the onset times and the HC^2/NOx was identified by trial and error. A purely empirical approach was adopted to represent the observed onset time with a precursor concentration. For the isoprene system, this parameter was best represented by HC^2/NOx and a linear equation produced the best fit to the dataset. Although the correlation between the linear equation and the six datasets is very strong no attempt is made to explain this relationship and it appears in this work as an observation and used as an empirical representation. The only thing that is obvious from this relationship is that both the HC and NOx concentration influence the onset for SOA formation and the onset time is more sensitive to the HC concentration than the NOx concentration.

6.3 Development of SOAPEM

The correlation between the temporal evolution of SOA formed during the isoprene experiments and the fitted sigmoidal equation was consistently strong, as shown in Table 6.1. The sigmoidal equation has four parameters shown in Figure 6.2. Since the sigmoidal equation is used as a platform for the empirical model, the four parameters are therefore defined in terms of the two key observations, onset time and maximum aerosol mass concentrations. Determination of the onset time and maximum aerosol mass from the initial hydrocarbon and NOx concentrations (as described in Section 6.2), are the reference points from which the other model parameters are determined. In this section, all the equations chosen to represent the relationship between the model parameters and the chamber observations (like precursor concentrations, onset times) have been chosen as either an exponential curve or a linear fit depending on which returned the highest correlation with the data. This approach is consistent with the purely empirical nature of the model.

6.3.1 The *A1* parameter

The *A1* parameter for the four isoprene chamber experiments varied from 2.0×10^{-5} to 0.2 $\mu g/m^3$, as depicted in Table 6.1. In these experiments, the *A2* value was at least 40 times greater than the *A1* value. The *A1* value defines the minimum amount of SOA produced in the experiment which pertains to background levels. For these reasons, *A1* will be set to zero.

6.3.2 The *A2* parameter

The *A2* parameter is the maximum aerosol mass concentration produced in the experiment; in this work it is represented by its relationship with the initial hydrocarbon concentration as discussed in Section 6.2.1. As depicted in Figure 6.4, the relationship between the amount of isoprene consumed and the aerosol mass concentration can be represented by an exponential function that was fitted to the dataset with a 97.4% correlation as shown in Equation 6.2. The valid domain for Equation 6.2 is for x values between 200 and 700 $\mu g/m^3$ of isoprene.

6.3.3 The *tO* parameter

The pivot point of the sigmoidal curve is marked on the x axis by the *tO* parameter, as depicted in Figure 6.2. If the data fitted the sigmoidal curve perfectly, the *tO* parameter would occur mid-way between the time that the aerosol formation increases exponentially (defined as the time of onset) and the time that the aerosol reaches its maximum mass concentration (*A2*), referred to herein as the 'completion time'. A symmetry would be observed between the time between *tO* - onset time and completion time - *tO*. A relationship between *tO* and the onset time is shown in Figure 6.6.

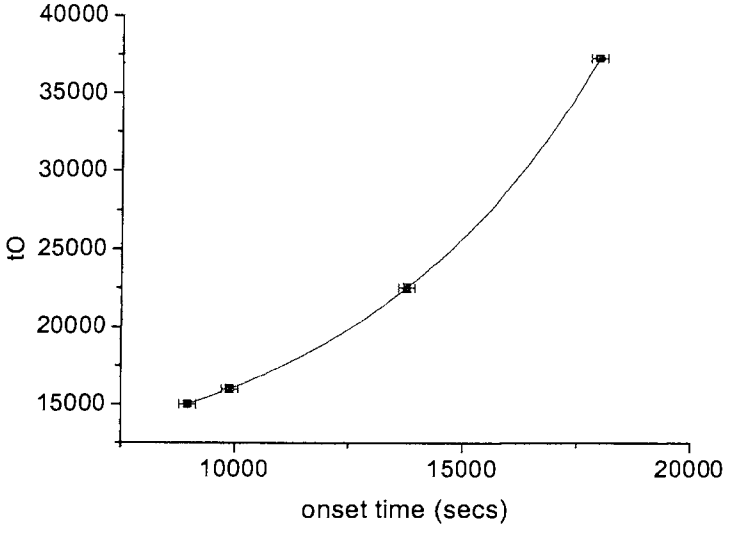

Figure 6.6: *tO* model values plotted against the onset time for the 4 experiments.

A correlation of almost 100% is observed between the curve and the data points, and the relationship representing this is given as Equation 6.4:

$$tO = (9523 \pm 28) + (1095 \pm 12)\, e^{x/(5572 \pm 37)} \qquad (6.4).$$

where x is the onset time (sec) between 5000 and 18 000 seconds.

Analysis of Figure 6.2 indicates that a relationship between the onset time and *tO* should be equal to half the time it takes to reach the completion time from the point of

onset, since the sigmoidal curve is symmetrical. The time it takes to reach the completion time (max. aerosol mass) for the four experiments is given in Table 6.3. If the sigmoidal curve fits the experimental aerosol profiles well, a similar relationship should still be observed. When the time taken to reach the completion time after onset is plotted against the time between onset and *tO*, a linear relationship is observed as shown in Figure 6.7.

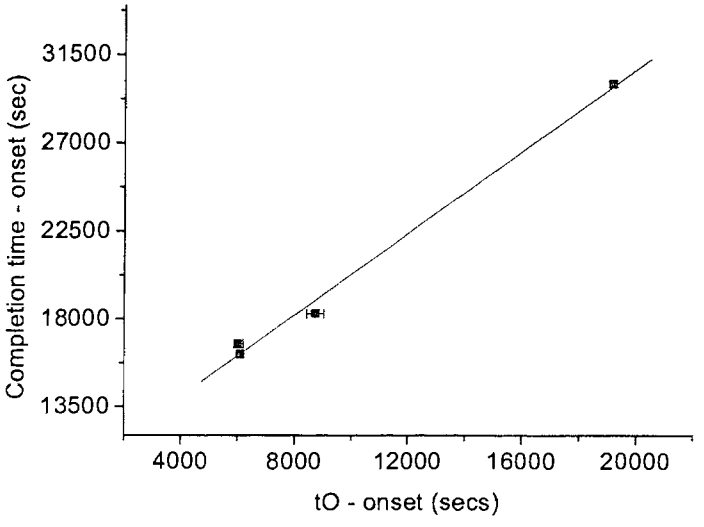

Figure 6.7: The difference in time between the onset time and tO is plotted against the time difference between the onset time and the completion time.

If the experimental SOA profiles were perfectly symmetrical, the completion time - onset time would be twice the *xO* - onset time value. Figure 6.7 illustrates that this is not the case for the isoprene experiments which may account for the 7% discrepancy between the SOA profiles and sigmoidal equation (given in Table 6.1).

6.3.4 The *dT* parameter

The *dT* value represents the width on the t-axis between the 30th and 70th percentile, which is usually slightly less than the time difference between the onset time and the completion time (as depicted in Figure 6.2). The *dT* parameter is a measure of the reactivity of the experiment; a low value (narrow width across the t-axis) indicates a

very rapid production of SOA, whereas a large *dT* value indicates a slow experiment. A relationship between the onset time and the *dT* parameter is shown in Figure 6.8.

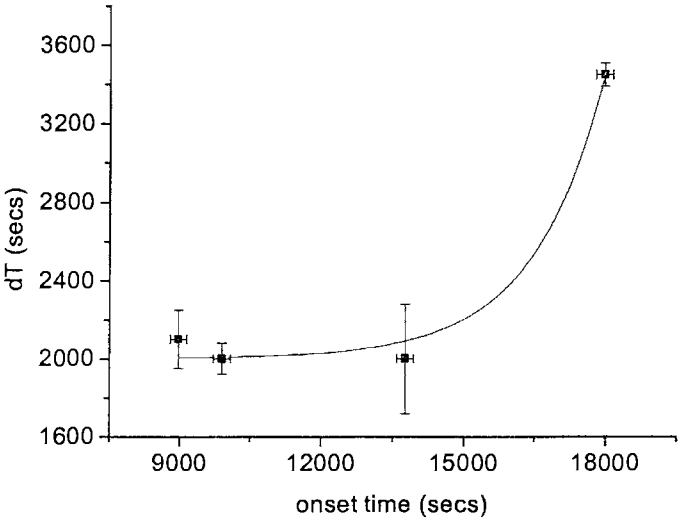

Figure 6.8: Onset time vs. the *dT* parameter.

An exponential function can be fitted to the experimental data with a strong correlation ($R^2 = 99\%$). The parameter value for *dT* can then be determined as:

$$dT = (2001 \pm 5) + (0.01 \pm 0.002)\, e^{x/(1522 \pm 43)} \tag{6.5}$$

where x is the onset time (sec) and the valid domain for Equation 6.5 is for an onset time between 8000 seconds and 18,000 seconds.

6.4 Model Profiles vs. Chamber Profiles

Once the maximum aerosol mass concentration (*A2*) and onset time were calculated from the initial isoprene and NOx concentration, using Equation 6.2 and 6.3 respectively, the other model parameter values were determined. The observed *A2* and onset times are compared to the *A2* and onset times determined by the model, which are presented in Table 6.3.

Table 6.3: A comparison between the observed and modelled *A2* and onset times.

Expt	Chamber A2 ($\mu g/m^3$)	Modelled A2 ($\mu g/m^3$)	% difference	Chamber Onset time (secs)	Modelled Onset time (secs)	% difference
303	13.6	12.8	6	9901	10678	8
304	2.6	2.0	23	18000	18110	1
308	5.8	6.7	16	8978	10947	22
309	1.95	2.4	23	13780	12006	13

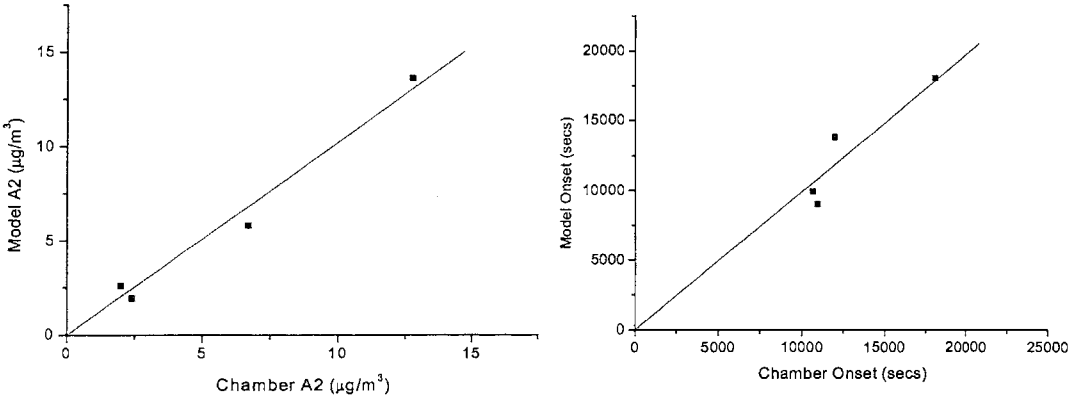

Figure 6.9: A comparison between the model output and the chamber data for the A2 parameter and for estimating the time of onset.

The largest difference between the observed *A2* values and the modelled values was 23% for both E304 and E309. The average for the four experiments was 17%. A comparison between the modelled onset times and the onset times observed for the chamber experiments (presented in Table 6.3) indicates that the maximum difference was 22% for E308 and the average for the four experiments was a difference of 11%, with one simulated result almost equalling the observation (E304).

A comparison between the model results and the chamber observations for the A2 parameter and the onset time are presented in Figure 6.9. A line was fitted to the datasets to identify the level of agreement between the model and the data using the same method described previously. A correlation of 99% and a standard deviation of 0.001 was observed for the A2 parameter which means that there is very good

agreement between the model and the data. A correlation of 93% and a standard deviation of 0.025 was found for the onset time dataset (model versus chamber) indicating less agreement between the model and the chamber data for this parameter but still, a good result.

Figure 6.10 illustrates a comparison between the SOA profiles determined from the model to the observed profiles returned from chamber experiments. As depicted in Figure 6.10, the model simulated the SOA profile best for E309, but underpredicts SOA formation for E304 and overpredicts SOA formation for the experiment E308. The difference between the observed maximum aerosol concentration and that produced by the model is at most $0.7\mu g/m^3$ for E304 which has a maximum aerosol mass concentration of 2.6 $\mu g/m^3$. In this experiment (E304), the aerosol profile looks as though the SOA mass concentration is about to plateau or decrease at the end of the experiment. This is assumed to be the case, although it could also account for the discrepancy between the observed and simulated SOA profiles. Although the results presented in Figure 6.10 are a comparison of the model against the same experimental data that was used to calibrate the model, these results indicate that the methodology is promising and further investigation and defining of parameter relationships with chamber data is warranted.

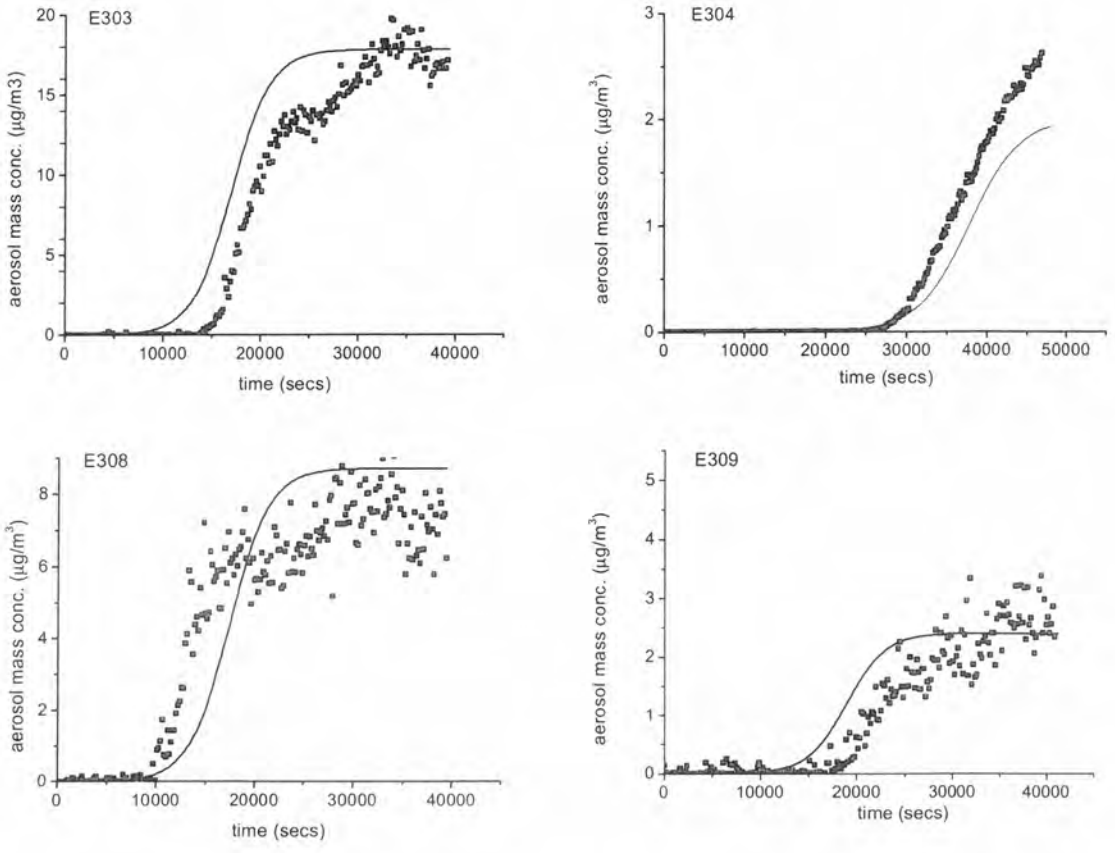

Figure 6.10: A comparison between observed SOA formation over time (symbols) and the simulated profile (line) for four isoprene chamber experiments.

6.5 α-Pinene/NOx system

In this section, the methodology developed in the preceding sections for the isoprene / NOx system has been applied to the α-pinene / NOx system. The initial experimental conditions and observations for the α-pinene experiments are presented in Table 6.4. The four experiments presented in Table 6.4 have all reached a maximum aerosol mass concentration. The aerosol mass concentration plateaus once it has reached this peak mass concentration, unlike the isoprene experiments where the aerosol mass concentration gradually declined.

Table 6.4: Chamber experimental details for the α-pinene experiments.

Expt No.	Initial HC conc. (ppb)	Initial NO conc. (ppb)	Initial NO_2 conc. (ppb)	ROC/NOx	Observed onset time (secs)
230	309	241	3	8.3	4631
231	180	245	8	7.6	11421
311	225	55	0	40.9	3224
313	173	140	2	12.2	5183

6.5.1 Estimation of onset times

For the α-pinene experiments, the aerosol is initially observed to form with diameters between 100 and 200 nm. The onset time was calculated from the time the aerosol was observed in this range for three consecutive time steps. To clarify, the aerosol did not grow in this range and move to detectable limit as is thought to occur in the isoprene experiments, rather the SOA partitioned from the gas phase and appears in this range of diameters, initially as a result of homogeneous nucleation. In the isoprene system, a relationship between the HC^2/NOx initial concentrations and the time of onset was observed. A relationship between these two variables was also found for the α-pinene system as shown in Figure 6.11.

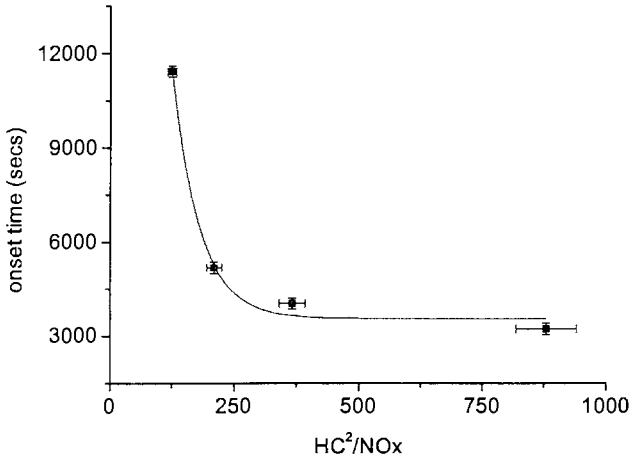

Figure 6.11: A correlation is observed between the time of SOA onset and the initial HC^2/NOx for the α-pinene / NOx system.

For the α-pinene system, onset times can be calculated from Equation 6.6;

$$Onset\ times = (3552 \pm 101) + (79231 \pm 1231)\exp^{-x/(55\pm10)} \quad (6.6)$$

where x is HC^2 / NOx, and where HC and NOx are in ppb and where the x-axis is between 125 and 1000.

A correlation of 99% is observed between the exponential curve and the onset time with the initial HC^2/NOx concentrations. In the isoprene system, the relationship between HC^2/NOx and onset times is represented by a linear function, whereas in the α-pinene system it is represented by an exponential curve. Interestingly, the inverse of HC^2/NOx when plotted against the onset times of the α-pinene experiments shows a relationship that could be represented as a linear function (like in the isoprene system). This might be attributed to either the lower number of data-points available for the α-pinene system or it may account for the difference in structures between isoprene (with two double bonds) and α-pinene (with one double bond).

6.5.2 Estimation of the other model parameters

A strong correlation is evident between the SOA formed from α-pinene chamber experiments over time and the sigmoidal equation. The model parameters determined from the chamber data and the correlation with the sigmoidal equation are given in Table 6.5.

Table 6.5: Sigmoidal equation fits to SOA formed during α-pinene photooxidation.

Expt.	R^2(%) Sigmoidal fit	Sigmoidal Equation Parameters			
		A1 (μg/m^3)	A2 (μg/m^3)	tO (sec)	dT (sec)
230	99.6	-0.13±0.002	101.5±0.6	10100±33	670±30
231	98.9	0.12±0.01	26.5±0.3	17050±80	1300±71
311	99.3	-1.98±0.28	458.1±0.2	7000±75	800±40
313	95.0	0.154±0.034	13.0±0.2	7700±70	370±65

As shown in Table 6.5, the *A1* values for the α-pinene experiments are much larger than for the isoprene experiments. For the four experiments presented in Table 6.5, the *A1* value ranged from 0.12 to -1.98. The negative value is indicative of the uncertainty associated with the model's prediction of the background aerosol. Since it is unreasonable to use a negative value and the *A1* parameter values are a small fraction of the *A2* values, a value of 0.0 was substituted as the *A1* value.

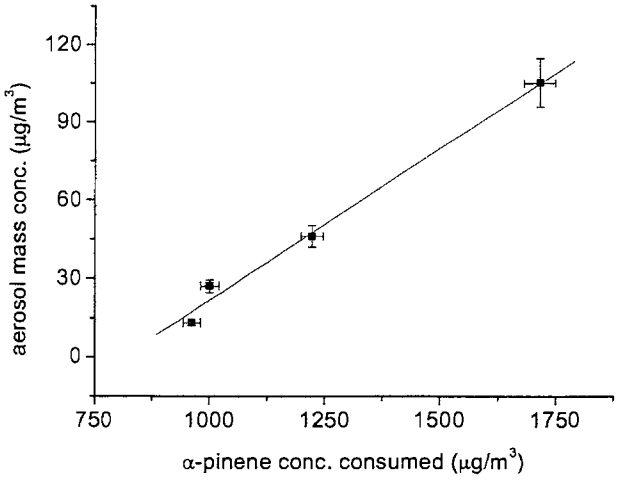

Figure 6.12: The amount of aerosol mass concentration formed versus the amount of α-pinene consumed.

A relationship between the maximum concentration of aerosol mass produced during an experiment and the amount of hydrocarbon consumed is also observed for α-pinene. A strong correlation (R^2 = 99.5%) is evident between the line of best fit and the data-points. In reference to Figure 6.12, estimates of the *A2* parameter can be determined from Equation 6. 7:

$$A2 = (0.116 \pm 0.002)x - (94.35 \pm 8.8) \tag{6.7}$$

where x is the amount of α-pinene consumed (μg/m^3) within the range of 800 and 1800 μg/m^3.

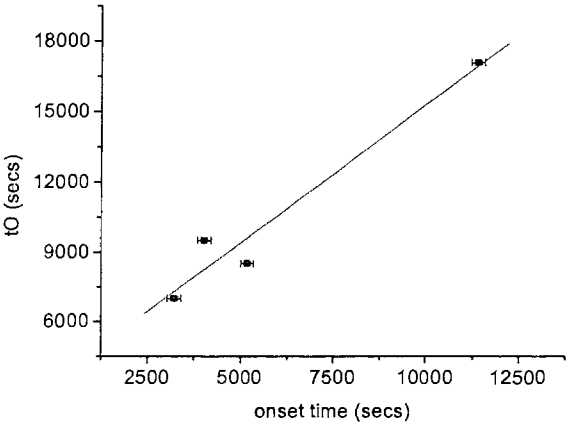

Figure 6.13: The onset time and the tO parameters values.

A relationship between *tO* and the onset time for SOA formation for the α-pinene experiments is shown in Figure 6.13. A straight line represents the relationship between the onset time and *tO*. A correlation of 96% was determined for the fit of the straight line to the data, and so Equation 6.8 can be used to calculate the *tO* parameter value;

$$tO = (3515 \pm 231) + (1.17 \pm 0.8)x \tag{6.8}$$

where x is the onset time (sec) within the range of 2500 and 12500 seconds..

In the isoprene system, a relationship between the completion time — onset time and the *tO* — onset time parameter values was observed. A similar relationship is also observed for the α-pinene system, as shown in Figure 6.14.

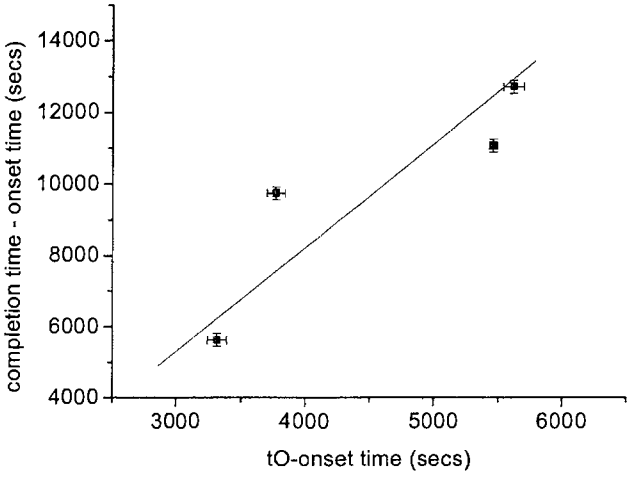

Figure 6.14: The completion time — onset time is plotted against the tO — onset time.

The final step in defining the empirical model for α-pinene is to determine a method of calculating *dT* from the maximum aerosol mass concentration, initial experimental conditions or from the onset time. In the isoprene system, a relationship between the *dT* parameter and the onset time was identified, which is also applicable to the α-pinene system as illustrated in Figure 6.15.

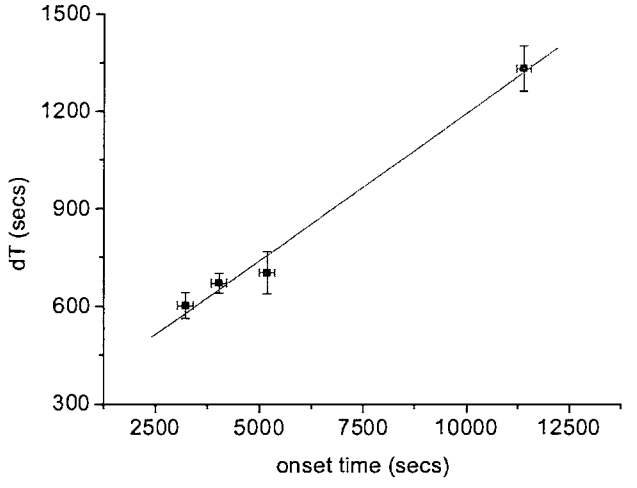

Figure 6.15: Onset times versus the *dT* model parameter values.

A 99% correlation between the fitted straight line and the dT value versus the onset time for the four α-pinene chamber experiments. The parameter dT can be calculated using Equation 6.9:

$$dT = (287 \pm 5.5) + (0.09 \pm 7E-04)x \quad (6.9).$$

where x is the onset time (secs).

6.5.3 Simulated profile vs. chamber profile

A comparison between the simulated SOA profile and the chamber derived SOA profile is presented in Figure 6.16. The final aerosol mass concentration of E230 is well represented by the simulated SOA profile. E231 is underrepresented by the model by 30% and the model was found to overestimate E313 by 31%. Although the model represents the maximum amount of aerosol formed for E311, it does not fit the aerosol profile well. The aerosol in E311 (ROC/NOx of ~41), is formed very rapidly which is not well represented by the model. The overall performance of the SOAPEM when applied to the α-pinene chamber data is again limited by the number of datasets available. As with the isoprene system, gathering data from more experiments would greatly refine the relationships between the observation data and the model parameters.

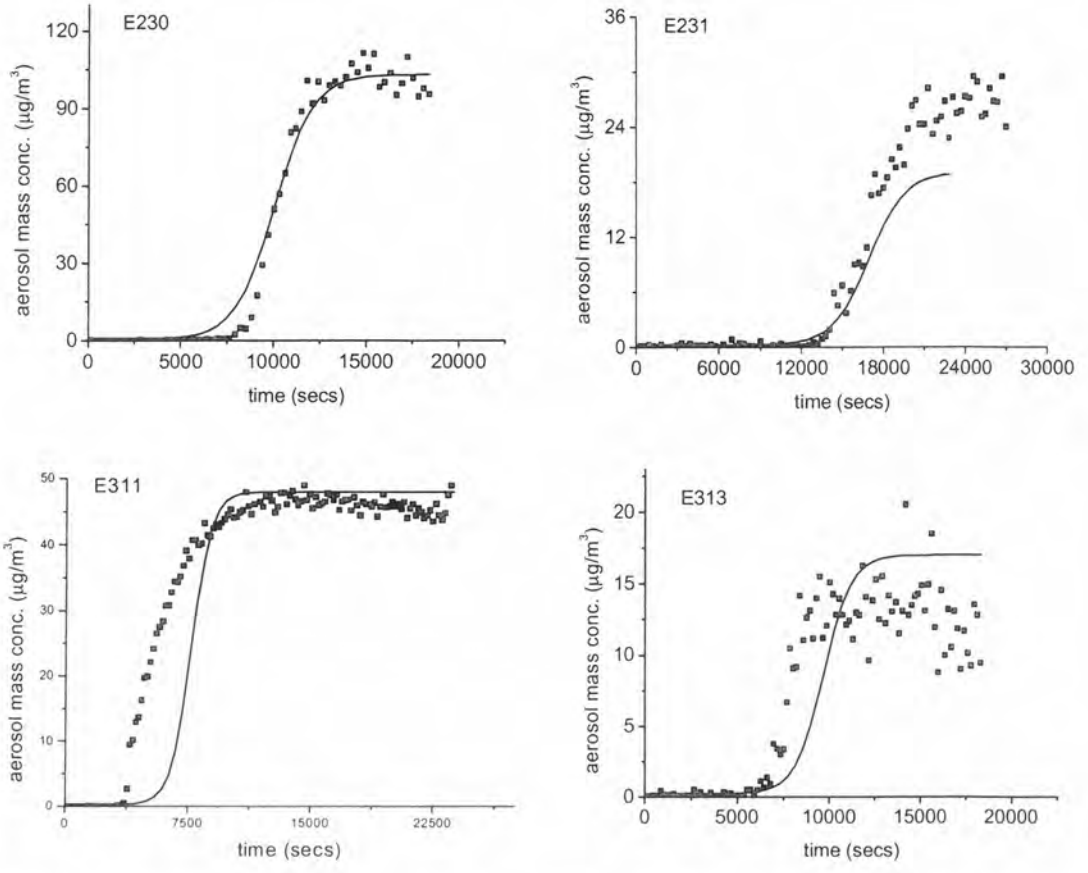

Figure 6.16: A comparison between the simulated SOA profile (line) and the observed SOA profile (symbols) for four α-pinene / NOx chamber experiments.

6.6 Discussion

The SOAPEM is a simplistic representation of a very complex system. In Chapter 4 it was observed that for the isoprene / NOx system, the composition of the SOA varies according to different ROC/NOx ratios and at different times throughout an experiment. The empirical model provides an estimate of SOA mass which is independent of the SOA formation pathways occurring throughout an experiment.

Modelling the isoprene and α-pinene systems has tested the ability of the empirical model to predict the temporal formation of SOA for two different systems. The SOA produced in the isoprene system has been largely associated with the OH reaction with isoprene (Surratt et al., 2006; Dommen et al., 2006), whereas in the α-pinene system a large contribution to overall SOA yield results from the ozonolysis reaction particularly at night time (Kamens et al., 1999). This is reflected in the -OH and -O_3 rate constants for the isoprene and α-pinene. k(OH) at 298K is 101E-12 for isoprene and 53.7E-12 for α-pinene and k(O_3) at 298K is 12.8E-18 and 86.6E-18 for isoprene and α-pinene respectively.

Overall, SOAPEM produces reasonable results for the isoprene and α-pinene / NOx systems. The range of ROC/NOx ratios modelled ranged from 6.8 to 14.4 for isoprene and 7.7 to 40.7 for α-pinene. The model over-predicts SOA formation for the isoprene experiment E308 by 17% which has a ROC/NOx of 13.2. The model under-predicts the formation of SOA for the experiment E309 by 23%, which has a ROC/NOx of 14.4. The closest fit in the isoprene suite occurred for E303 which had a ROC/NOx ratio of 11.3. When comparing the model's performance to ROC/NOx ratios for the isoprene experiments, no dependence was observed. This observation was true for the α-pinene experiments as well.

The mass of SOA produced in the isoprene experiments is much less than that produced in the α-pinene experiments. The model performed better for the experiments with more mass and once the mass concentration was less than about 2 $\mu g/m^3$ the model results

were less accurate, as in E304 and E309. The mass of SOA produced in the α-pinene experiments was greater than 12 $\mu g/m^3$. Figure 6.3 demonstrates that the yield is not a constant value for a specific system, which is an assumption used in many air quality models. The notion of a varying yield is implicit in the empirical model and does, in part, account for the relatively good results.

The onset time for the α-pinene system appears to be much lower than for the isoprene system for the same HC (ppbC) to NOx ratio. This may be indicative of the structure of these compounds: the isoprene species has two double bonds and the α-pinene species has only the one double bond but is a ring-shaped structure. The reaction rate for OH attack for the isoprene species, which is 101E-12, is faster than that for α-pinene, which is 53.7E-12. The reaction rate for O_3 reaction with α-pinene (86.6E-18) is seven times faster than the O_3 reaction with isoprene (12.8E-12), which may account for the faster onset time. Ozonolysis has been identified as a key SOA formation pathway for α-pinene accounting for the production of 77% of the SOA, whereas 23% was attributed to the reaction with OH (Griffin et al., 1999).

The main limitation of SOAPEM at the moment is the lack of experimental data used to identify the relationships between the model parameters and the chamber observations. For this reason, the relationship equations have a limited domain consistent with the dataset used. Once more data is available it is anticipated that the relationship can be more accurately defined and applicable across a greater range of precursor concentrations. At this stage the methodology presented for the isoprene and α-pinene experiments can be used for any suite of experiments given that all of the physical chamber variables are consistent such as J_{NO_2}, temperature and humidity.

In summary, the empirical model is presented as a work-in-progress and introduces a very different approach to SOA modelling. The empirical model presented here can only be applied to the isoprene and α-pinene CSIRO chamber experiments. The methodology, however, presents a possible way of developing a predictive, simple

model that can be applied to any hydrocarbon or mixture of hydrocarbons when there is ample chamber data available to support and define it.

There is a possibility that SOAPEM could be transferred to model ambient conditions if rigorous chamber experiments were undertaken to simulate the mixed hydrocarbon burden found in the atmosphere. Physical variables such as radiation intensity, humidity, temperature variation throughout the photochemical window of about 8 hours a day would similarly need to be considered when planning an experimental program. Variations in the hydrocarbon burden in terms of the chemical composition of air would also need to be considered in the experimental program so that all variables (chemical and physical) in the real world that impact on the formation of the SOA are accounted for in the model.

Chapter 7: Modelling the Contribution of SOA in Air Pollution Events – a Melbourne Case Study

7.1. Introduction

SOA may comprise a significant proportion of photochemical smog. Baltensperger et al. (2006) estimates that up to 50% of the annual average $PM_{2.5}$ is comprised of carbonaceous aerosol, and up to 90% of the total mass comprises SOA.

Many studies have used the OC/EC method to determine the quantity of SOA in the ambient environment. The assumption behind this method is that elemental carbon (EC) and organic carbon (OC) are produced from the same source and so an area will have a representative ratio of OC to EC. If the measured OC/EC is greater than the expected ratio, the amount of OC in excess is then considered to be derived through secondary processes, hence is assumed to be SOA (Strader et al., 1999). Until recently, this method was the only way of estimating SOA mass concentrations from measurements in the ambient environment. Aerosol mass spectrometers have been used successfully to determine primary versus secondary organic aerosol mass concentrations in ambient air (Robinson et al., 2007). Modelling methods have continued to evolve and are employed to relate the components of the atmosphere (chemistry and physics) to the observations as well as providing an insight into the actual formation processes, as presented in Chapter 4.

Models have difficulty in estimating the temporal and spatial variation of SOA due to the number of variables that could impact on SOA formation. Some air quality models have been developed to estimate the net SOA mass derived from the more abundant hydrocarbons or lumped groups of hydrocarbon monitored in the airshed. These measurements are based on the assumption that all condensable organic products will behave as quasi-ideal solutions, and their partitioning characteristics are determined accordingly (Pankow et al., 1994).

The United States Environmental Protection Agency (EPA) describe on their website the recently developed legislation, known as the regional haze rule, which requires the States to implement strategies to improve visibility conditions to natural background levels by 2064. Since a large component of fine and ultrafine particles is derived from SOA processes, the development of SOA modules is of emerging importance in the United States.

An air quality model employed extensively in the United States is the Community Multi-scale Air Quality (CMAQ) model. The SOA module developed for the CMAQ model has recently been modified so that it includes SOA formation from sesquiterpenes, monoterpenes, isoprene products, toluene and xylene species (Morris et al., 2006). A dominant SOA formation process occurs via the partitioning of the condensable organic species from the gas to the aerosol phase. Partitioning coefficients have been estimated for each of the condensable products derived from the photooxidation of the five hydrocarbons. In order for the species to partition to the aerosol phase, the CMAQ SOA module requires that the saturation concentration of the condensable product is greater than a specified condensation concentration. A unique feature of the CMAQ SOA module is that 50% of the net SOA formed at each time-step is retained as polymerised material over a period of 20 hours to simulate an oligomerisation function.

Another SOA module developed for application with an air quality model is the secondary organic aerosol model (SORGAM) developed by Schell et al. (2001). The SORGAM includes several common elements to the CMAQ SOA module, such as the incorporation of the gas/aerosol partitioning mechanism based on the model proposed by Odum et al. (1996). SORGAM doesn't, however, consider condensed phase oligomeristion reactions included in CMAQ's SOA module. The precursor hydrocarbons considered in the SORGAM include toluene, xylene, cresol, higher alkanes, higher alkenes, α-pinene and limonene. Product yields and partitioning coefficients were calculated from chamber data presented in other literature. The saturation concentrations (inverse of the partitioning coefficients) are calculated in the

SORGAM as a function of temperature, and the temperature dependence of SOA partitioning was highlighted as an important process by Schell et al. (2001).

This chapter describes the development of an SOA module that has been coupled to a 3D atmospheric model named The Air Pollution Model – Chemical Transport Mechanism (TAPM-CTM). TAPM-CTM has been widely applied to airshed studies in Australia and New Zealand and incorporates an emissions inventory, meteorology and a chemical transport module featuring the Carbon Bond 99 (CB99) chemical mechanism. The SOA module is designed to be a stand-alone module that has no impact on the CB99 mechanism. Within the CB99 mechanism, the species olefins, paraffins, xylene and terpene are treated as lumped species, whereas toluene and isoprene are treated explicitly. The SOA module incorporates the formation of SOA from six hydrocarbon precursors, namely olefins, paraffins, xylene, toluene, terpene and isoprene. In line with the CMAQ SOA module, this module also includes the formation of SOA via the oligomerisation process.

The absorption gas/aerosol partitioning model developed by Odum et al. (1996) has been fitted to chamber data to define the modelling parameters; which are the SOA product yield, α, and partitioning coefficients, $K_{om,}$ of the hypothetical products produced from the reaction of the six hydrocarbons with a primary oxidant. In most cases parameter information was available from the literature where the Odum model had been fitted to chamber data. The exceptions occurred for the 1-octene system, where chamber data were sourced from Forstner et al. (1997) and fitted to the Odum model, and for the isoprene system where chamber experiments previously presented in Chapters 5 and 6 were fitted to the Odum model to derive parameter information.

7.2 SOA Module Development

There are two factors that combine to make a species a dominant SOA producer: one is the abundance of the species in ambient air, and the other is the SOA forming ability of the species. Guenther (1995) estimated that 1150 $TgCyr^{-1}$ are produced from biogenic sources and 98 $TgCyr^{-1}$ from anthropogenic sources. Guenther et al. (1995) found that

500 TgC of isoprene is emitted annually which means that it is the most abundant emission in the atmosphere. The SOA yield, however, produced from isoprene is much smaller than from many other hydrocarbons. This is due to the fact that the SOA produced by the isoprene system are relatively small and in low quantities. The maximum aerosol diameter in the isoprene system is approximately 100nm (after 16 hrs of photooxidation), whereas, in the α-pinene system, the aerosol diameter sizes can grow to be 1μm after only 6 hrs of photooxidation. Isoprene is considered to potentially be a major SOA producer because of its abundance in the ambient environment, not because of its aerosol forming ability.

The SOA module has been designed as a stand-alone module that couples to TAPM-CTM. Figure 7.1 identifies the role and position of the SOA module in relation to the TAPM-CTM system. The CB99 chemical mechanism is the basis of TAPM-CTM chemistry. The CB99 photooxidation reactions that have been included in the chemical compiler to form condensable products CG1 to CG9 are presented in Table 7.1.

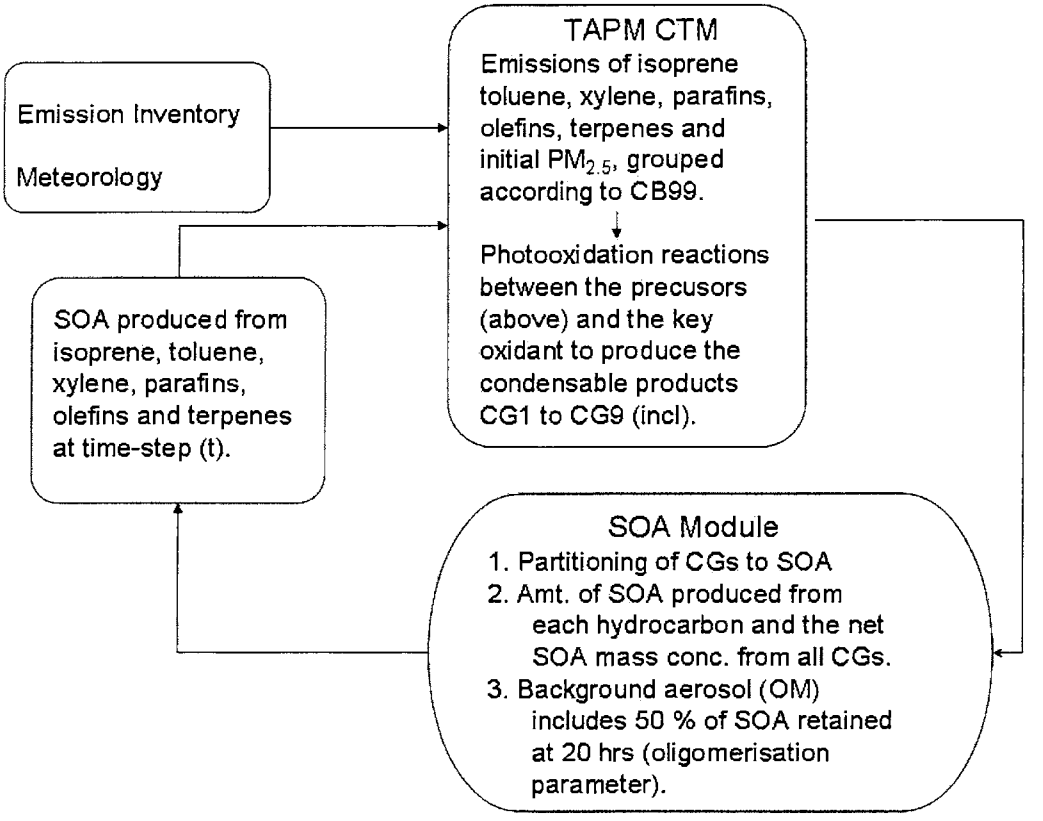

Figure 7.1: The relationship between the SOA Module and TAPM-CTM.

Table 7.1: The photooxidation reactions and the reaction rate equations.

Chemical Reaction	Reaction equation type and parameters
OLE + OH => OLE +OH + 0.029*CG1 + 0.0043*CG2	CONS ; 3.2E-11
PAR + OH => PAR + OH + 0.13*CG3	CONS ; 8.1E-13
XYL + OH => XYL + OH + 0.075*CG4 + 0.105*CG5	ARRH ; 1.7E-11,-116
TOL + OH => TOL + OH + 0.34*CG6	ARRH; 1.8E-12,-355
TERP + OH => TERP + OH + 0.26*CG7	ARRH ; 1.5E-11,-449
ISOP + OH => ISOP + OH + 0.0788*CG8 + 0.0062*CG9	ARRH ; 2.54E-11,407.6

Where OLE is olefins, PAR is paraffins, XYL is xylenes, TOL is toluene, TERP is terpenes and ISOP is isoprene. The reactions in Table 7.1 noted as ARRH are

temperature dependent reactions, where $k = Ae^{-C/T}$ and the first parameter value listed in the table is A and the second is C. The other reaction type presented in Table 7.1 is a constant rate coefficient (CONS) in which the reaction rate coefficient is also listed. These reaction rate coefficients are taken from the CB99 chemical mechanism (Gery et al., 1994).

The reactions and reaction rate coefficients listed in Table 7.1 are used to determine the amount of CG1 to CG9 produced for each time-step. The branching ratios (the ratio of the amount of product like CG1 produced from the precursor OLE) have been determined using the Odum model and will be discussed in detail later in this chapter. It is important to note that the species denoted as CG* may be aerosol or gas phase and represent the concentration of the product species in both phases. These products are treated as gas phase species in the chemical transport mechanism until they are partitioned to the aerosol species and become CA* species. So, within this context, the amount of product in the gas phase is equal to CG* - CA*. The six hydrocarbon groups or species have a dominant OH oxidant reaction (Griffin et al., 1999). The productions of CGs are included in the existing CB99 mechanisms but the OH is not consumed in the reaction. The SOA module, in this instance, does not impact on the gas phase chemistry and is described as a stand-alone module.

The species chosen to be included in the SOA module were selected because they represented the dominant hydrocarbons in the Australian airshed. Toluene, m-xylene, p-xylene and o-xylene, in addition to the olefins and paraffins, were the dominant species identified in an extensive analysis of non-methane hydrocarbon concentrations in Sydney's air (Nelson et al., 1982). This study did not include an analysis of biogenic emissions. The dominant biogenic emissions recognised globally are isoprene and terpenes (Kanakidou et al., 2005). Chung et al. (2000) found that more SOA is produced from biogenic emissions than from anthropogenic emissions. However, the aerosol forming potential of many biogenic species has yet to be determined.

A distinction between the isoprene and isoprene-product species has not been made in this SOA module since the chamber experiments encompass the photooxidation of isoprene as a system, and so SOA is produced via primary, secondary and further oxidation events. The model parameters (α and K_{om}) were determined by fitting the Odum model to chamber experimental data and represent theoretical species. As discussed in Chapter 5, these theoretical products are representative of the whole isoprene / NOx system.

The CMAQ SOA module also includes the SOA formation from sesquiterpenes, which it considers to be one of the largest sources of SOA (Morris et al., 2006). A review of recent literature indicates that although sesquiterpenes do produce high yields of SOA, their actual concentration in the Australian airshed is not well understood. The emissions inventory does not include sesquiterpenes. Similarly, precursor species cresol and limonene are considered in the SORGAM but are not included in this module. Pun et al. (2006) suggest that from a computational efficiency perspective, the ideal number of precursor species should be at most 6. So with this in mind, the dominant 6 species were chosen for inclusion in the SOA module.

7.2.1 Determination of product yields and partitioning coefficients

The equilibrium absorption gas / aerosol partitioning model presented by Odum et al. (1997) is used extensively in the SOA module as a means of estimating the condensable product yield, α, resulting from the initial hydrocarbon photooxidation reaction, and as a means of estimating the partitioning coefficients, K_{om}, of each condensable product. The product yields, partitioning coefficients and literature source applied to the SOA module are presented in Table 7.2.

As discussed in Chapter 5, the Odum model can be applied to chamber data in many ways. The most common method is to fit the model (given in Equation 5.2) to chamber data to define the parameter values for two hypothetical products. This is the method described in Section 5.3.3 and is employed here in order to determine parameter values

for 1-octene which was reported by Forstner et al. (1997). 1-octene has been adopted as a representative species of the olefin group. The fit of the Odum model to the 1-octene data is presented in Figure 7.2. For the condensable products in the olefin system, the product yields for CG1 and CG2 were determined to be 0.0017 and 0.4505 respectively. The partitioning coefficients were 1.0 and 0.0005 for CG1 and CG2 respectively. The Odum fit suggests that all of CG1 will partition to the aerosol phase but only minor amounts of this product will be produced (0.0017 of the olefin concentration). CG2 will be formed more readily than CG1 but only a fraction of it will partition to the aerosol phase.

Table 7.2: Odum's model parameter values and literature source.

Oxidation reaction	Product yields (1 or 2 products)	Partitioning Coefficient/s ($m^3/\mu g$)	Literature Source (refer to references section)
OLE + OH	0.0017 (CG1), 0.4503 (CG2)	1.000 (CG1), 0.005 (CG2)	Data from Forstner et al. (1997) 1-octene as an analogy.
PAR + OH	0.130 (CG3)	0.0044 (CG3)	Parameters and data from Takakawa et al. (2003). n-Undecane as analogy
XYL + OH	0.075 (CG4), 0.105 (CG5)	0.1390 (CG4) 0.0100 (CG5)	Parameters and data from Carter et al. (2005)
TOL + OH	0.340 (CG6)	0.0057 (CG6)	Parameters and data from Takakawa et al. (2003).
TERP + OH	0.260 (CG7)	0.0069 (CG7)	Parameters and data from Takakawa et al. (2003). α-pinene as an analogy
ISOP + OH	0.0788 (CG8), 0.0105 (CG9)	0.0062 (CG8), 0.202 (CG9)	Determined from CSIRO chamber experiments.

The majority of the isoprene experiments undertaken in the CSIRO chamber were performed at very low concentrations. As a result, the majority of experiments produced minimal amounts of SOA. The CSIRO chamber experiments are compared to the unseeded isoprene photooxidation experiments performed by Dommen et al. (2006) and are presented as Figure 7.3.

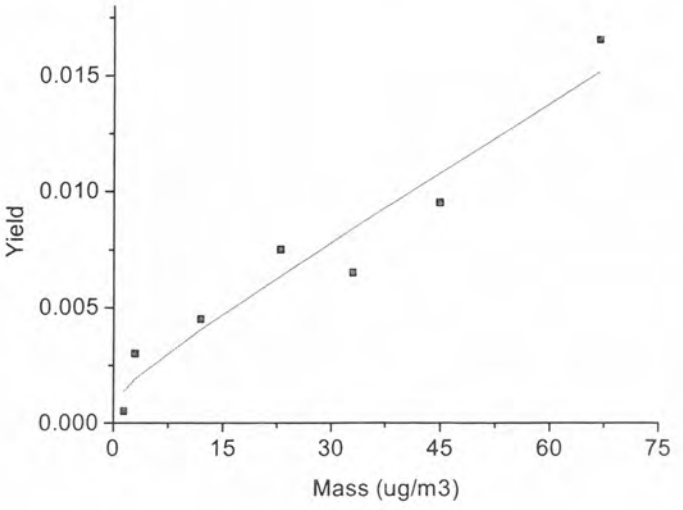

Figure 7.2: The Odum model is fitted to the chamber data for 1-octene reported by Forstner et al., 1997.

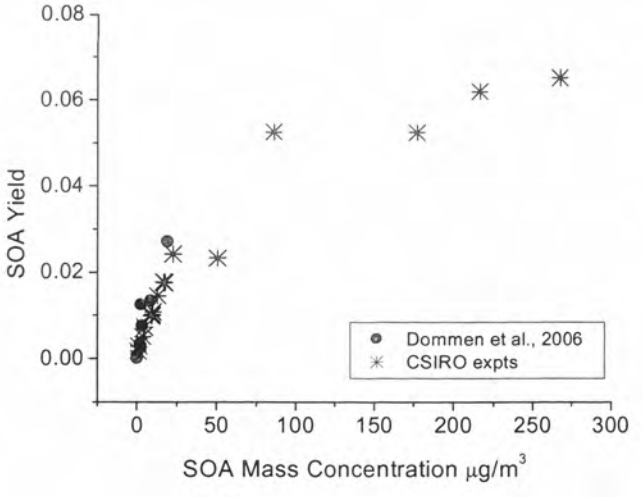

Figure 7.3: Isoprene photooxidation experiments performed by Dommen et al. (2006) are compared with the CSIRO experiments.

Expected page number is not

in original print copy

The amount of aerosol produced in chamber experiments was found to be temperature dependent (Odum et al., 1996; Hoffmann et al., 1997). Temperature influences the degree of partitioning as expressed by the K_{om} as defined in Chapter 5. Takakawa et al, (2003) developed a method to determine K_{om} at one temperature given K_{om} at another. Takakawa's equation is based on the relationship between temperature and saturation vapour pressure, as follows:

$$K_{T_1,i} = K_{T_2,i} \frac{T_1}{T_2} \exp\left[B_i\left(\frac{1}{T_1} - \frac{1}{T_2}\right)\right] \tag{7.1}$$

where $K_{T_2,i}$ is $K_{om,i}$ at temperature T_2 and B_i is $\Delta H_{vap,i}$ /R which is the enthalpy of vapourisation over the ideal gas constant.

7.2.2 Calculating the SOA produced from each hydrocarbon reaction

Once the product yields and partitioning coefficients for the condensable products CG1 to CG9 were determined, the amount of SOA partitioned from the products was calculated using Equation 7.2 (Pun et al., 2003):

$$CA_i = \frac{CG_i \; M \; K_{om}}{(1 + K_{om} M)} \tag{7.2}$$

where CA is the amount of SOA partitioned from the condensable product CG, i is the number of condensable products, M is the amount of organic mass in the system and K_{om} is the partitioning coefficient determined for the CG.

Ambient mass concentrations of $PM_{2.5}$ are imported into the SOA module at each time step (and completely exported later in the same time-step) to provide an absorbing organic mass for the partitioning of the CG's. At this stage no discrimination is applied to primary organic material or secondary organic aerosol. The amount of SOA produced from each hydrocarbon reaction and the net amount of SOA produced is reported for each time-step. This information is transported through the TAPM-CTM so that spatial and temporal SOA concentrations can be determined. The CG and CA concentrations are persistent throughout the model simulation. The formation of condensed phase species through oligomerisation processes have been accounted for in the SOA module

in line with the approach adopted for the CMAQ module. 50% of the SOA over a 20 hour period has been retained as oligomerised non-volatile mass (Morris et al., 2006).

7.3 Isoprene Chamber Experiments

Initially the SOA module was tested against the isoprene chamber data. The amount of isoprene consumed in each experiment was substituted into the SOA module as an isoprene emission and the amount of SOA produced by the box model was compared to the amount of SOA produced in the chamber experiment. The box model is a simplified version of TAPM-CTM without the emissions inventory input and minimal meteorology capabilities and has been developed by Dr Martin Cope from CSIRO, Centre for Marine and Atmospheric Research. The box model simulation was run for the duration of each of the experiments. The initial experimental conditions like the relative humidity, amount of ultraviolet radiation and temperature, in addition to the initial isoprene and NOx concentrations, were required to run the box model. The results presented in Table 7.3 compare the estimates derived from the SOA module (with and without the oligomerisation function) to the experimental results. These results are also presented in Figures 7.5 and 7.6.

Table 7.3: Experimental chamber concentrations (bold) versus model results for the SOA module with and without the oligomerisation function.

Expt No.	**Experimental concentrations**		Model Simulation with oligomerisation		Model Simulation w/o oligomerisation	
	Mass $\mu g/m^3$	**C5H8 $\mu g/m^3$**	Mass $\mu g/m^3$	C5H8 $\mu g/m^3$	Mass $\mu g/m^3$	C5H8 $\mu g/m^3$
202	**0.014**	**285**	0.0107	250	0.00326	250
207	**0.015**	**522**	10.3	537	0.0041	537
304	**0.030**	**187**	0.414	203	0.0904	203
204	**0.285**	**556**	10.6	559	8.37	559
203	**1.752**	**530**	0.0037	514	0.00204	514
205	**2.530**	**1039**	22.1	954	19.1	954
308	**5.800**	**645**	12.0	645	10.3	645
303	**13.600**	**716**	14.9	715	0.00576	715

The model simulation of the isoprene concentration for each experiment is the same for the SOA module with, and without the oligomerisation function. This is due to the fact that the concentration of isoprene is not a function of oligomerisation. The box model has done a reasonable job of simulating the amount of SOA mass produced from the SOA module with and without the oligomerisation function as shown in Figures 7.5 and 7.6. These results are a reflection of the initial fit of chamber data to the Odum model (Figure 7.4). Note that the model was fitted to a combination of the CSIRO chamber data and the data reported by Dommen et al. (2006).

The impact of the oligomerisation function on the model results is quite variable. The difference in results for the oligomerised versus non-oligomerised SOA module is minimal for E203, E204 and E205 but relatively large for E202, E207, E303 and E304. In the oligomerised SOA module a component of SOA is retained in the system during the simulation, more aerosol is therefore available for the absorption process and so there is more SOA produced with this module. For E302 and more so for E303, the oligomerisation function has had a large impact on the overall SOA mass produced, bringing it more in line with the mass of SOA produced in the chamber experiment. Better results for E207 were obtained without the oligomerisation function but this is an exception to the overall results. E207 had a high background aerosol mass concentration (at least ten times the background of the other experiments), and it is likely that the amount of SOA produced in this experiment will be larger than similar experiments with a lower background. This may be one reason for the anomaly. Generally, the oligomerisation function has improved the results of the SOA module and its inclusion signifies that oligomerisation is an important process of SOA formation.

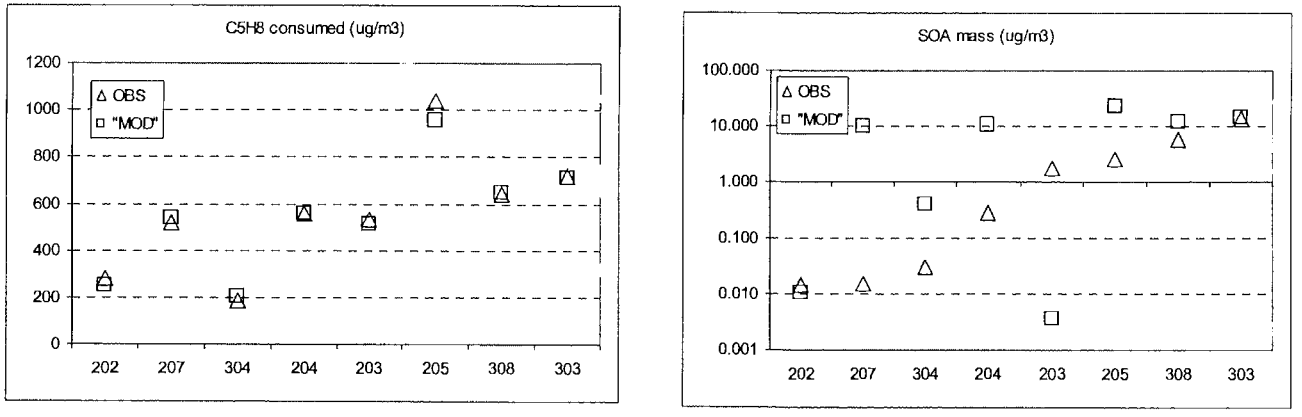

Figure 7.5 Chamber observations versus box model results for the amount of isoprene consumed and SOA mass produced with the oligomerised function active within the SOA module.

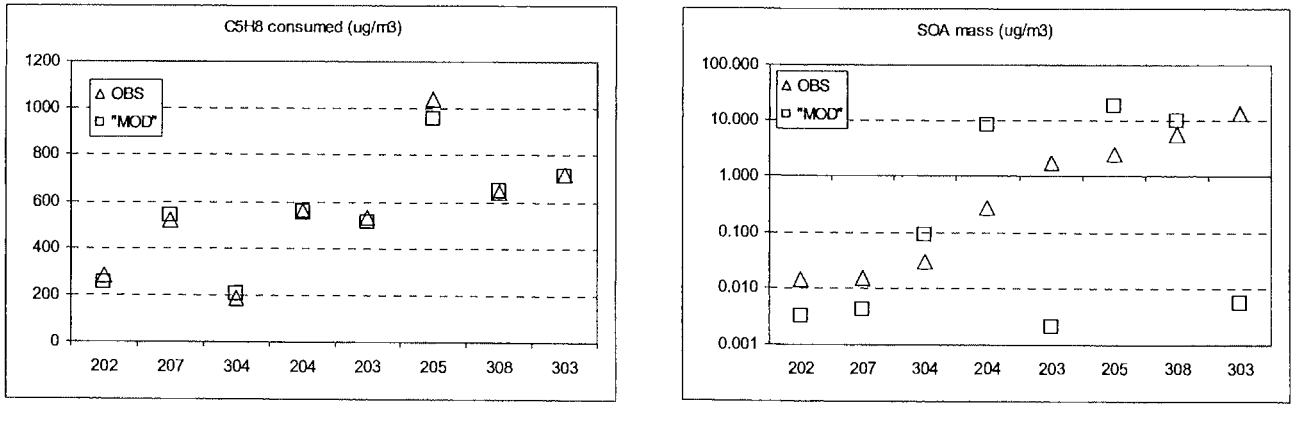

Figure 7.6: Chamber observations versus box model results for the amount of isoprene consumed and SOA mass produced with the oligomerised function not active within the SOA module.

7.4 TAPM-CTM Simulations

The work presented in this section is part of a collaboration between CSIRO Centre for Marine and Atmospheric Research and the writer. In this section the coding of the SOA module (into Fortran 99) and the coupling of the SOA module to TAPM CTM was undertaken by Dr Martin Cope (of CSIRO, CMAR).

The SOA module was coupled to the TAPM-CTM model to produce simulations for Melbourne, Australia, over a 3 day photochemical smog episode during 3-5 January 2001. The study area is centred on Melbourne city which is shown in Figure 7.7. Port Phillip Bay is recognisable in this figure and comprises a large portion of the study area. A 30km, 10km and a 3km grid spacing can be used across the study area. For this work, a 3km x 3km grid was applied to the model and the study region is pictured in Figure 7.8. Note that the 3km x 3km grid is the smallest grid depicted in Figure 7.8, the contours is this image are of elevation.

Figure 7.7: The study region, Melbourne CBD which is circled in yellow.

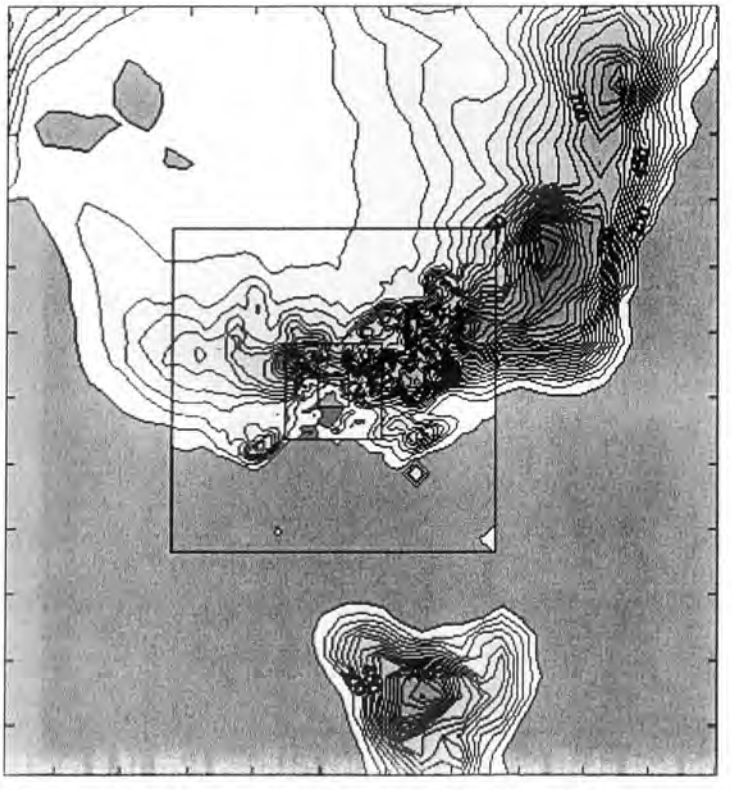

Figure 7.8: The smallest square is the 3km study area used in this study.

7.4.1 Model performance

The TAPM-CTM model was coupled to the SOA module (referred to herein as CTM-SOA) so that a comparison between model estimates and ambient data collected at EPA field stations can be made. Concentrations of O_3, NOy, NO, NO_2 and SO_2 measured at the Paisley EPA monitoring station were compared to model simulations and are presented below as Figures 7.10 and 7.11. Monitoring data for the CO concentrations were not available.

For the model simulations, input emissions data were sourced from the emissions inventory which was developed from the ambient field measurements compiled at numerous EPA monitoring stations. The biogenic component of the emissions inventory was supplemented with addition data. Two classes of emitters were considered in the biogenic inventory supplement, they are eucalypt trees and pasture. The trees emit isoprene and α-pinene which were mapped to isoprene and terpene species in the CB99

chemical mechanism. The pasture emits isoprene, pinene, methanol, ethanol, acetone and aldehydes which were similarly mapped to these species in CB99. Default canopy emissions were taken from a biogenic emission study undertaken by CSIRO in 2004 (Nelson et al., 2004) and default pasture emissions were taken from another CSIRO study by Kristine et al. (1998). The daily fluctuations in the total VOC biogenic emissions (kg/hr) and the NOx emissions for the 3km x 3km grid identified in Figure 7.8 are presented in Figure 7.9 during local summer time.

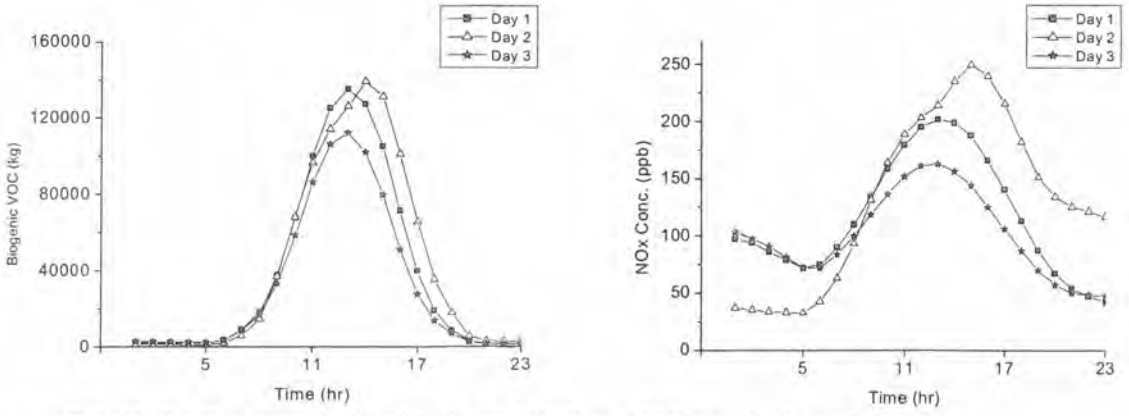

Figure 7.9: Daily fluctuations in simulated VOC and NOx emission rates.

As anticipated, the total biogenic VOC concentration peaked at about 1 – 2pm each day which is generally the hottest period of the day. The highest concentration was experienced on Day 2 (January 4th 2001) at 2pm. The total biogenic VOC emissions at that time were just over 140,000 kg/h. The NOx emission rates depicted in Figure 7.9 show that the peak concentration varies throughout the modelling period. The NOx peak occurs at 1pm on the first two days and a peak and shoulder is observed on Day 2 with the highest peak occurring at 3pm. NOx is thought to be generated primarily from traffic and industry, it is therefore unusual to observe peaks occurring outside of peak hour traffic periods. Most of the NOx was observed during the 11am - 2pm window.

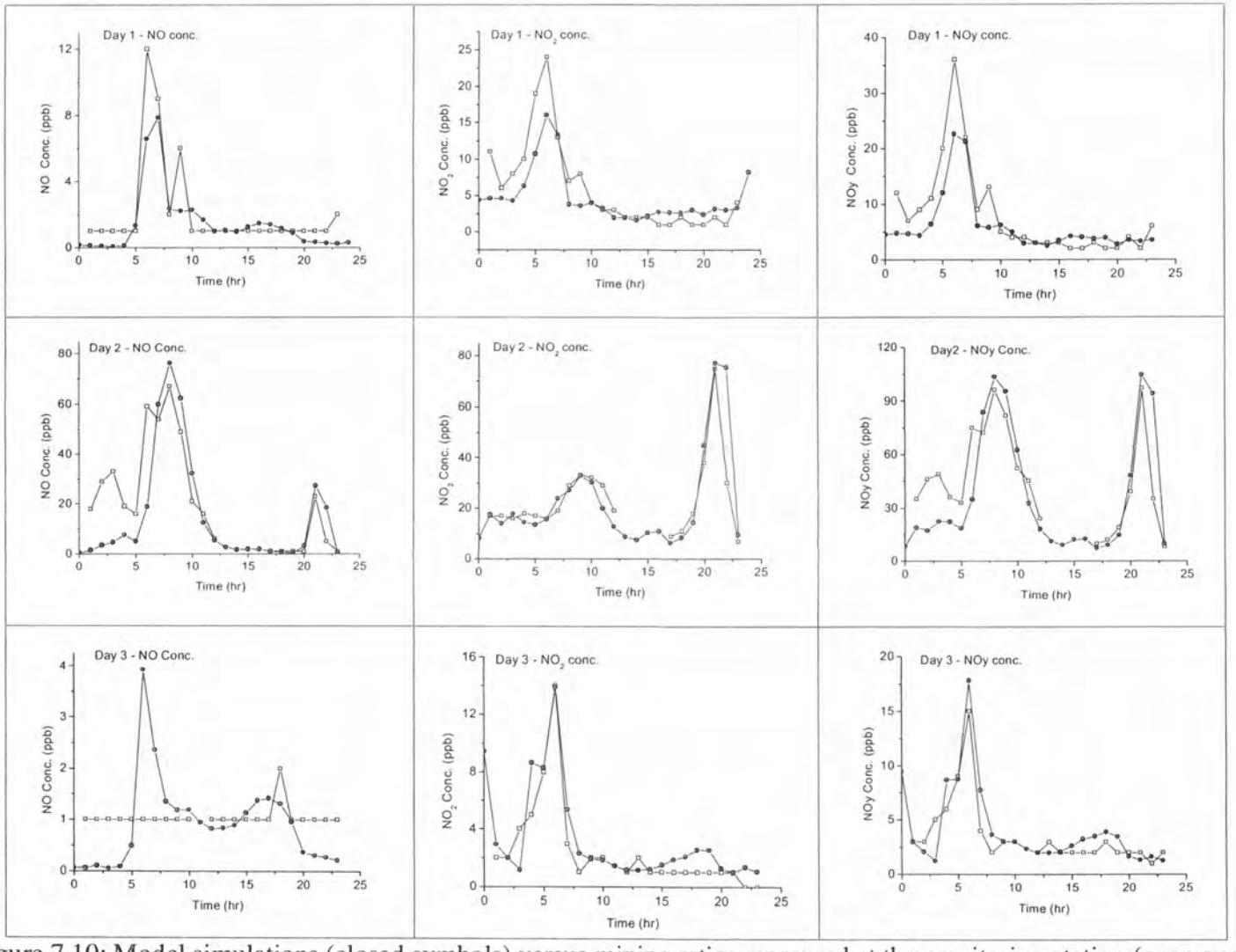

Figure 7.10: Model simulations (closed symbols) versus mixing ratios measured at the monitoring station (open symbols).

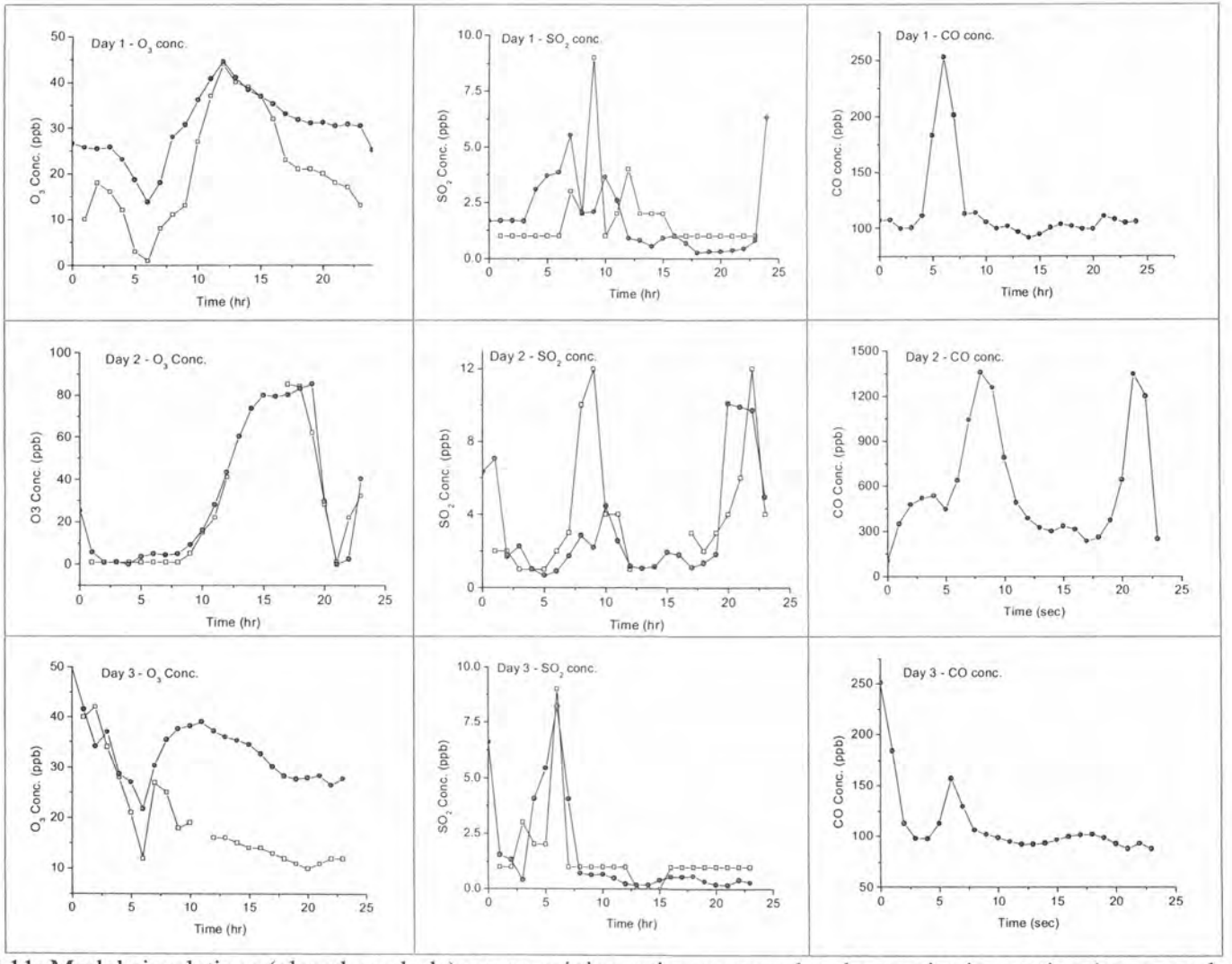

Figure 7.11: Model simulations (closed symbols) versus mixing ratios measured at the monitoring station (open symbols).

NB: Monitoring data is not available for the CO emissions.

An O_3 event is captured in the monitoring data of measured ambient concentrations and simulated quite well by the CTM-SOA. The variation in the NOx and O_3 concentrations over the 3 day period is large and the CTM-SOA is successful in capturing most of these variations. Figure 7.10 indicates that the model does very well at predicting the NOy, NO and NO_2 concentrations. The model tracks the NO concentrations over the first 2 days with some success; the NO ambient concentrations vary from a peak of 12pb in the first day, to about 70ppb in Day 2. The NO analyzer has failed on Day 3 but a simulated NO concentration profile on Day 3 estimates a peak of 4ppb on Day 3. The model similarly predicts a peak of about 8ppb on Day 1 and about 75ppb on Day 2. The timing of the simulated NO profile represents the observed NO profile quite well. The observed NO_2 peaks are very closely represented by the model, particularly on Day 2 and Day 3. The observed NOy concentrations are underestimated by the model on Day 1 by about 30% but are quite well simulated by the model on Days 2 and 3.

The model is challenged by the SO_2 and the O_3 observations, particularly at the initial periods of the simulation in which O_3 is overestimated by the model and SO_2 is underestimated. During the simulation of Day 1, the model was not very successful in capturing the O_3 profile, although the model was able to predict the O_3 peak occurring on this day. During the Day 2 simulation, the model is able to capture the O_3 profile extremely well but appears to underestimate the observed decline in O_3 concentrations in the later part of Day 3. The simulated SO_2 profile for Day 2 looks to follow the same peaks as the observed SO_2 profile, however the model often underestimates the maximum SO_2 peaks. Day 3 of the simulation was the best day for estimating SO_2 concentrations and there is a good correlation between the observed ambient data and those modelled.

Overall, the model does quite well at estimating the concentrations of NO, NO_2, NOy, SO_2 and O_3 for the 3 day simulation. Improvements could be made in the short term by adjusting the initial O_3 and SO_2 concentrations, although it may take some time before it can more accurately predict these ambient concentrations.

7.4.2 SOA simulations

The spatial distribution of the peak 24 hour concentrations of $PM_{2.5}$ (primary and secondary aerosol) during the three day study period is presented in Figure 7.12. The highest concentrations of $PM_{2.5}$ are centred around the commercial business district (CBD) which is located to the north of Port Phillip Bay. It is likely that the majority of $PM_{2.5}$ are, therefore, produced from anthropogenic sources and may represent primarily the emissions from vehicle exhausts that are representative of urban centres. The isoprene concentrations in the gas phase (ppb) and the concentration of the isoprene products ($\mu g/m^3$) are shown in Figure 7.13 at the end of the 3 day simulation. The other precursors that produced reasonably high concentrations of SOA are the olefins and terpenes, which are presented in Figures 7.14 and 7.15.

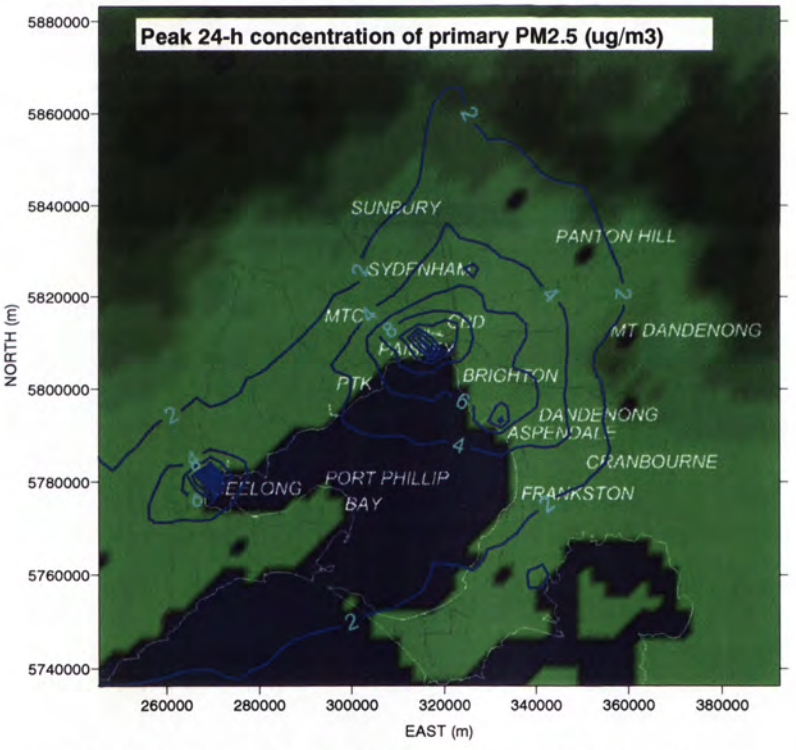

Figure 7.12: The spatial distribution of PM2.5 in $\mu g/m^3$.

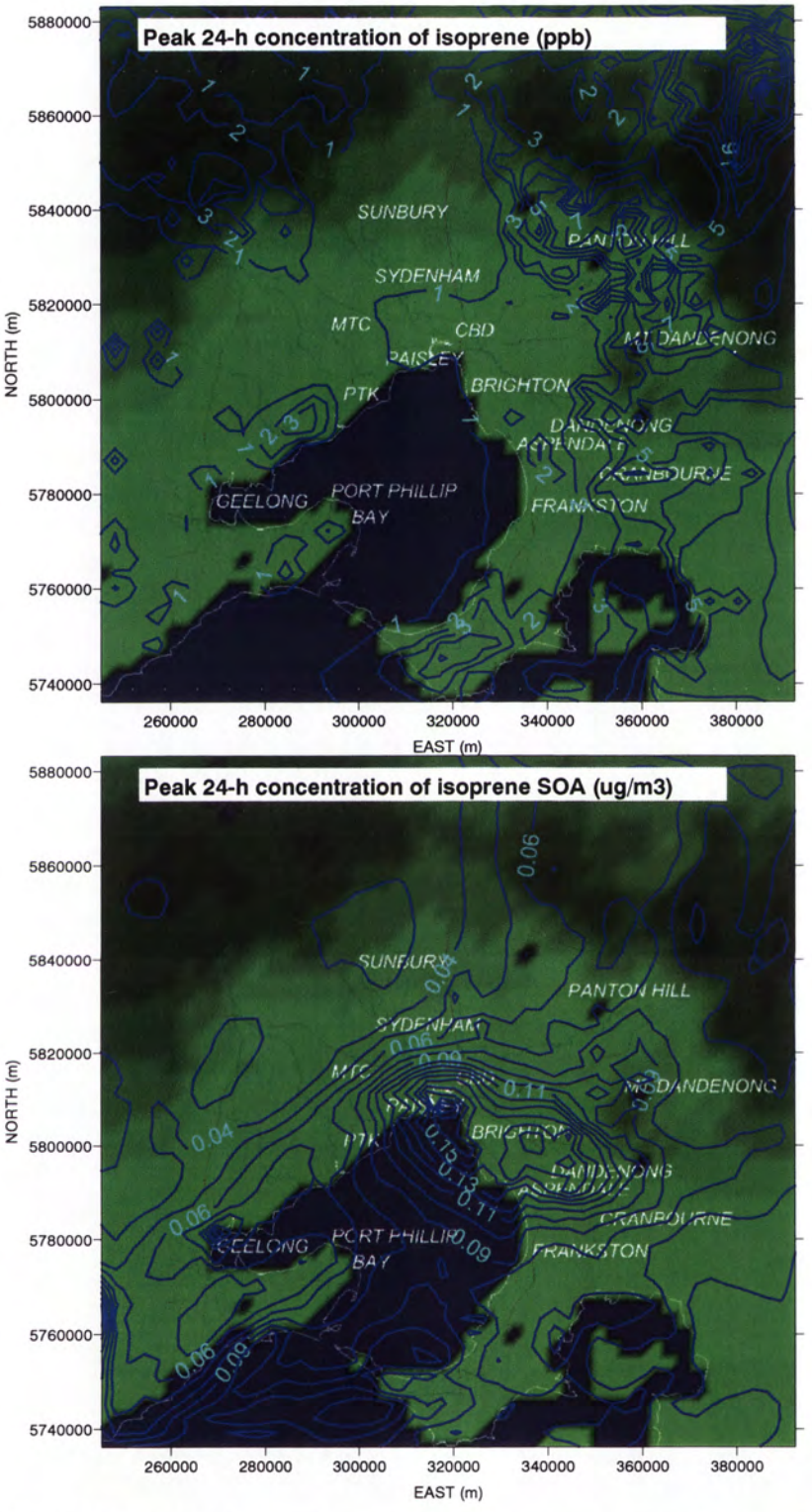

Figure 7.13: Spatial contours plots of isoprene concentrations (ppb) and SOA produced from isoprene ($\mu g/m^3$).

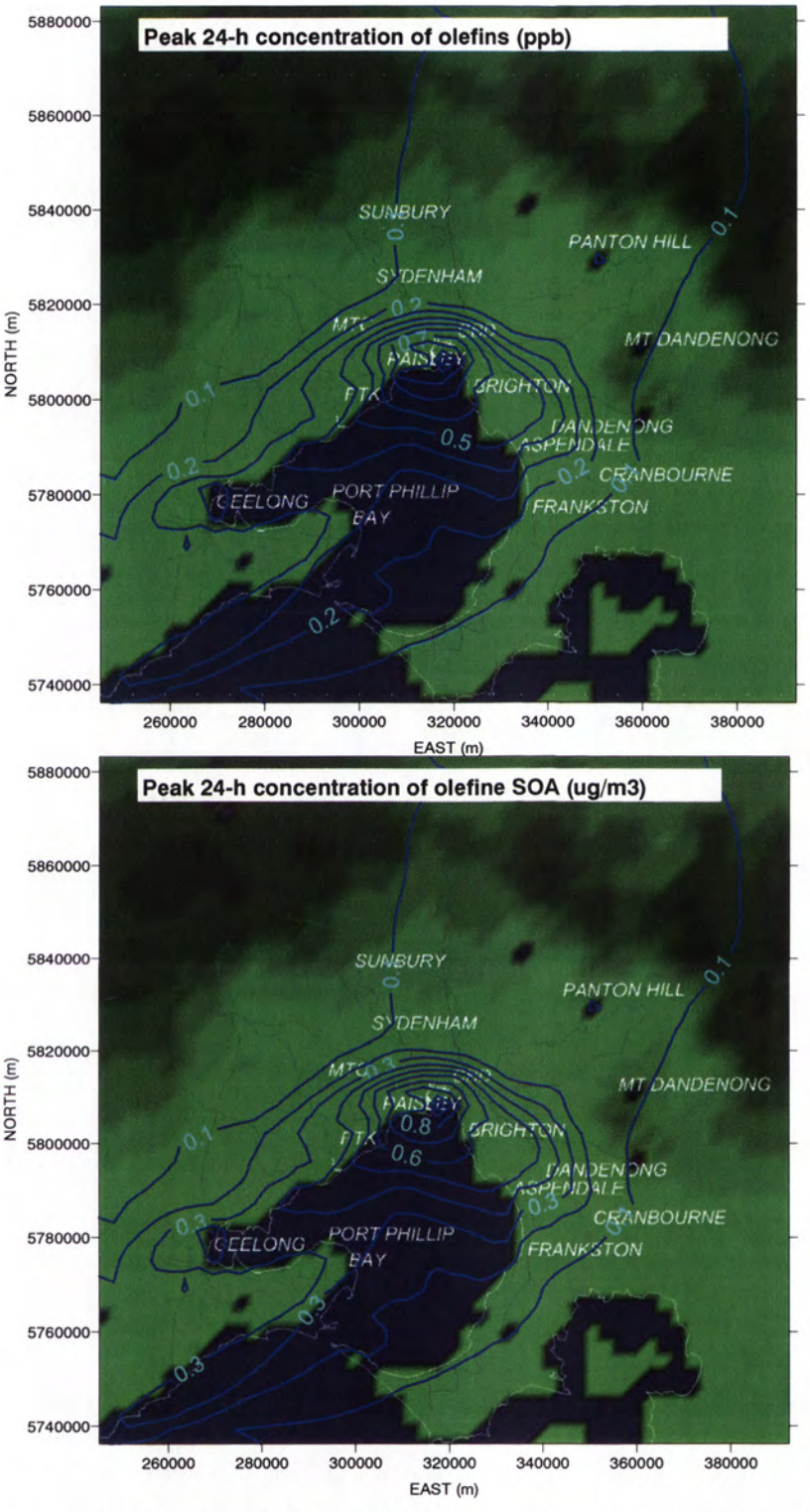

Figure 7.14: Spatial contour plot of olefins (ppb) and the SOA produced from the olefins ($\mu g/m^3$).

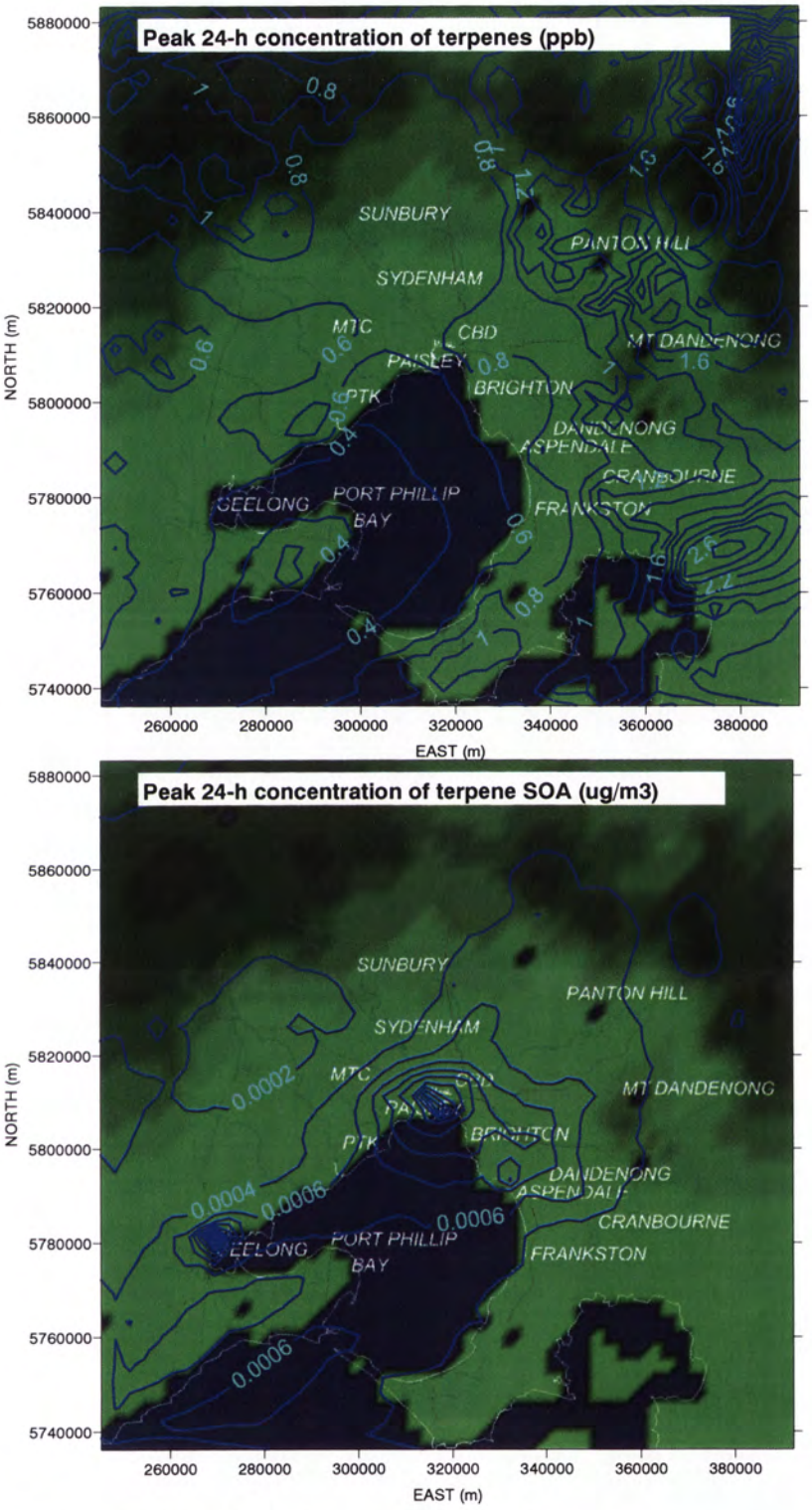

Figure 7.15: Spatial contour plots of the terpene concentrations (ppb) and the SOA produced from the terpenes ($\mu g/m^3$).

As shown in Figure 7.13, the peak concentrations of isoprene are observed in the north eastern region which is an area of high elevation as depicted by the shading of

the contour plot. This result suggests that the highest elevations are likely to be the most vegetated. The lowest concentrations are observed around the northern side of Port Phillip Bay which is where the CBD is located and as expected there is far less vegetation. Since isoprene is predominantly a biogenic emission the contour plot looks reasonable. It is interesting to note the difference between the isoprene concentration in the gas phase and the isoprene product's SOA concentration depicted in Figure 7.13. There appears to be little spatial correlation between the isoprene product's SOA mass and the precursor concentration. The peak concentrations of SOA in these figures are centred around the CBD rather than the highly vegetated areas and are most likely more sensitive to the $PM_{2.5}$ concentrations than the isoprene concentrations. This may be due to the fact that the SOA module is based on the absorption model defined by Odum et al. (1996) which focuses on the absorption mode of SOA formation. $PM_{2.5}$ is imported into the SOA module as available seed aerosol from which SOA can form, and so embodied within the module is the assumption that more SOA can be partitioned from the gas phase if there is more seed available for absorption.

The emissions of olefins depicted in Figure 7.14 are centred around the CBD, as are the $PM_{2.5}$ pictured in Figure 7.12. The SOA produced from olefins, not surprisingly, also follows this spatial pattern. The concentration of SOA produced from the olefins is the dominant class of SOA produced by the SOA module. The spatial distribution of the terpenes is similar to that of isoprene indicating a biogenic origin, although like isoprene, the SOA produced from the terpenes is located around the CBD in response to the higher $PM_{2.5}$ concentrations found in that area.

7.5 Discussion

The SOA module was found to represent the production and emission of some gas phase species monitored by the EPA's monitoring stations quite well. The SOA mass simulated by the SOA module was found to represent some of the chamber experiments extremely well and others not well at all. This is likely a result of fitting the Odum model to the chamber data. Some experiments correlated strongly to the line of best fit represented by the Odum model while others were not as close, hence, a mixture of results is obtained. The Odum model was fitted to the CSIRO

experiments in addition to the data obtained from Dommen et al. (2006). The model parameters determined for the two hypothetical Odum products therefore represent this whole system rather than the CSIRO subset. Although there is a compromise when comparing the SOA module only to the CSIRO experiments, it is considered that the wider range will be more appropriate to ambient conditions.

The largest mass of SOA was produced from the olefins relative to the other precursor species. Isoprene produced the second largest mass of SOA, presumably because the isoprene emission fluxes are about 100 times greater than the terpene emission fluxes. The other hydrocarbon precursors produced minimal amounts of SOA. The other key finding is that there is also not a lot of spatial coincidence between the biogenic VOC emission regions and the isoprene and terpene derived SOA peaks. The most likely explanation for this observation has been discussed previously and relates that the formation of SOA from the olefin precursor is centred around the CBD region where the mass concentration of $PM_{2.5}$ is greater, hence a larger amount of absorbing organic material.

In this chapter, the first stage of development of the SOA module has been presented with encouraging results. A crude representation of the oligomerisation processes occurring in the isoprene system (as a percentage) has improved the simulated results to more closely resemble chamber experiments. It is likely that further examination of the impact of the oligomerisation processes on SOA formation will provide insights into a more accurate way of parameterising this important process.

The model is very sensitive to the amount of $PM_{2.5}$ in the system and currently a distinction between the organic and inorganic fraction of $PM_{2.5}$ has not been made. Similarly, discrimination between the primary and secondary organic aerosol components of $PM_{2.5}$ has not been attempted. This is a limitation in the current CTM-SOA model that could be addressed in the next stage of development.

Chapter 8: Conclusion

The focus of this study has been to examine and develop methods of estimating the formation of secondary organic aerosols (SOAs). The models developed to achieve this outcome include:

1. A near explicit chemical mechanism that predicts the SOA composition and formation pathways derived from the photooxidation of isoprene;
2. A simple empirical model named the Secondary Organic Aerosol Profile Empirical Model (SOAPEM), that predicts the temporal SOA mass concentration produced throughout a chamber experiment;
3. A SOA module that is coupled to an atmospheric airshed model so that a prediction of SOA mass concentrations on a spatial and temporal grid can be made.

A series of isoprene / NOx and α-pinene / NOx chamber experiments was undertaken at the CSIRO, Lucas Heights facility to provide the necessary data required for the development of these models. The experimental set-up has been described in detail in Chapter 3, so it is sufficient to say in these closing remarks that the results returned from these experiments have been compared to the work of other researchers with similar results.

The modelling and experimental components of this study have focussed on the isoprene species. During the initial period of this work, isoprene was thought to produce negligible amounts of SOA in the ambient environment. In 2004, Claeys et al. (2004) reassessed this finding, and in doing so, encouraged many other researchers to investigate the SOA forming properties of isoprene. The work presented in Chapter 4 builds on an existing gas phase chemical mechanism that was found to estimate our gas phase chamber observations surprisingly well. The SOA mechanism that was developed in this study focuses the observations and findings of other researchers into a modelling domain.

Two other popular SOA models were examined to support the development of the SOA module that is coupled to the atmospheric airshed model. The work presented in Chapter 5 found that the popular method of substituting parameter values of

known primary products (resulting from the photochemical reaction of a hydrocarbon with an oxidant) into the Odum model produces estimates of yield that are not similar to the experimental yield. The products used in the Odum model were found to have theoretical properties that represented the whole system rather than a single species. Similarly, the assumption of a constant yield value for a hydrocarbon was also found to not hold for different experimental conditions. The main limitations constraining the use of the Odum and Hoffmann models in atmospheric airshed models is their inability to estimate the SOA mass concentrations produced from a system of mixed hydrocarbons. The current method (which is also employed in Chapter 7) is to add the yield of the individual systems to derive a yield of the mixed system and assume that the mixed system yield is a sum of its components. Work undertaken with toluene and propene by Lack et al. (2004) indicated that this is not the case. To the author's knowledge there are no methods currently employed in airshed models that counter this limitation.

The identification of this limitation in airshed modelling was the impetus for the development of the SOAPEM. At this moment, the SOAPEM is, at best, an alternative approach to this problem. The key feature of the SOAPEM is its simplicity, in that once it has been defined by numerous chamber experiments only the initial hydrocarbon and NOx concentrations are required to predict the SOA mass concentration produced throughout a chamber experiment (given that the physical variables are constant throughout the experimental program). The SOAPEM was applied to isoprene and α-pinene chamber experiments and although it was defined by only 4 experiments, it produced reasonable representations for both systems. This illustrates the ability of the SOAPEM to be applied to different SOA forming regimes. The structure and aerosol forming potentials of each hydrocarbon, isoprene and α-pinene, vary significantly.

The inherent simplicity of SOAPEM means that it could potentially be applied to mixed chamber experiments that represent the airshed hydrocarbon burden. If the experimental program that supports the mixed hydrocarbon SOAPEM is thorough, it is likely that the model could be coupled to an atmospheric model to provide SOA estimates spatially over time. In order to develop SOAPEM to the extent that it

could be applied to airshed studies, the impact of the physical variables (like UV intensity, temperature and relative humidity) on the aerosol mass concentration time-series profile needs to be explored. This would be the next stage of development for the SOAPEM.

The final piece of work presented in this study was developed in collaboration with CSIRO, Atmospheric Research, and it is anticipated that the SOA module will be packaged in the next release of The Air Pollution Model (TAPM) product. Collaboration has focussed on the upgrade of the CB4 to CB5 mechanism for the Chemical Transport Mechanism (CTM), which is a component of TAPM. The collaborators on this project have also been instrumental in coupling the SOA module to TAPM.

The SOA module has been developed to predict the formation of SOA from six groups of hydrocarbons: paraffins, olefins, toluene, xylene, terpenes and isoprene. One or two condensable organic products are formed by the photooxidation of these hydrocarbons and the Odum model is employed to estimate the model parameters of these products. As a result of the work presented in Chapter 5, care has been taken to use parameter values from the literature that has applied the Odum model to chamber data correctly. The products are therefore theoretical products. Where this information was not available, the Odum model was applied to chamber data reported in the literature or to chamber experiments undertaken in this study. In line with Morris et al. (2006), an oligomerisation function was applied to the SOA produced in each time-step. Its unlikely that the oligomerisation rate is constant for all hydrocarbons and their products, or for all time-steps, but it is the best approximation available. This is an area of SOA modelling that has been identified as requiring further intensive research. The formation of oligomers from condensed phase reactions has been identified as a dominant SOA forming process in the last few years. More information about this process is required before it can be adequately parameterised in air quality models.

From a holistic view of the SOA modelling efforts presented in this study, two dominant challenges have emerged. The first is to identify the SOA formation

pathways of mixed systems where a hydrocarbon may contribute to the concentration of condensable organic products held in the gas phase without any tangible signs of contribution in the aerosol phase. The other major challenge for SOA modelling is to allow for the formation of SOA via condensed phase reactions to form oligomers. This is a relatively new development in this field of science and the physical and chemical processes that govern these reactions are not well understood. The mass of SOA produced from hydroscopic reactions is another area of growth emerging in this field and adds further complexity to the estimation of SOA mass concentrations produced in a mixed system, like the atmosphere. A purely empirical approach like the one presented as SOAPEM may be one possible pathway until further understanding of these processes emerges.

References

Angove, D.E.; Halliburton, B.W., and Nelson, P.F. (CSIRO Energy Technology, North Ryde). 2000, 'Development of a new indoor environmental chamber at MRL, North Ryde', Proceedings of the *15th International Clean Air and Environment Conference; Sydney, Australia, 1: 270-274.*

Angove, D. E., Fookes, C. J. R., Hynes, R. G., Walters, C. K., and Azzi, M., 2006. The characterization of secondary organic aerosol formed during the photodecomposition of 1,3-butadiene in air containing nitric oxide. *Atmospheric Environment* **40**, 4597-4607.

Atkinson, R., 1987. A structure-activity relationship for the estimation of rate constants for the gas-phase reactions of OH radicals with organic compounds. *International Journal of Chemical Kinetics* **19**, 799-828.

Atkinson, R. and J. Arey, Gas-phase tropospheric chemistry of biogenic volatile organic compounds: a review. *Atmospheric Environment, 37, Supplement 2, 2003, 197-219*

Baltensperger, U., Kalberer, M., Dommen, J., Paulsen, D., Alfarra, M.R., Coe, H., Fisseha, R., Gascho, A., Nyeki, S., Sax, M., Steinbacher, M., Prevot, A.S.H., Sjögren, E.Weingartner and R.Zenobi. 2005. Secondary Organic Aerosols from anthropogenic and biogenic precursors. *Faraday Discussions.* **130**, 265-278.

Barthelmie and Pryor (1999). A model mechanism to describe oxidation of monoterpenes leading to SOA 1. Alpha and Beta Pinene. *Journal of Geophysical Research*, **104/19**, 23,657 – 23,699.

Böge O., Y. Miao et al. 2006. Formation of secondary organic particulate phase compounds from isoprene gas-phase oxidation products: An aerosol chamber and field study. *Atmospheric Environment*

Bowman, F.M., Odum, J.R., and Seinfeld, J.H. 1997, 'Mathematical model for gas partitioning of SOA', *Atmospheric Environment* **31/23**:3921-2931.

Camps, Francis E (Ed.) (1976). "Gradwohl's Legal Medicine, 3rd edition" *Bristol: John Wright & Sons Ltd*, ISBN 0 7236 0310 3. page 236 (referenced from wikipedia website).

Carter, W., Cocker III, W., Fits, D., Malkina, I., Bumiller, K., Sauer, C., Pisano, J., Bufalino, C., Song, C. 2005, A new environmental chamber for evaluation of gas-phase chemical mechanisms and secondary aerosol formation, *Atmospheric Environment*, **39**, 7768-7788.

Chung, S. H., Seinfeld, J. H., 2000. Global distribution and climate forcing of carbonaceous aerosols. *Journal of Geophysical Research* **107**, 4407 – 4411
Claeys, M., Graham, B., Vas, G., Wang, W., Vermeylen, R., Pashynska, V., Cafmeyer, J., Guyon, P., Andreae, M., Artaxo, P., Maenhaut, W., 2004a. Formation of secondary organic aerosol through photooxidation of isoprene. *Science* **303**, 1173-1176.

Claeys, M., Wang, W., Ion, A., Kourtchev, I., Gelencsér, A., Maenhaut, W., 2004b. Formation of secondary organic aerosol from isoprene and its gas-phase oxidation products through reaction with hydrogen peroxide. *Atmospheric Environment* **38**, 4093-4098.

Clancy L, Goodman P, Sinclair H, Dockery DW. 2002. Effect of air-pollution control on death rates in Dublin, Ireland: an intervention study. *Lancet* **360**: 1210 - 1214.

CSIRO Media Release 2004. Air Pollution death toll needs solutions. Ref 2004/31 Mar02, 2004

Czosche, N., Jang, M., Kamens, R. 2003. Effect of acidic seed on biogenic secondary organic aerosol growth. *Atmospheric Environment* **37** 4287-4299

Dockery, D., Pope III, C.A., Xu, X., Spengler, J.D., Ware, J.H., Fay, M.E., Ferris, Jr, B.G. & Speizer, F.E. 1993, 'An association between air pollution and mortality in six US cities', *New England Journal of Medicine*, **329**, pp.1753–9

Dommen, J., Metzger, A., Duplissy, J., Kalberer, M., Alfarra, M.R., Gascho, A., Weingartner, E., Prevot, A.S.H., Verheggen, B., Baltensperger, U., 2006. Laboratory observation of oligomers in the aerosol from isoprene / NOx photooxidation. *Geophysical Research Letters*, **33**, L13805.

Edney, E. O., Kleindienst, T. E., Jaouri, M., Lewandowski, M., Offenberg, J. H., Wang, W., Claeys, M., 2005. Formation of tetrol and 2-methylglyceric acid in secondary organic aerosol from laboratory irradiated isoprene/ NOx/ SO_2/air mixtures and their detection in ambient $PM_{2.5}$ samples collected in the eastern United States. *Atmospheric Environment* **39**, 5281-5289.

Finlayson-Pitts and Pitts 2000, Chemistry of the Upper and Lower Atmosphere *Academic Press*, U.K.

Forstner, H., Flagan, R.C. and Seinfeld, J. 1997, Molecular Speciation of SOA from photooxidation of the higher alkenes: 1-octene and 1-decene. *Atmospheric Environment*, **31**, 13, 1953-1964

Gao S., M.Keywood et al. 2004. Particle phase acidity and oligomer formation in secondary organic aerosol . *Environmental Science and Technol.* **38**, 6582- 6589.

Griffin, R., Cocker III, D., Flagan, R. and Seinfeld, J. 1999. Organic aerosol formation from the oxidation of biogenic hydrocarbons. *Journal of Geophysical Research*, **104**, D3, 3555- 3567.

Griffin, R., Nguyen, K., Darbub, D. and Seinfeld, J. 2003, A coupled hydrophobic – hydrophilic model for the predicting SOA formation, *J. Atmospheric Chemistry*, **44**, 171-190

Grosjean, D. 1989 Parameterisation of the formation potential of SOAs, *Atmospheric Environment*, **23**, 5, 1733-1749.

Guenther, A., Nicholas Hewitt, C., Erickson, D., Fall., R., Geron, C., Graedel, T., Harley, P., Klinger, L., Lerdau, M., McKay, W. A., Pierce, T., Scholes, B., Steinbrecher, R., Tallamraju, R., Taylor, J., Zimmerman, P., 1995. A global model of natural volatile organic compound emissions. *Journal of Geophysical Research* **100**, D5, 8873-8892.

Hegg, D.A. and Y.J. Kaufman. 1998. Measurements of relationships between submicron aerosol number and volume concentration. *Journal of Geophysical Research* **103**, D5, 5671-5678.

Hildermann et al., 1994. Seasonal Trends in Los Angeles Ambient Organic Aerosol by High Resolution Gas Chromatography, *Aerosol Science Technology*, **20**, 303-317.

Hoffmann, T., Odum, J.R., Bowman, F., Collins, D., Klockow, D., Flagan, R.C., Seinfeld, J.H.,1997.'Formation of organic aerosols from the oxidation of biogenic hydrocarbons', *Journal of Atmospheric Chemistry*, **26** 189-222.

Houghton J.T., Y. Ding, et al. (2001). IPCC 2001: Climate Change 2001: The Scientific Basis. Contributions of the working group 1 to the third assessment report of the intergovernmental panel on climate change. Cambridge, United Kingdom and New York, NY, USA, *Cambridge University Press.*

Hynes, R. G., Angove, D. E., Saunders, S. M., Harverd, V., Azzi, M., 2005. Evaluation of two MCM v3.1.1 alkene mechanisms using indoor chamber data. *Atmospheric Environment* **39**, 7251-7262.

Ion, A. C., Vermeylen, R., Kourtchev, I., Cafmeyer, J., Chi, X., Gelencsér, A., Maenhaut, W., Claeys, M., 2005. Polar organic compounds in rural $PM_{2.5}$ aerosol K-

puszta, Hungary during a 2003 summer field campaign: sources and diel variations. *Atmospheric Chemistry and Physics,* **5,** 1805-1814.

IPCC 2007. Climate Change 2007: The Physical Science Basis. Summary for policymakers. Working Group 1.

Jang and Kamens, (2001). Atmospheric SOA formation by heterogeneous reactions of aldehydes in the presence of a sulfuric acid catalyst, *Environmental Science and Technology*, **35**, 4758-4766.

Jaoui. M, and Kamens. R 2001. Mass balance of gaseous and particulate products analysis from α-pinene / NOx / air in the presence of natural sunlight. *Journal of Geophysical Research*, **106**, D12, 12,541-12,558

Jenkin, M. E., Saunders, S. M., Pilling, M. J., 1997. The tropospheric degradation of volatile organic compounds: a protocol for mechanistic development. *Atmospheric Environment* **31**, 81-104.

Jenkin, M. E., 2004. Modeling the formation and composition of secondary organic aerosol from α- and β-pinene ozonolysis using MCM v3. *Atmospheric Chemistry and Physics,* **4**, 1741-1757.

Johnson, D., Jenkin, M., Wirtz, K., Martin-Reviejo, M., 2004. Simulating the formation of secondary organic aerosol from the photooxidation of toluene. *Environmental Chemistry* **1**, 150-165.

Kanakidou,M., Seinfeld, J.H., Pandis, S.N., Barnes, I., Dentener, F.J., Facchini, M.C., Van Dingenen, R., Ervens, B., Nenes, A., Nielsen, C.J., Swietlicki, E., Putaud, J.P., Balkanski, Y., Fuzzi, S., Horth, J., Moortgat, G.K., Winterhalter, R., Myhre, C.E.L., Tsigaridis, K., Vignati, E., Stephanou, E.G. and Wilson, J.2005 Organic aerosol and global climate modeling: review. *Atmospheric .Chemistry and Physics.*, **5**, 1053-1123.

Kamens, R., Jang, M., Chien, C-J., and Leach, K. 1999. Aerosol formation from the reaction of α-pinene and ozone using a gas-phase kinetics-aerosol partitioning model. *Environmental Science and Technology* **33**, 1430-1438.

Kalberer, M., Sax, M. and Samburova, V. 2006. Molecular size evolution of oligomers in organic aerosols collected in urban atmospheres and generated in a smog chamber. *Environmental Science and Technology*, **40**, 5917-5922.

Kavouras, I.G, Mihalopous, N., Stephanou, E.G., 1998. Secondary Aerosol Formation vs. primary organic aerosol emission: in situ evidence for chemical coupling between monoterpene acid photochemical products and new particle formation over forests. *Environmental Science and Technology*, **33**, 1028-1037.

Kourtchev, I., Ruuskanen, T., Maenhaut, W., Kulmala, M., Claeys, M., 2005. Observation of tetrol and related photooxidation products of isoprene in boreal forests aerosols from Hyytiälä, Finland. *Atmospheric Chemistry and Physics Discussions* **5**, 2947-2971.

Kirstine W., Galbally I.E, Ye Y., and Hooper M.A., 1998.Emissions of volatile organic compounds (primary oxygenated species) from pasture. *J. Geophys. Res.*, **103**, 100605-10620.

Kroll, J. H., Ng, N. L., Murphy, S. M., Flagan, R. C., Seinfeld, J. H., 2005. Secondary organic aerosol from isoprene photooxidation under high-NOx conditions. *Geophysical Research Letters* **32**, L18808.

Kroll, J. H., Ng, N. L., Murphy, S. M., Flagan, R. C., Seinfeld, J. H., 2006. Secondary organic aerosol formation from isoprene photooxidation. *Environmental Science and Technology* **40**, 1869-1877.

Kwok, E. and Atkinson,R. (1995) *Atmospheric Environment29 1685*

Lack, D., Bofinger, N. and Wiegand, A. 2003. The effect of propene on secondary organic aerosol formation from toluene and m-xylene. PhD thesis. *Queensland University of Technology*.

Liggio, J. and R. McLaren, An optimized method for the determination of volatile and semi-volatile aldehydes and ketones in ambient particulate matter, *International Journal of Environmental Analytical Chemistry* **83** (2003), pp. 819–835

Limbeck, A., Kumala, M., Puxbaum, H. 2003, Secondary organic aerosol formation in the atmosphere via heterogeneous reaction of gaseous isoprene on acidic particles. *Geophysical Research Letters*, **30**, 1996-1999.

Matsunaga, S. N., Wiedinmyer, C., Guenther, A. B., Orlando, J. J., Karl, T., Toohey, D. W., Greenberg, J. P., Kajii, Y., 2005. Isoprene oxidation products are a significant atmospheric aerosol component. *Atmospheric Chemistry and Physics Discussion* **5**, 11143-11156.

Morgan, G et al. 1998, 'Air Pollution and Daily Mortality in Sydney, Australia, 1989 to 1993', *American Journal of Public Health* **88**(5) 759-64.

Morris, R., Koo, B., Guenther, A., Yarwood, G., McNally, D., Tesche, T., Boylan, J. and Brewer, P. 2006. Model sensitivity for organic using two multi-pollutant air quality models that stimulate regional haze in the southeastern United States. *Atmospheric Environment*, **40**, 4960-4972.

Nelson, P.F., Quigley, S. and M.Y.Smith, 1982. *Atmospheric hydrocarbons in Sydney: Ambient concentrations and relative source strengths.* The Urban Atmosphere – Sydney, a case study. CSIRO, Australia

Nelson P.F., Azzi M., Cope M., Stuart D., Halliburton B., Huber G., Tibbett A., Bentley S., Galbally I., Gillett R., Lawson S., Meyer M., Selleck P., Weeks I. & Kirstine W., 2004. Biogenic Emission in the Greater Sydney Region. Final Report to

the NSW Environmental Trust, Environmental Research Program Grant. 2000/RD/6004. CSIRO Energy Technology

NEPC, 2001, 'The Need for a PM2.5 Standard in Australia', Issues Paper, May, http://www.nepc.gov.au/pdf/issues_paper.pdf

Ng, N.L., Kroll J.H., Keywood, M. Bahreini, R., Varutbangkui, V., Flagan, R., and Seinfeld, J. 2006. Contribution of first versus second generation products to secondary organic aerosols formed in the oxidation of biogenic hydrocarbons. *Environmental Science and Technology* **40**, 2283-2297.

Odum, J.R., Hoffmann, T., Bowman, F., Collins, D., Flagan, R.C., Seinfeld, J.H. 1996. 'Gas/particle partitioning and secondary organic aerosol formation. *Environmental Science and Technology*, **30**(8): 2580-2585.

Odum, J., Jungkamp, T., Griffin, R., Forstner, H., Flagan, R. and Seinfeld, J. 1997, Aromatics, reformulated gasoline and atmospheric organic aerosol formation. *Environ. Science and Technol.*, **31**, 1890-1897.

Ostro, B.D. and Rothschild, S. Air pollution and acute respiratory morbidity: An observational study of multiple pollutants. 1989. *Environmental Research*, **50**, 2, 238-247.

Pandis, S.N., Paulson, S.E., Seinfeld, J.H. and Flagan., 1991 Aerosol formation in the photo-oxidation of isoprene and β-pinene. *Atmospheric Environment*, **28**(2): 189- 93.

Pankow, J. F., 1994. An absorption model of gas-particle partitioning involved in the formation of secondary organic aerosol. *Atmospheric Environment* **28A**, 189-193.

Pinho, P. G., Pio, C. A., Jenkin, M. E., 2005. Evaluation of isoprene degradation in the detailed tropospheric chemical mechanism, MCM v3, using environmental chamber data. *Atmospheric Environment* **39**, 1303-1322.

Pilinis C.P. P.Pandis et al., 1995 Sensitivity of direct climate forcing by atmospheric aerosols to aerosol size and composition. *Journal of Geophysical Research* 100 D9 18739-18754.

Presto, A., Huff Hartz, K. and Donahue, N. 2005. Secondary organic aerosol production from terpene ozonolysis. 2. Effect of NOx concentration. *Environmental Science and Technology* **39**, 7046-7054.

Pun, B., Wu, S-Y., Seigneur, C., Seinfeld, J., Griffin, R. and Pandis, S. 2003, Uncertainties in modeling SOA: 3D Modelling studies in Nashville / Western Tennessee, *Environmental Science and Technol.*, **37**, 3647-3661.

Pun, B., Seigneur, C., Lohman, K. 2006. Modelling secondary organic aerosol formation from multiphase partitioning with molecular data. *Environmental Science and Technol.*, **40**, 4722-2731

Report on Carcinogens, Eleventh Edition. Substance Profiles. 2007

Rissel CE. Clinicians prescribing exercise: is air pollution a hazard [letter with other letters by du Plessis and Sharman] 2005 *Medical Journal of Australia*, **183** 334-336.

Robinson DL. 2005 Air pollution in Australia: review of costs, sources and potential solutions. *Health Promotion Journal of Australia* **16** 213-220.

Samet, J et al, 2000, 'Fine Particulate Air Pollution and Mortality in 20 U.S. Cites, 1987-1994', *New England Journal of Medicine* **343**(24).

Schell, B., Ackermann, I., Hass, H. Binkowski, F., Ebel, A. 2001. Modeling the formation of SOA within a comprehensive air quality model system, *J. Geophysical Research*, **106**, 22, 28,275-28,293.

Seinfeld, J.H. and Pandis, S.N. Atmospheric chemistry and physics. *John Wiley Press* New York. 1998

Seinfeld et al., 2001. Modelling the formation of SOA. 2. The predicted effects of relative humidity on aerosol formation in the pinene, sabinene, carene and cyclohexene – ozone systems' *Environmental Science and Technology* **35**, 9, 1806-1817.

Shine K.P. and P.M. Forstner. 1999 The effects of human activity on radiative forcing of climate change: A review of recent developments. *Environmental Science and Technology*

Simpson, R. Dension, L. Petroeschevsky, A, Thalib, L. and G. Williams. 2000 Effects of ambient particulate pollution on daily mortality in Melbourne 1991-96. *J. Expo Anal. Environ. Epidemiol.* 10(5) 488-96.

Skov, H., Hjorth, J., Lohse, C., Jensen, N. and G. Restelli.1992 Products and mechanisms of the reactions of the nitrate radical (NO_3) with isoprene, 1,3-butadiene and 2,3-dimethyl-1,3-butadiene in air, *Atmospheric Environment.* 26, 15, 2771-2783

Stein, S. E., Brown, R. L., 1994. Estimation of normal boiling points from group contributions, *Journal of Chem. Inf. Comp. Sci.* **34(3),** 581-7.

Song, C., Na, K. and Cocker, D. 2005, Impact of the hydrocarbon to NOx ratio on SOA formation, *Environmental Science and Technol.*, **39**, 3143-3149.

Strader, Lurmann and Pandis (1999), Evaluation of SOA formation in winter' *Atmospheric Environment* **33**, 4849 – 4863.

Stroud, C. A., Makar, P. A., Michelangeli, D. V., Hastie, D. R., Barbu, A., Humble, J., 2004. Simulating organic aerosol formation during the photooxidation of Toluene/NOx mixtures: Comparing the kinetic and equilibrium assumption. *Environmental Science and Technology* **38**, 1471- 1477.

Surratt, J. D., Murphy, S. M., Kroll, J.H., Ng, N.L., Hildebrandt, L., Sorooshian, A., Szmigielski, R., Vermeylen, R., Maenhaut, W., Claeys, M., Flagan, R., Seinfeld, R., 2006. Chemical Composition of Secondary Organic Aerosol Formed from the Photooxidation of Isoprene, *Journal of Physical Chemistry* **A110**, 9665-9690.

Takakawa, H., Minoura, H. amd Yamazaki, S. 2003. Temperature dependence of secondary organic aerosol formation by photo-oxidation of hydrocarbons. *Atmospheric Environment* **37** 3413-3424.

Turpin, B.J. and Huntzicker, J.J (1995). 'Identification of SOA episodes and quantification of primary and secondary organic aerosol concentration during SCAQS". *Atmospheric Environment* **29B**, 3527-3544.

Urbinato, David 1994. EPA Journal, Summer. referenced from the US EPA website http://www.epa.gov/history/topics/perspect/london.htm

Walser, M. L., Park, J., Gomez, A. L., Russell, A. R., and Nizkorodov, S. A., 2007. Photochemical aging of secondary organic aerosol generated from the oxidation of d-limonene. *Journal of Physical Chemistry* **A111**, 1907-1913.

Wang, W., Kourtchev, I., Graham, B., Cafmeyer, J., Maenhaut, W., Claeys, M., 2005. Characterisation of oxygenated derivatives of isoprene related to 2-methyltetrol in Amazonian aerosol using trimethylsilylation and gas chromatography/ ion trap mass spectrometry. *Communications in Mass Spectrometry* **19**, 1343-1351.

WHO and World Bank publication, World report on road traffic injury prevention, 2004).